All the X in one basket: X-ray constraints on sub-GeV dark matter

Elena Pinetti

PADUA – 7th September 2023

This talk is based on…

INTEGRAL X-ray constraints on sub-GeV Dark Matter

Marco Cirelli [a], Nicolao Fornengo [b],
Bradley J. Kavanagh [c], Elena Pinetti [a,b]

[a] *Laboratoire de Physique Théorique et Hautes Energies (LPTHE), UMR 7589 CNRS & UPMC, 4 Place Jussieu, F-75252, Paris, France*

[b] *Dipartimento di Fisica, Università di Torino & INFN, Sezione di Torino, via P. Giuria 1, I-10125 Torino, Italy*

[c] *Instituto de Física de Cantabria, (IFCA, UC-CSIC), Av. de Los Castros s/n, 39005 Santander, Spain*

Phys.Rev.D 103 (2021) 6, 063022

Putting all the X in one basket: Updated X-ray constraints on sub-GeV Dark Matter

Marco Cirelli [a], Nicolao Fornengo [b],
Jordan Koechler [a], Elena Pinetti [c,d], Brandon Roach [e]

JCAP 07 (2023) 026

This talk is based on…

INTEGRAL X-ray constraints on sub-GeV Dark Matter

Marco Cirelli [a], Nicolao Fornengo [b], Bradley J. Kavanagh [c], Elena Pinetti [a,b]

[a] Laboratoire de Physique Théorique et Hautes Energies (LPTHE), UMR 7589 CNRS & UPMC, 4 Place Jussieu, F-75252, Paris, France

[b] Dipartimento di Fisica, Università di Torino & I…
via P. Giuria 1, I-10125 Tor…

[c] Instituto de Física de Cantab…
Av. de Los Castros s/n, 390…

Phys.Rev.D 103 (2021) 6, 063022

$1\,\text{MeV} \leq m_\chi \leq 5\,\text{GeV}$

Putting all the X in one basket: Updated X-ray constraints on sub-GeV Dark Matter

Marco Cirelli [a], Nicolao Fornengo [b],
…Koechler [a], Elena Pinetti [c,d], Brandon Roach [e]

JCAP 07 (2023) 026

Outline

- ❑ Motivation for sub-GeV dark matter
- ❑ Theoretical prediction of dark matter flux
- ❑ X-ray telescopes
- ❑ Dark matter costraints
- ❑ Uncertainties & Prospects

Indirect detection of sub-GeV dark matter

$e^{\pm}$

ν

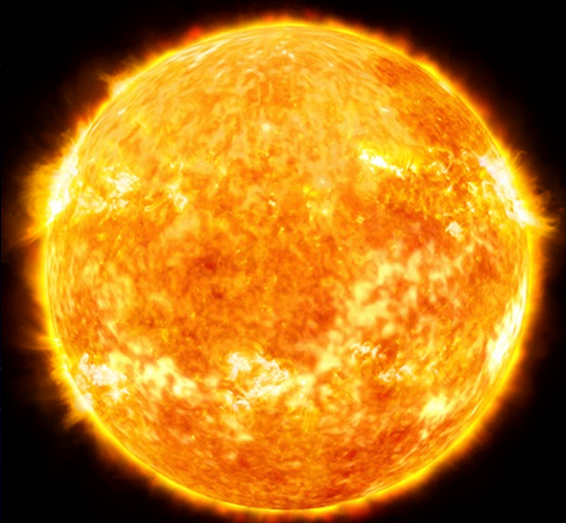

γ

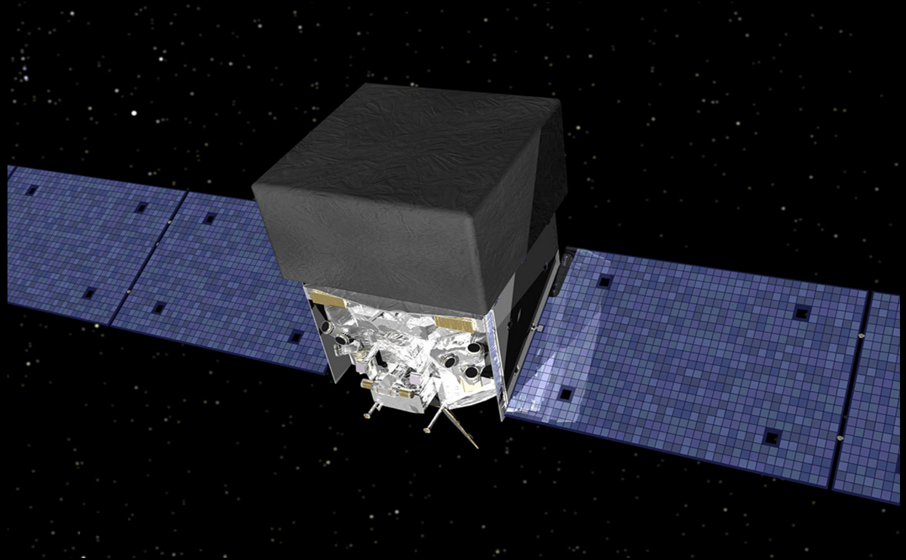

MeV gap

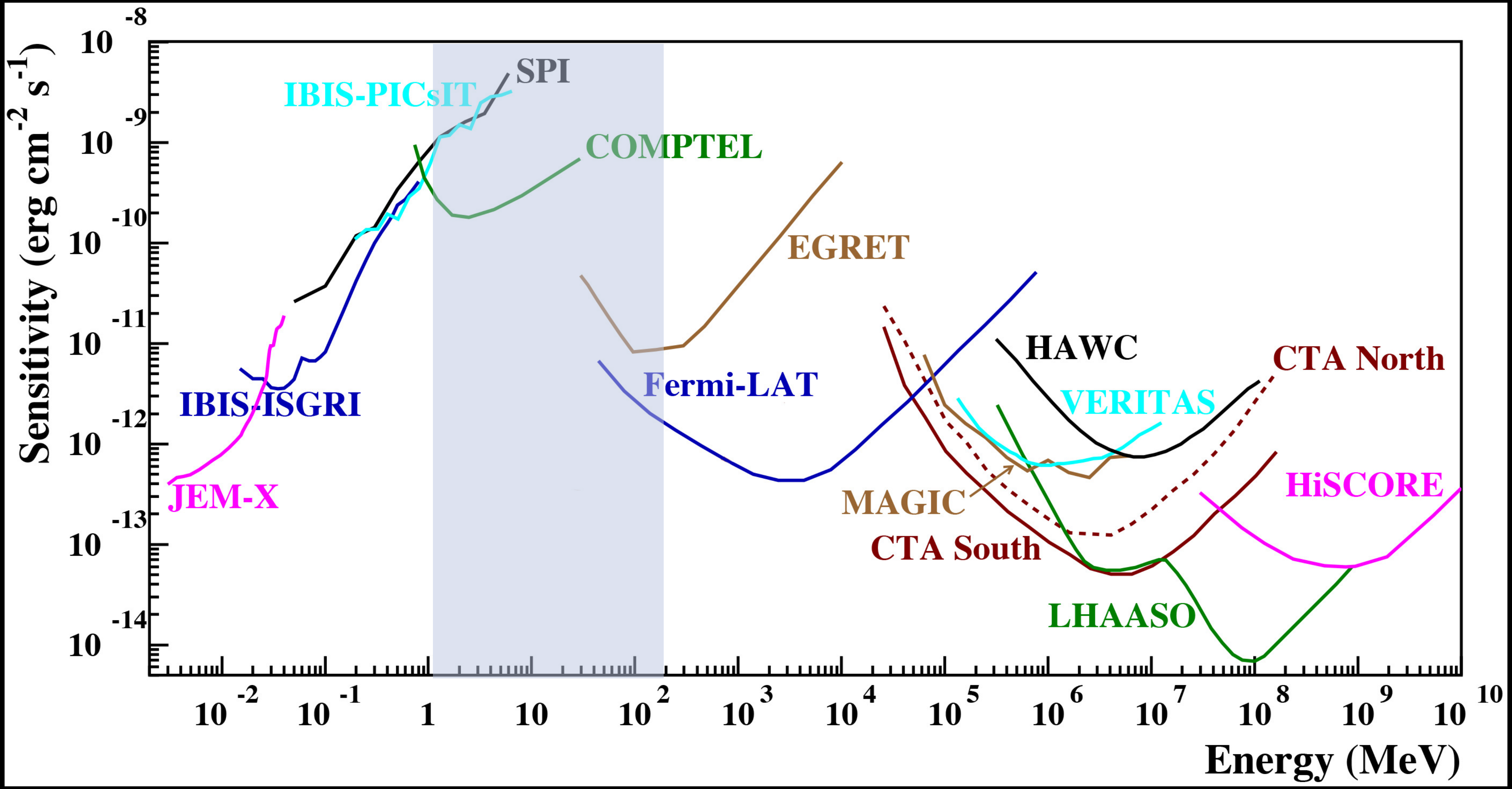

Figure adapted from Tatischeff+ arxiv:1805.06435

MeV gap

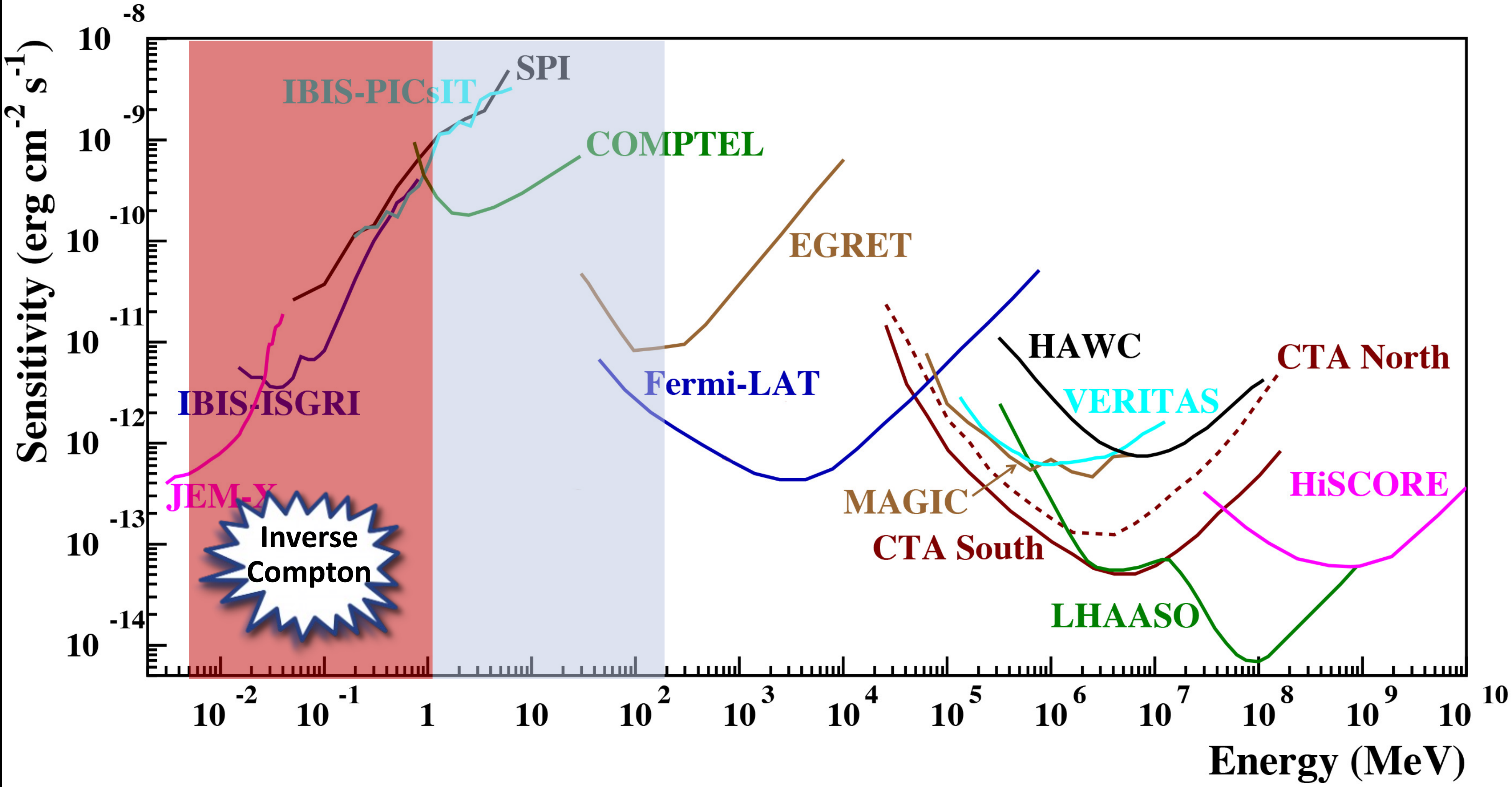

Figure adapted from Tatischeff+ arxiv:1805.06435

Production channels

$$1\ \text{MeV} < m_\chi < 5\ \text{GeV}$$

3 decay/annihilation channels:

$$\chi(\chi) \longrightarrow e^+e^-$$
$$\chi(\chi) \longrightarrow \mu^+\mu^-$$
$$\chi(\chi) \longrightarrow \pi^+\pi^-$$

Kinematically open: $m_\chi > (2)m_i \quad i = e, \mu, \pi$

Total Flux

$$\phi_{TOT} = \phi_{FSR} + \phi_{Rad} + \phi_{ICS}$$

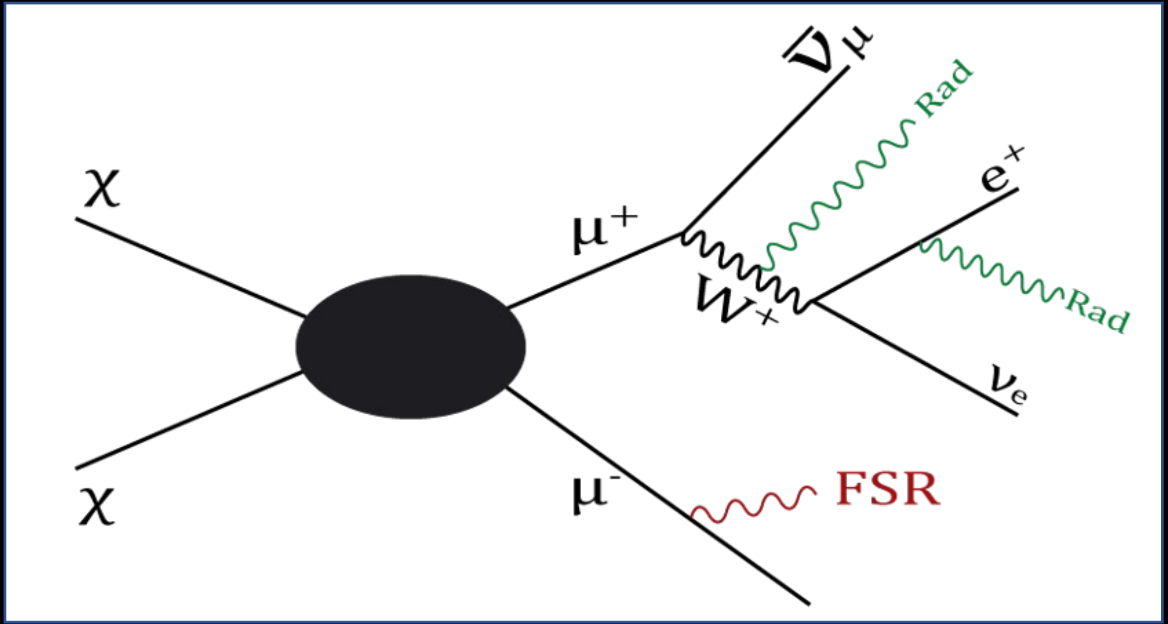

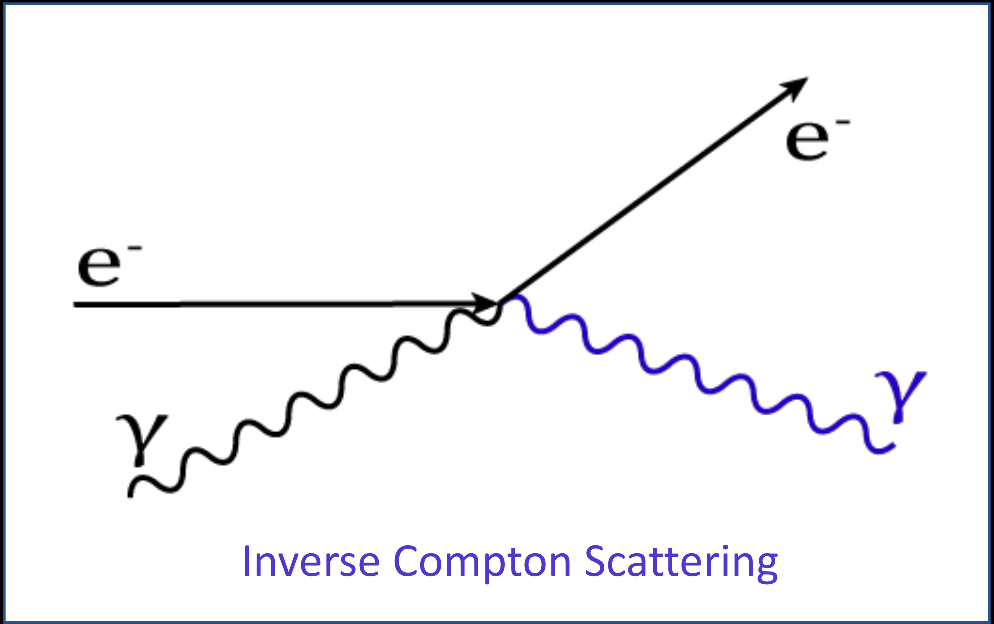

$\chi\chi \longrightarrow \mu^+\mu^-\gamma$ FSR

$\chi\chi \longrightarrow \mu^+\mu^-$ Rad

$\quad \hookrightarrow e^+\nu_e\bar{\nu}_\mu\,\gamma$

$\chi\chi \longrightarrow (\ldots) \rightarrow e^+\, e^-$

$e^- + \gamma \rightarrow e^- + \gamma$

Prompt components

Decaying dark matter:

$$\frac{d\phi}{dE_\gamma\, d\Omega}(E_\gamma, \theta) = \frac{1}{4\pi} \frac{1}{\tau\, m_{\rm DM}} \frac{dN}{dE_\gamma}(E_\gamma)\, D(\theta)$$

$$D(\theta) = \int_{l.o.s} \rho\big(s(r,\theta)\big) ds$$

Particle properties

Energy spectrum

D-factor

Annihilating dark matter:

$$\frac{d\phi}{dE_\gamma\, d\Omega}(E_\gamma, \theta) = \frac{1}{4\pi} \frac{\langle \sigma_{ann} v \rangle}{2 m_{DM}^2} \frac{dN}{dE_\gamma}\, J(\theta)$$

$$J(\theta) = \int_{l.o.s} \rho^2\big(s(r,\theta)\big) ds$$

Inverse Compton scattering

$$\chi\chi \longrightarrow (\dots) \rightarrow e^+ e^-$$

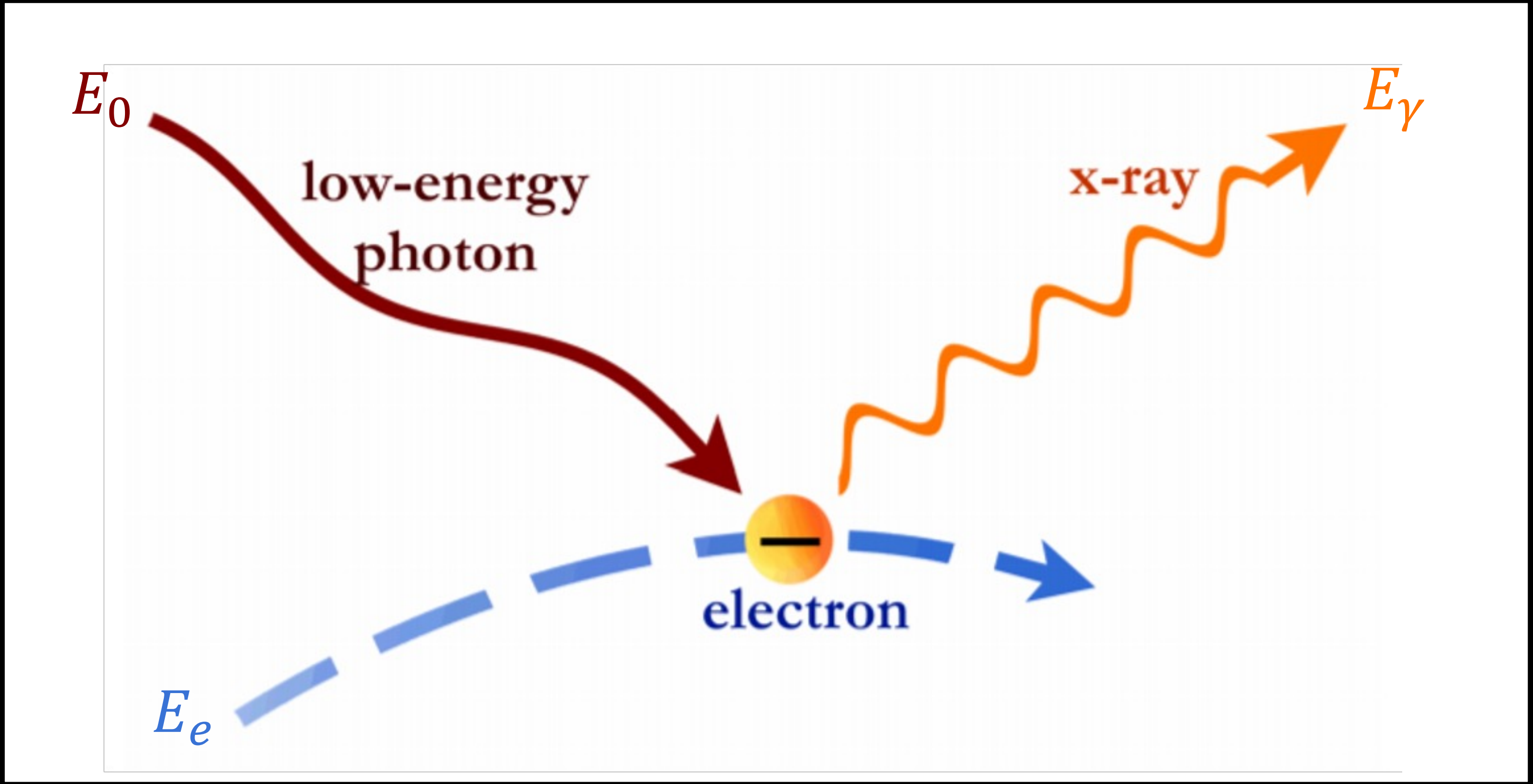

3 kind of photons:

- CMB
- IR (dust)
- Optical (starlight)

Inverse Compton scattering

$$\gamma = \frac{E_e}{m_e}$$

$$E_\gamma \approx 4\gamma^2 E_0$$

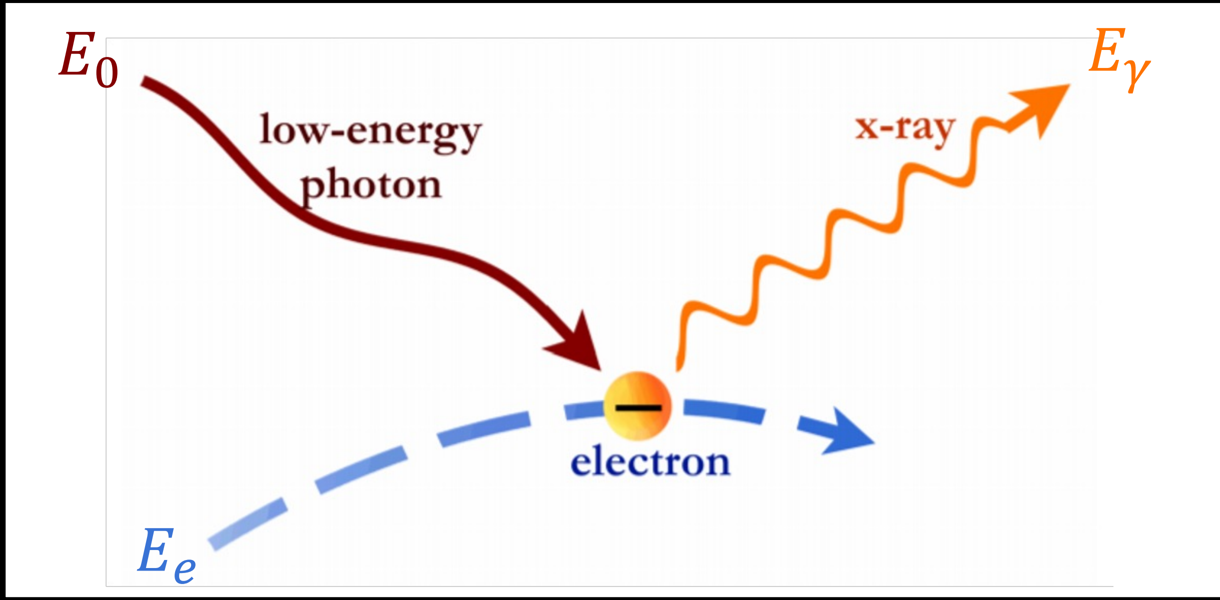

Type	E_0 [eV]	E_e [GeV]	E_γ [keV]
CMB	10^{-4}	5	40
IR	10^{-2}	0.5	40
Opt	10	0.05	400

X rays

Inverse Compton scattering

$$\frac{d\phi_{IC}}{dE_\gamma d\Omega} = \frac{1}{4\pi\, E_\gamma} \int_{l.o.s.} ds\, j\left(E_\gamma, \vec{x}(s,b,l)\right)$$

$$j(E_\gamma, \vec{x}) = 2 \int_{m_e}^{m_\chi} dE_e\, P_{IC}(E_\gamma, E_e, \vec{x}) \frac{dn_e}{dE_e}(E_e, \vec{x})$$

Emissivity

$e^{\pm}$

Differential Power

Number density

Photon energy distribution

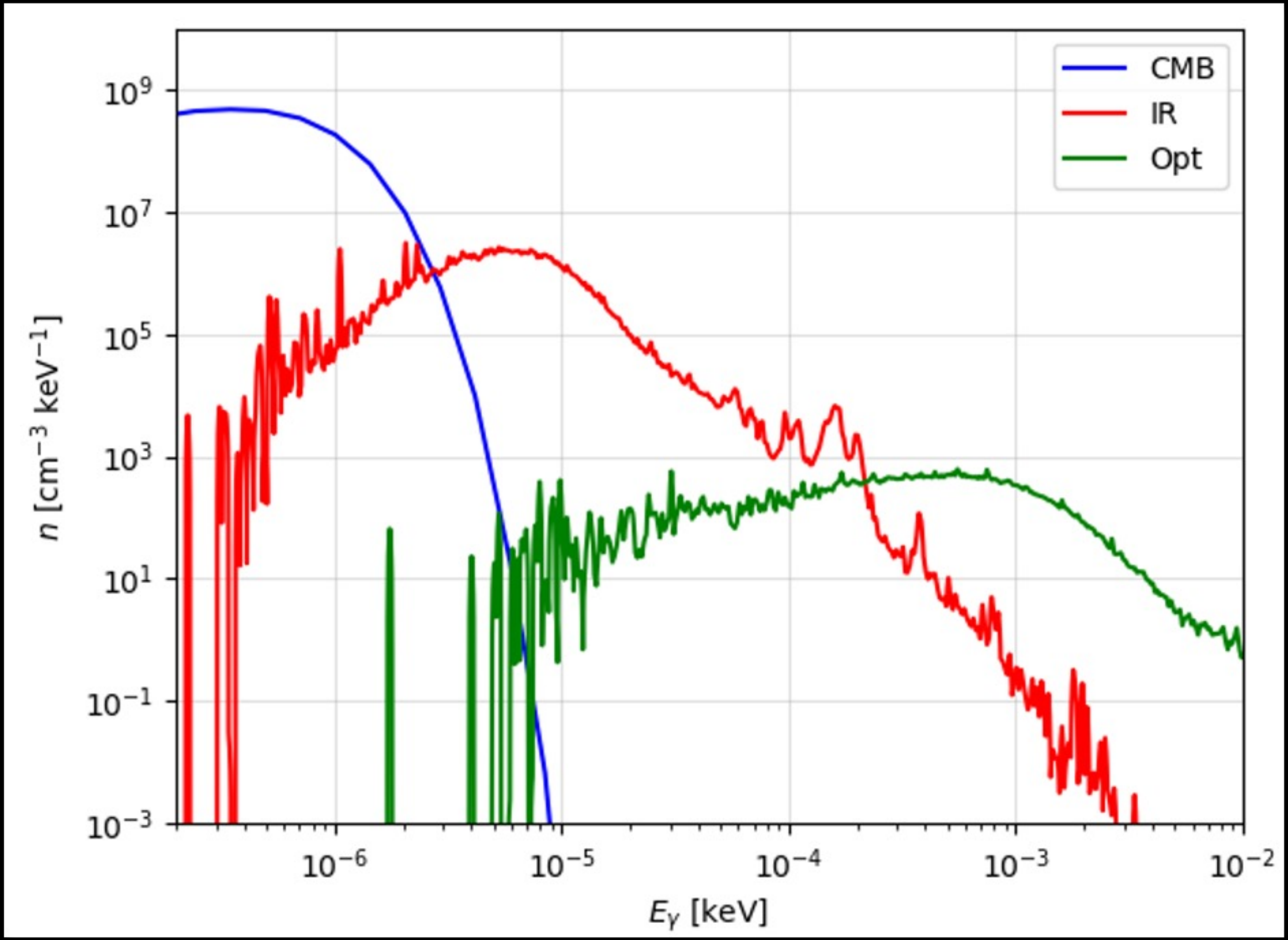

As implemented in GALPROP code

ICS Power

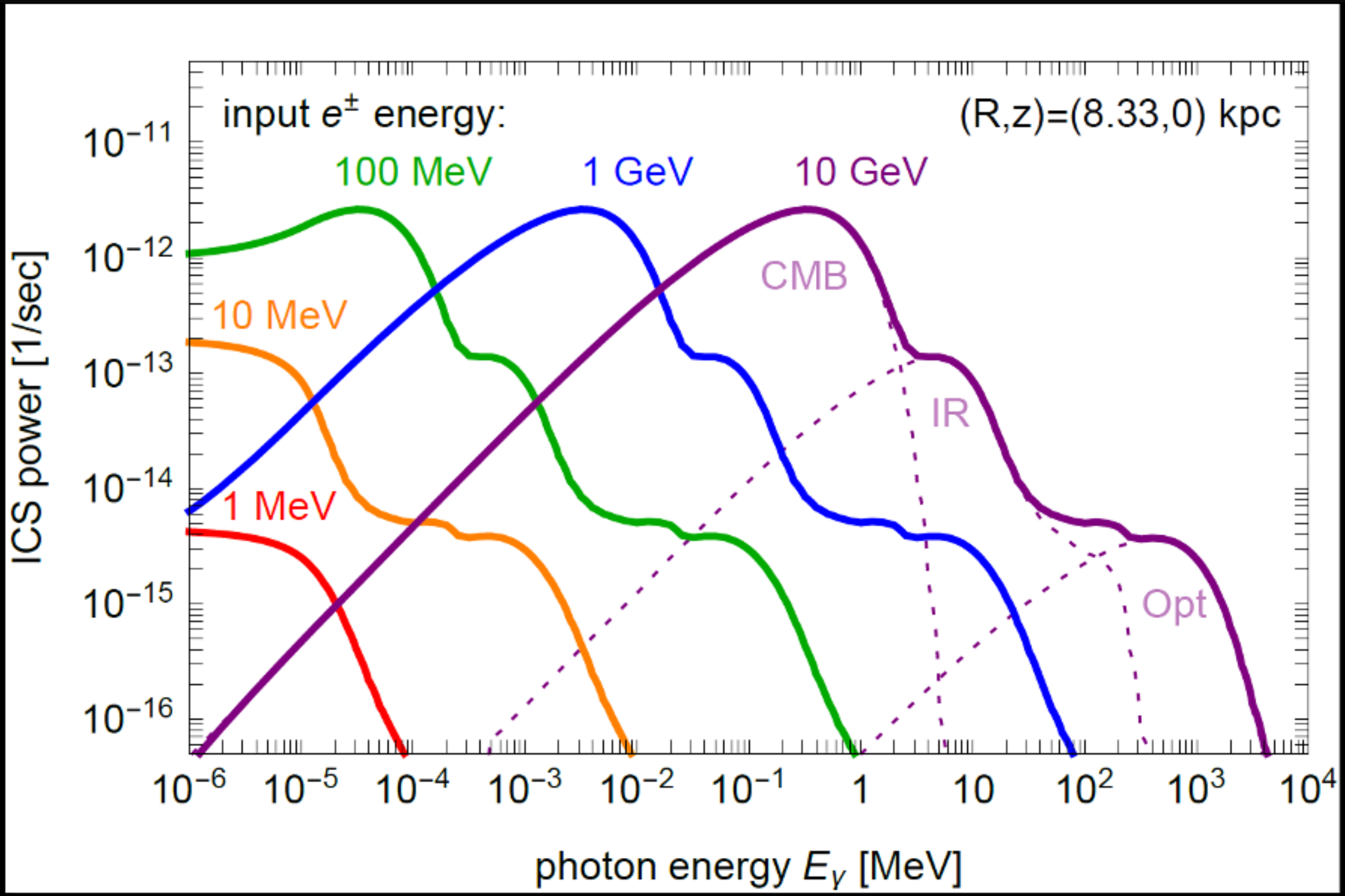

input $e^{\pm}$ energy:
(R,z)=(8.33,0) kpc
100 MeV
1 GeV
10 GeV
10 MeV
1 MeV
CMB
IR
Opt
ICS power [1/sec]
10^{-11}
10^{-12}
10^{-13}
10^{-14}
10^{-15}
10^{-16}
10^{-6} 10^{-5} 10^{-4} 10^{-3} 10^{-2} 10^{-1} 1 10 10^{2} 10^{3} 10^{4}
photon energy E_γ [MeV]

Energy losses

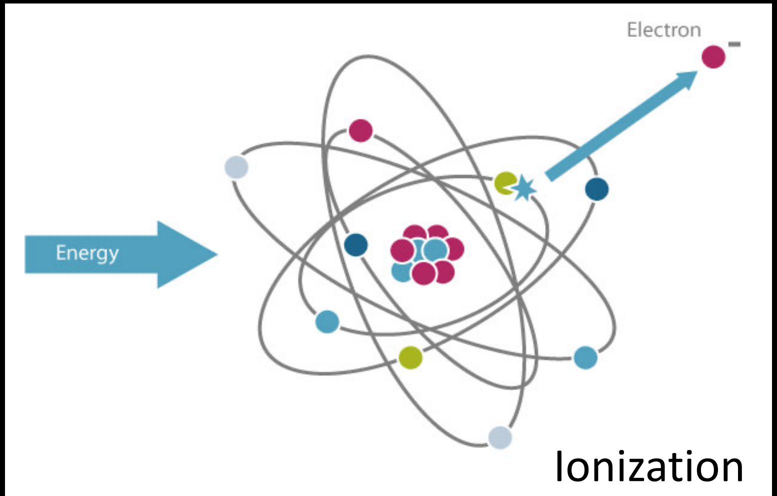

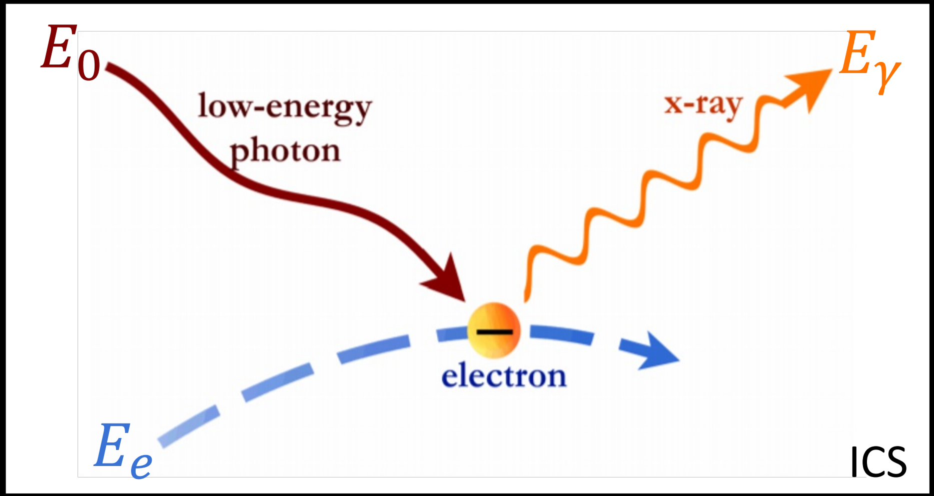

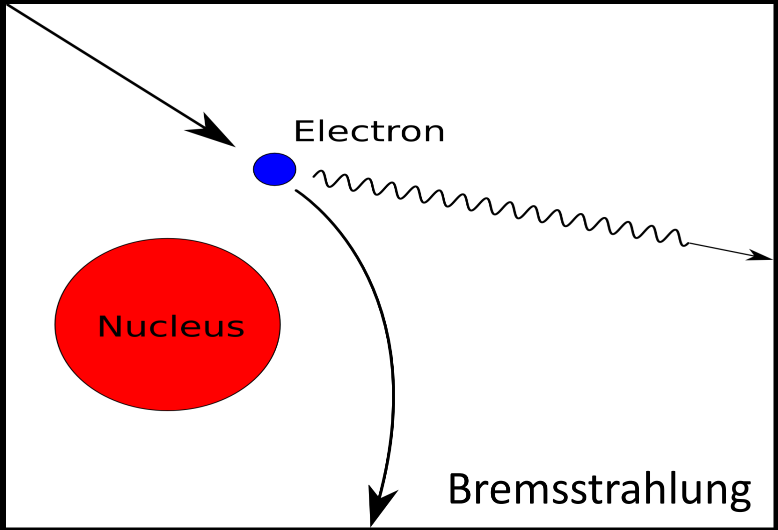

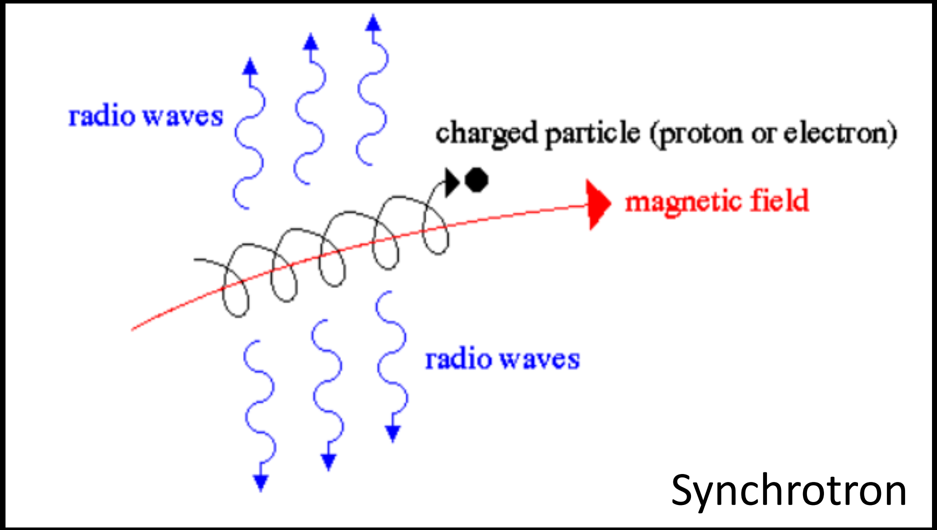

Electron number density

$$\frac{dn_{e^\pm}}{dE_e}(E_e,\vec{x}) = \frac{1}{b_{tot}(E_e,\vec{x})}\int_{E_e}^{m_\chi} d\tilde{E}_e\, Q_e(\tilde{E}_e,\vec{x})$$

$$Q_e(\tilde{E}_e,\vec{x}) = \frac{\langle\sigma_{ann}v\rangle}{2\, m_{DM}^2}\frac{dN_{e^\pm}}{d\tilde{E}_e}\rho_{DM}^2$$

Particle Properties

Energy spectrum

Density distribution

Energy losses $b_{tot}(E_e,\vec{x})$

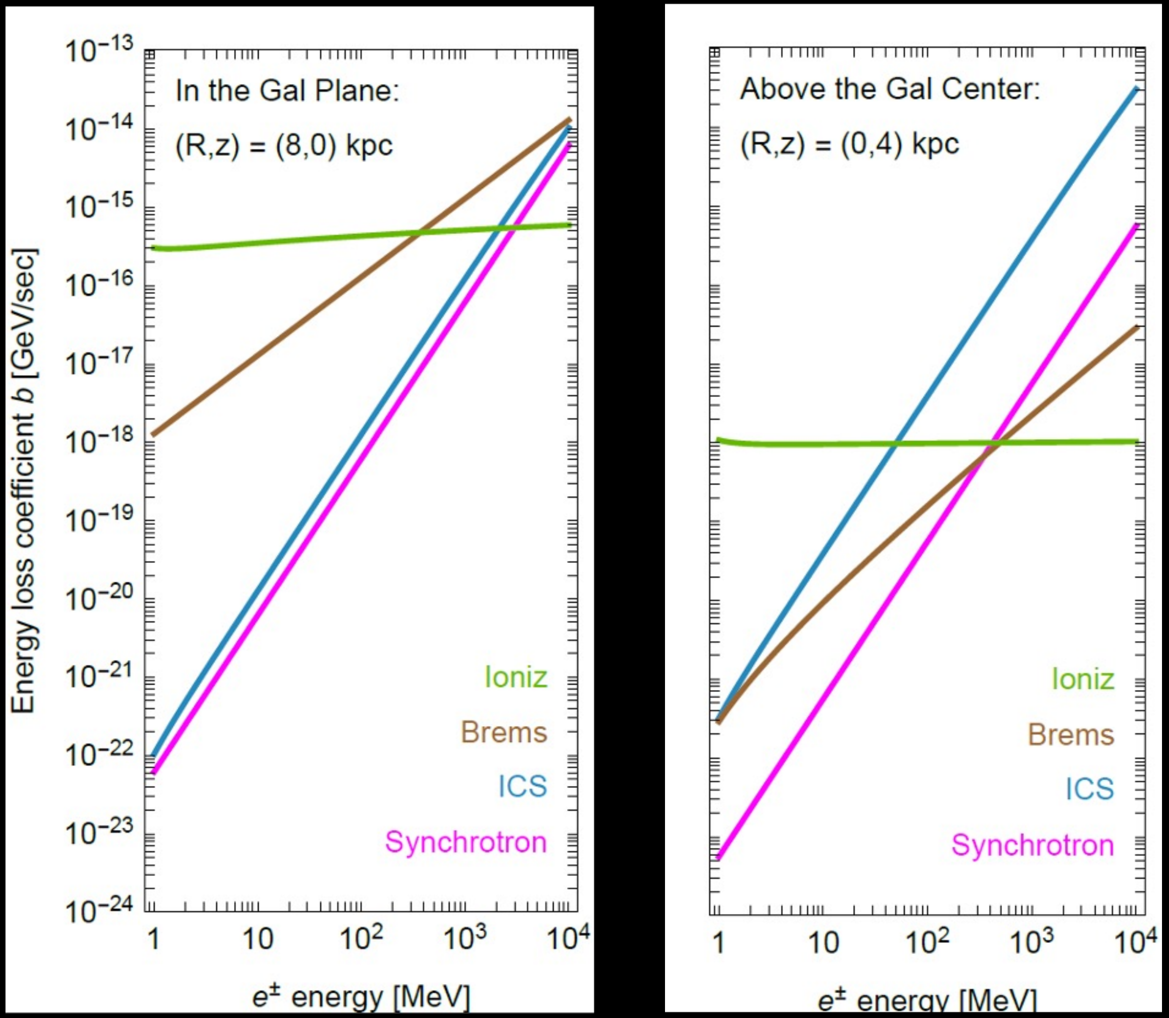

Total flux

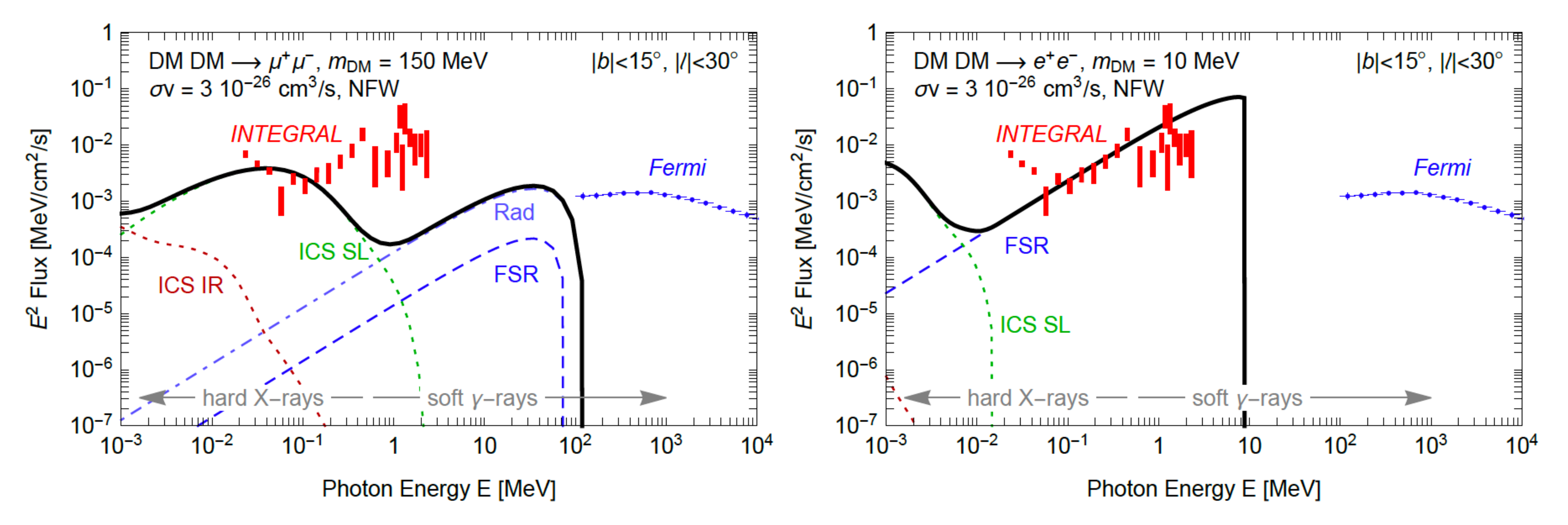

DM DM ⟶ μ⁺μ⁻, m_DM = 150 MeV
σv = 3 10⁻²⁶ cm³/s, NFW
|b|<15°, |l|<30°
INTEGRAL
Fermi
Rad
ICS SL
FSR
ICS IR
hard X–rays
soft γ–rays
E² Flux [MeV/cm²/s]
Photon Energy E [MeV]
DM DM ⟶ e⁺e⁻, m_DM = 10 MeV
σv = 3 10⁻²⁶ cm³/s, NFW
|b|<15°, |l|<30°
INTEGRAL
Fermi
FSR
ICS SL
hard X–rays
soft γ–rays
E² Flux [MeV/cm²/s]
Photon Energy E [MeV]

X-ray telescopes

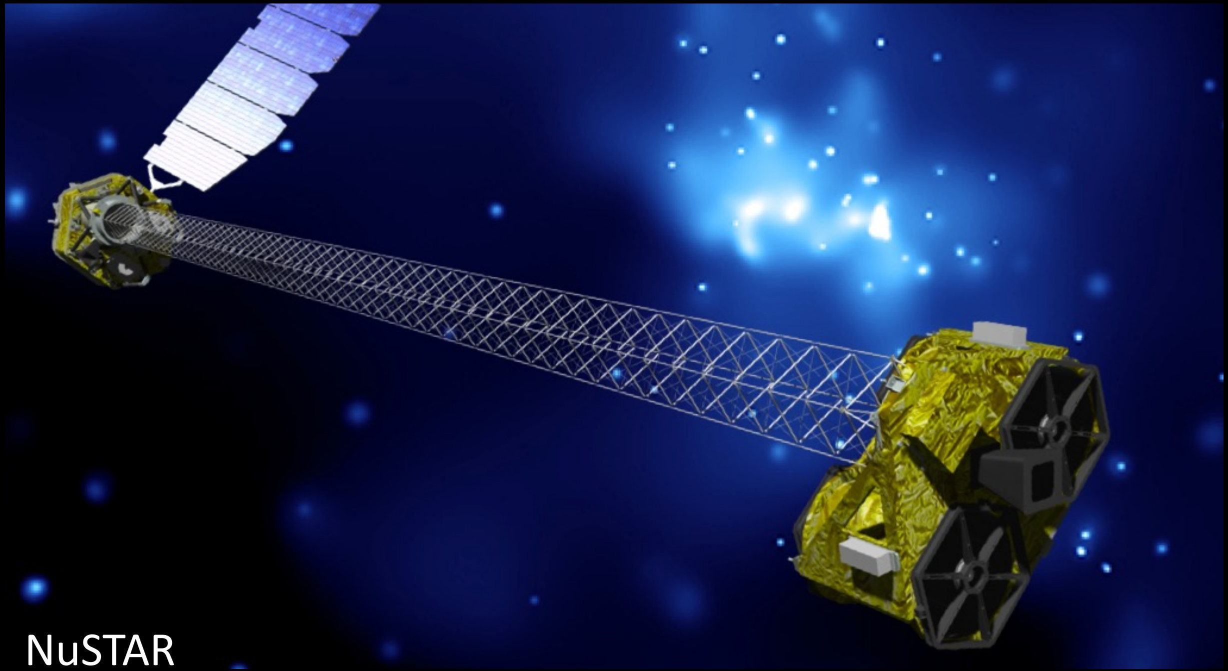

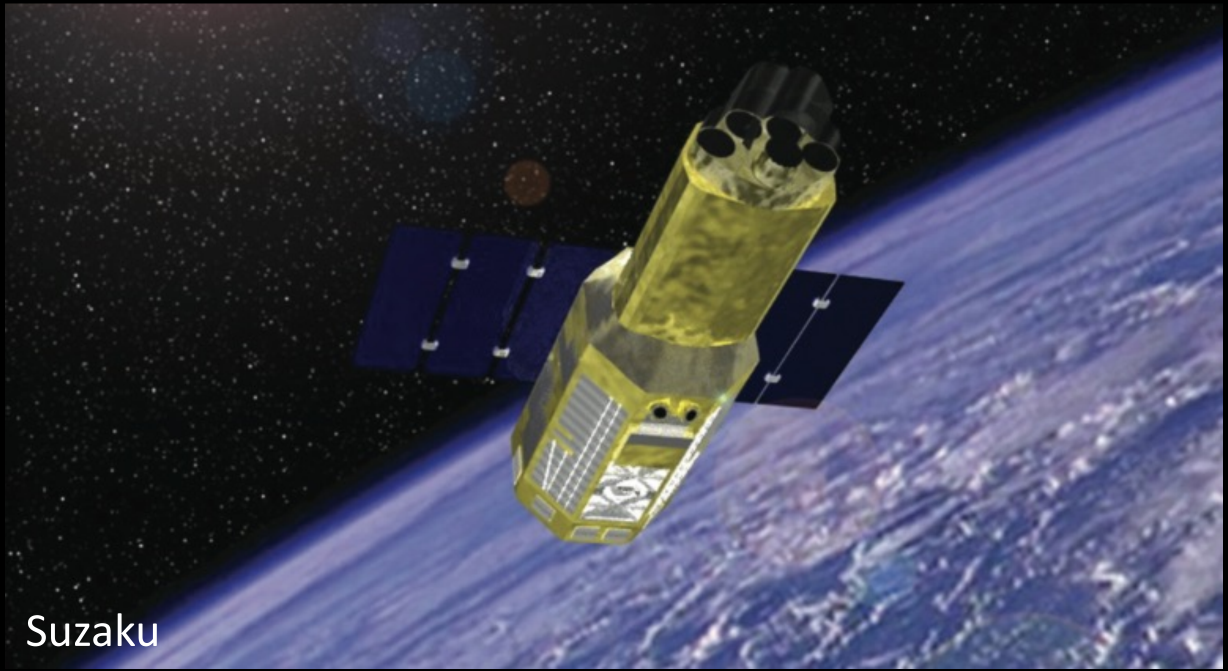

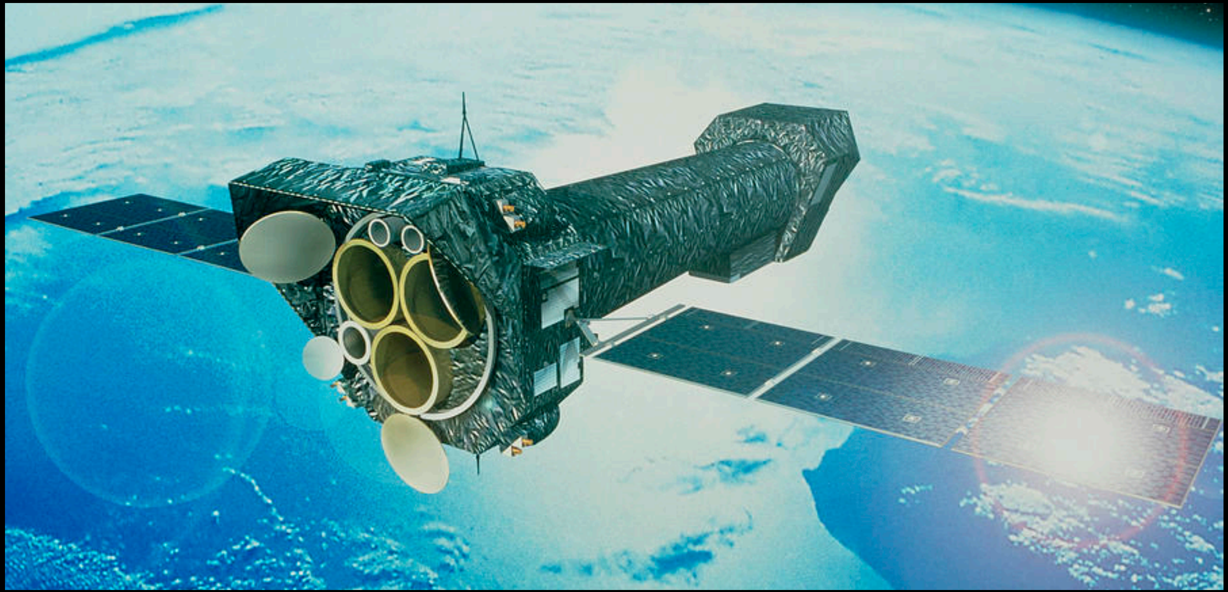

XMM-Newton

INTEGRAL

Energy range

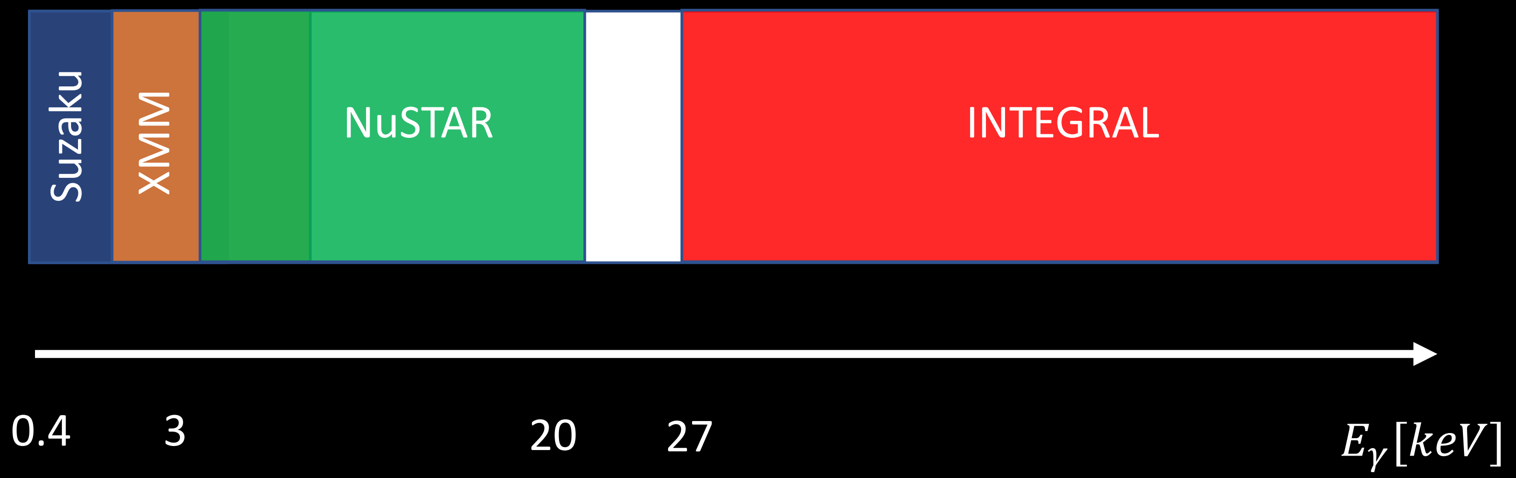

Suzaku: 0.4 keV – 5 keV

NuSTAR: 3 keV – 20 keV

XMM-Newton: 2.5 keV – 8 keV

INTEGRAL: 27 keV – 1.8 MeV

Observations

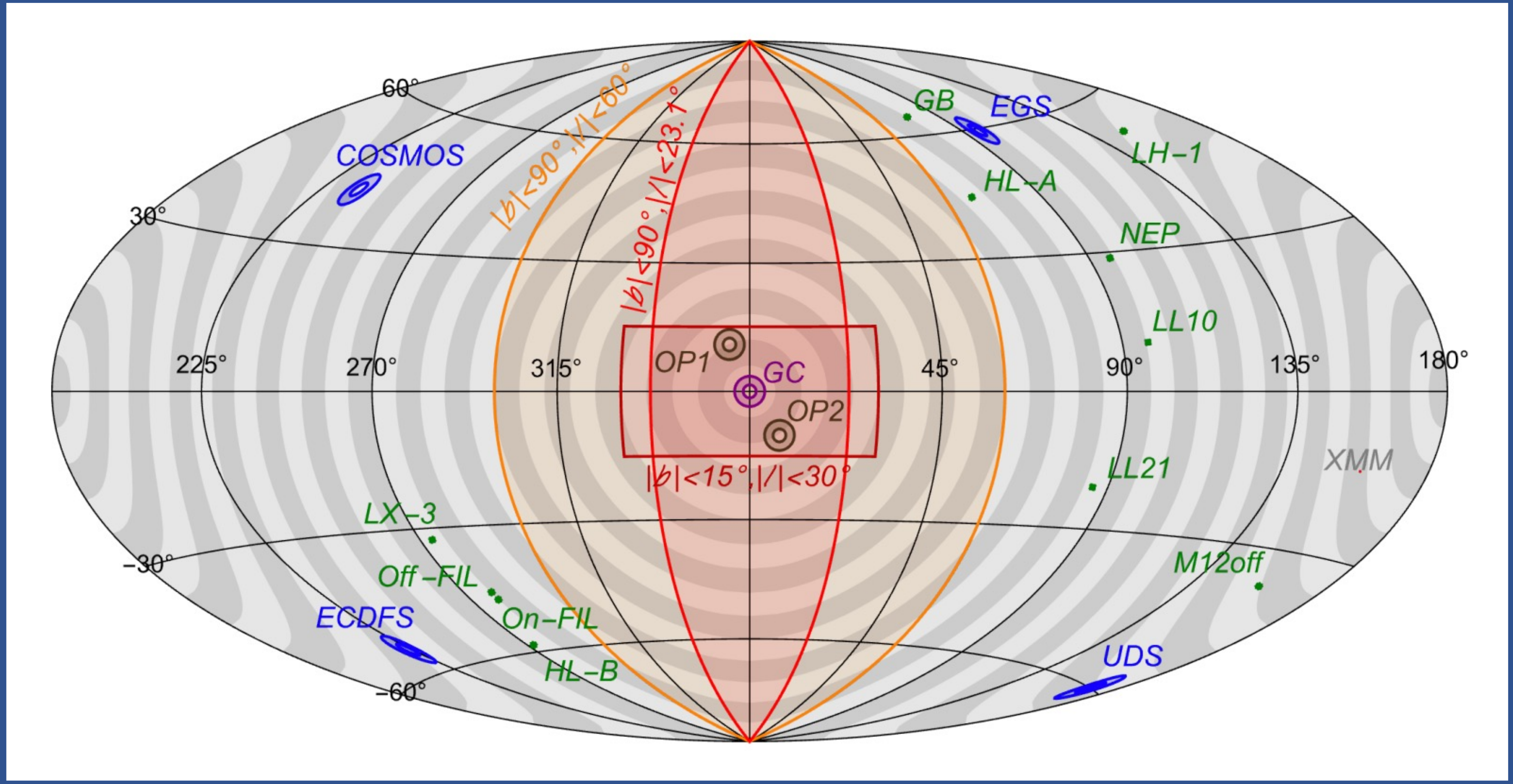

X-ray constraints

Constraints on electron channel

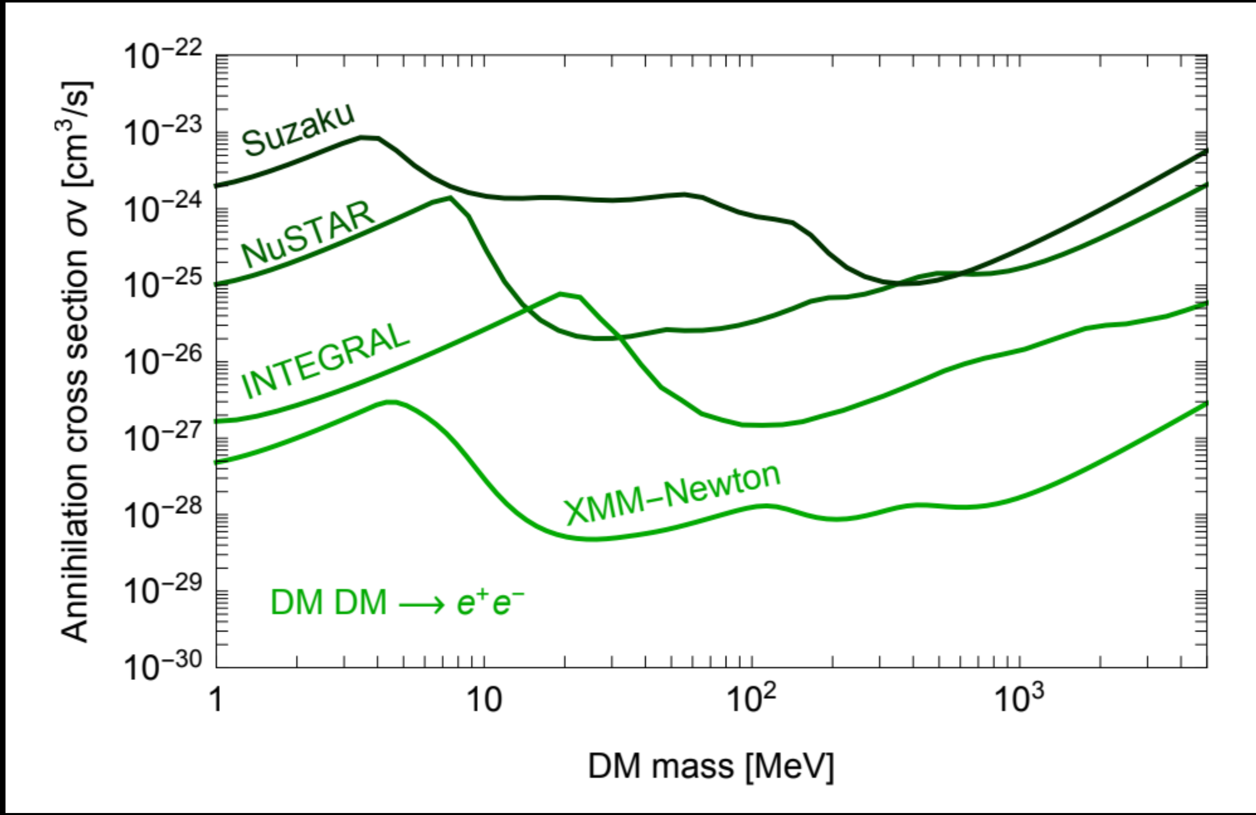

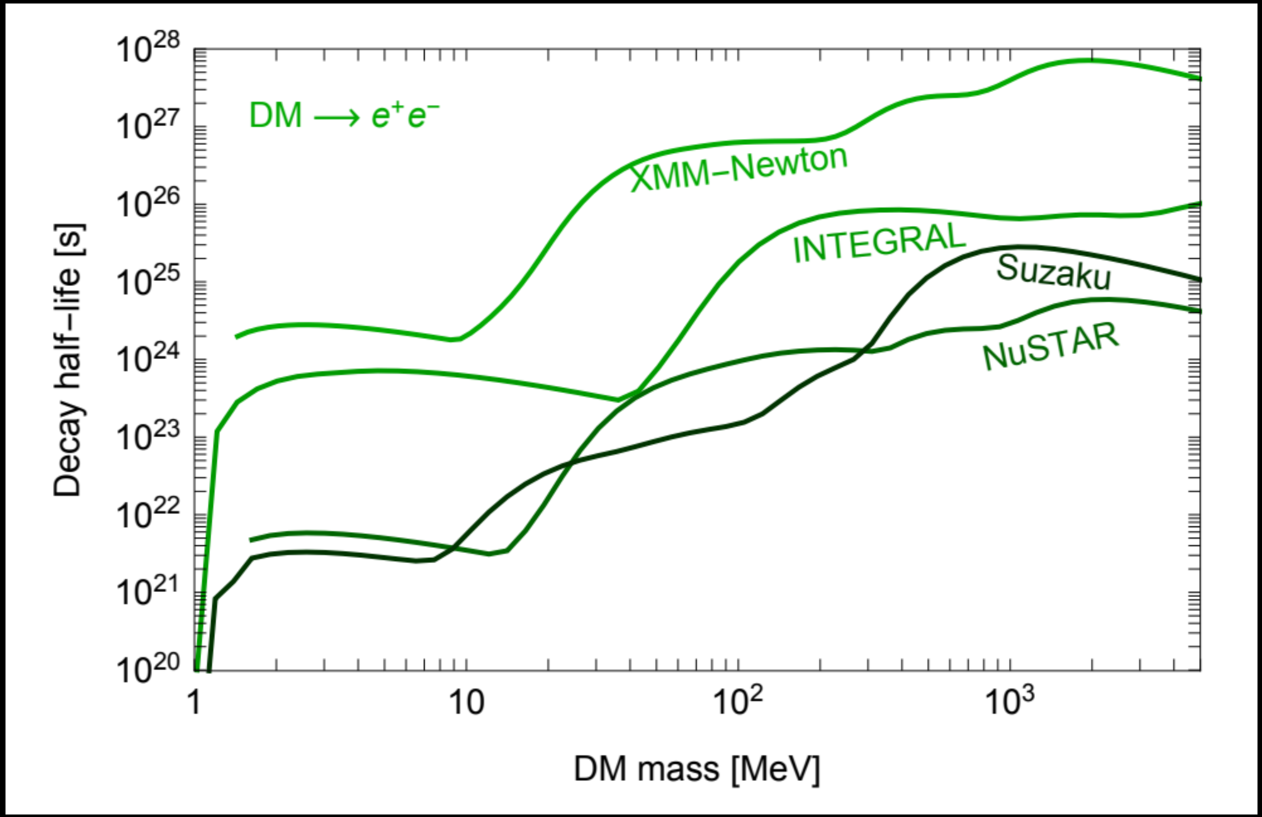

Constraints on muon and pion channel

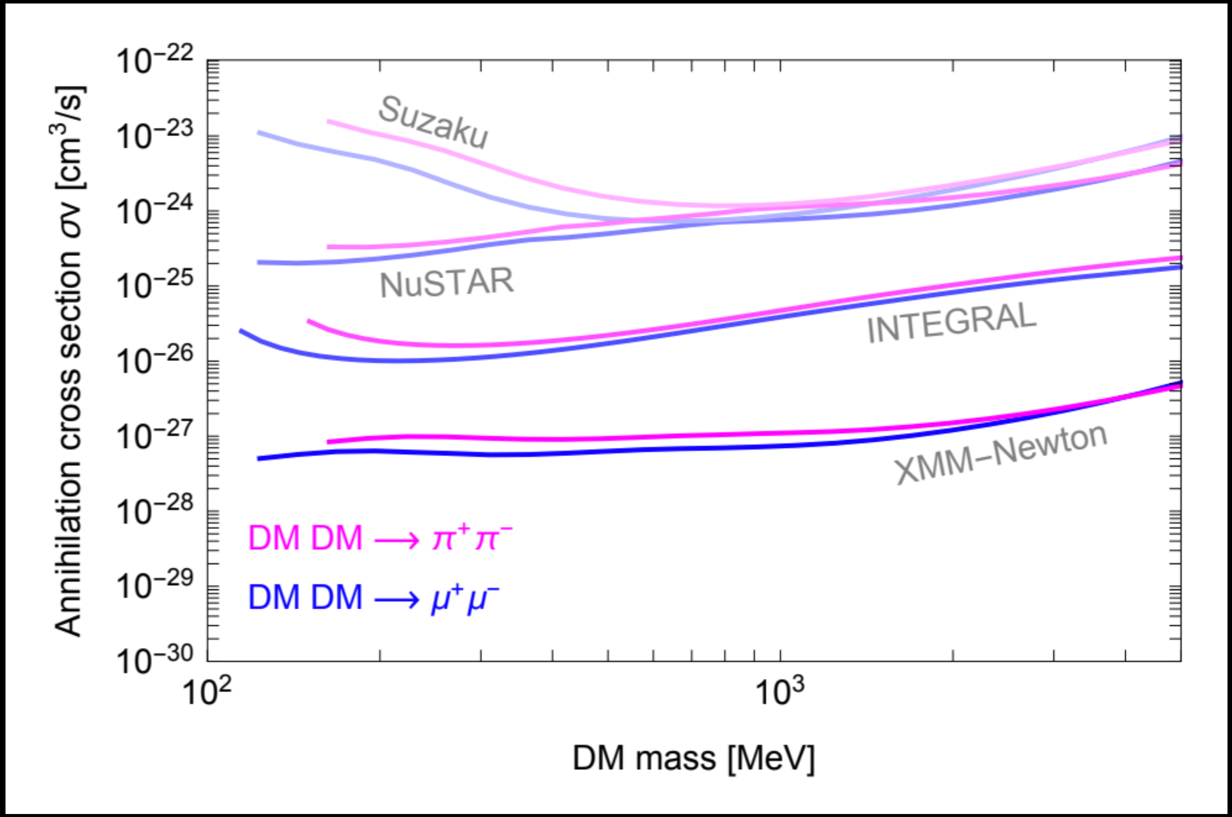

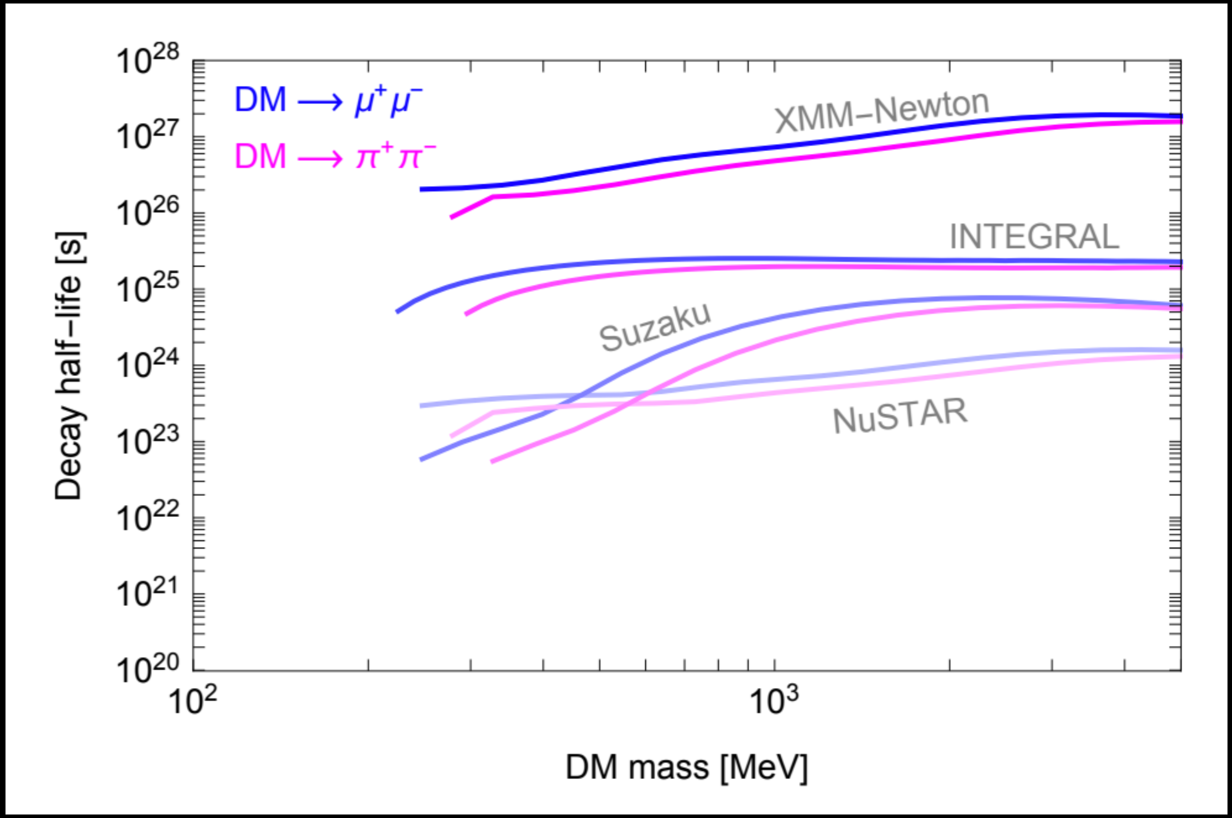

Comparison with the literature

Diffusive gamma-ray constraints

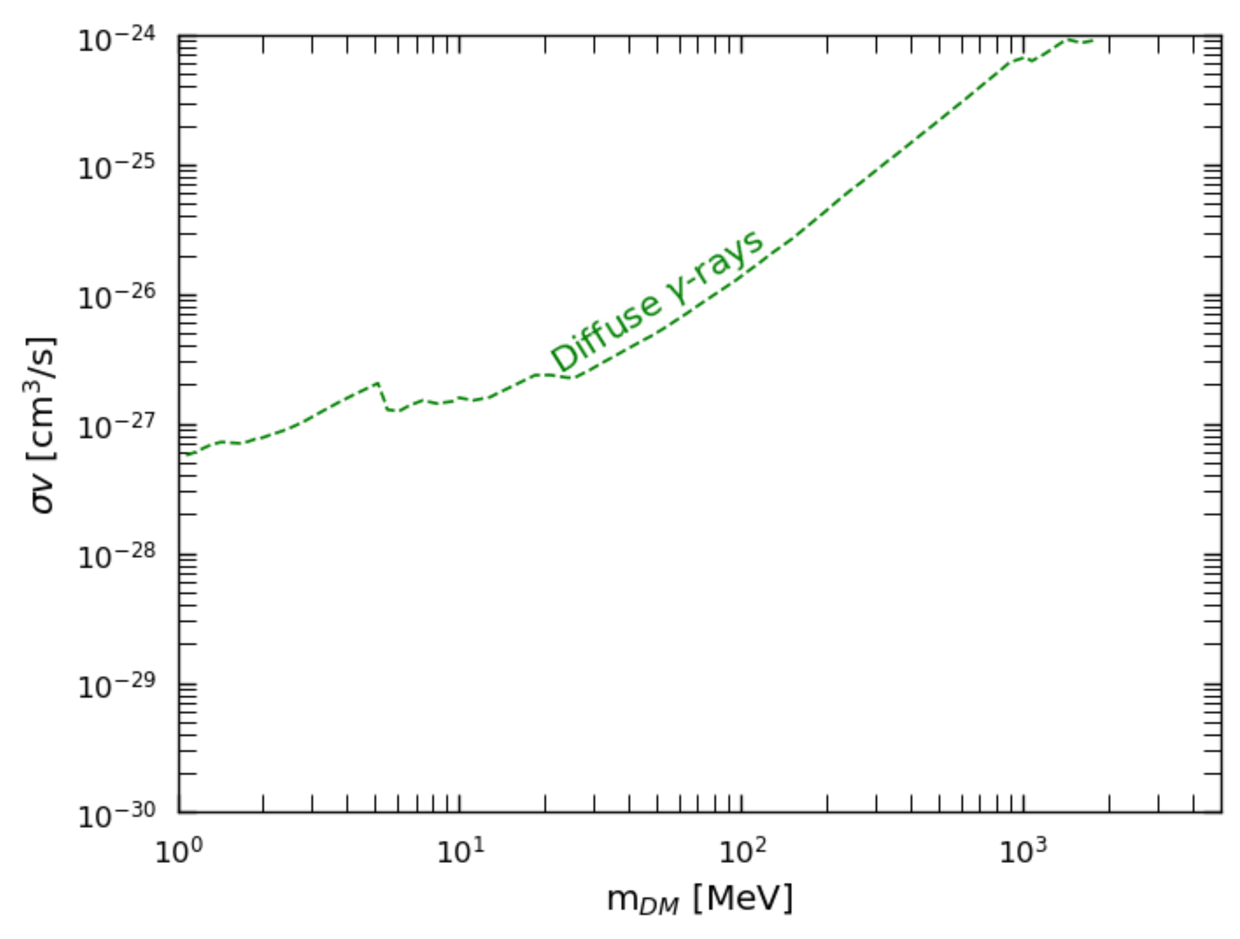

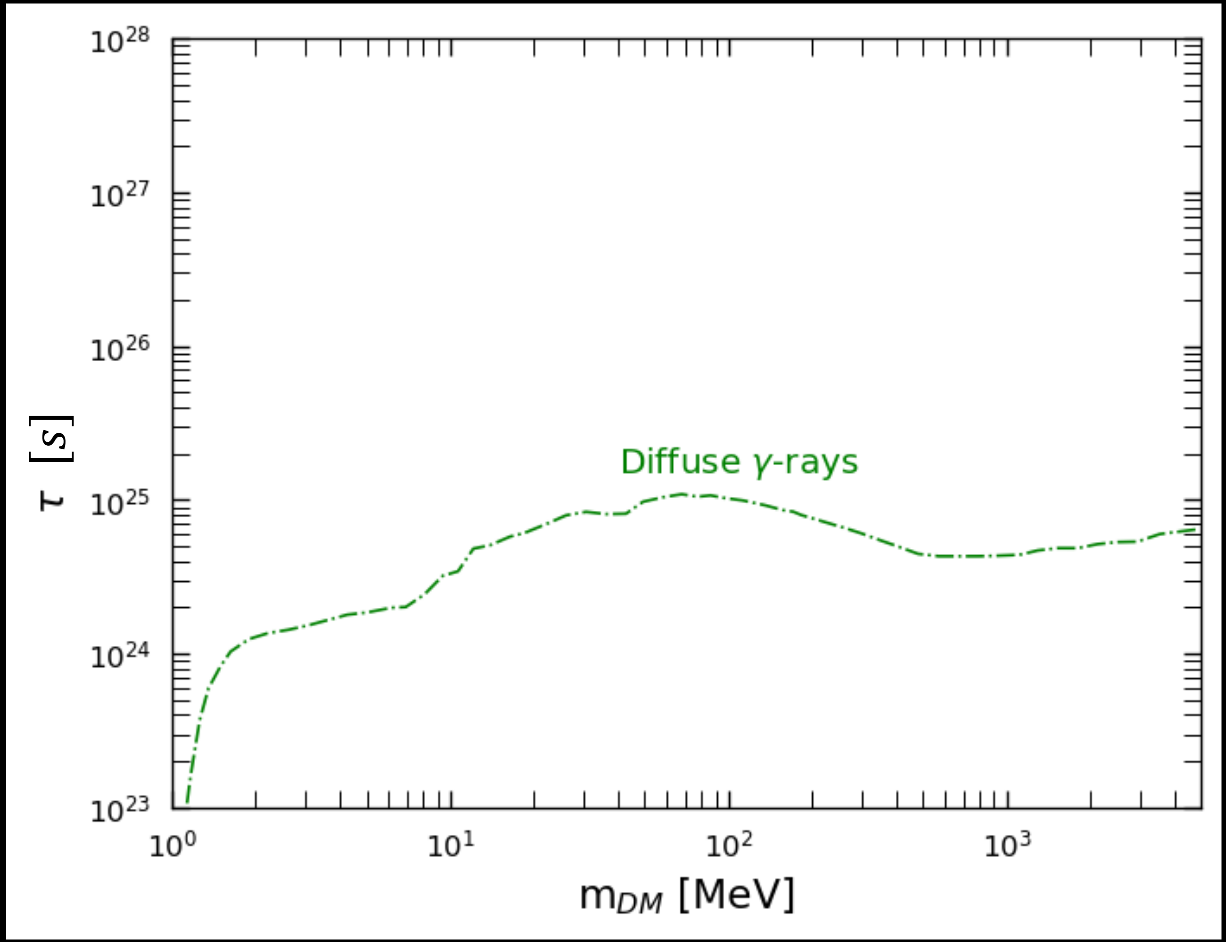

Essig+, JHEP 11 (2013) 193

Voyager constraints

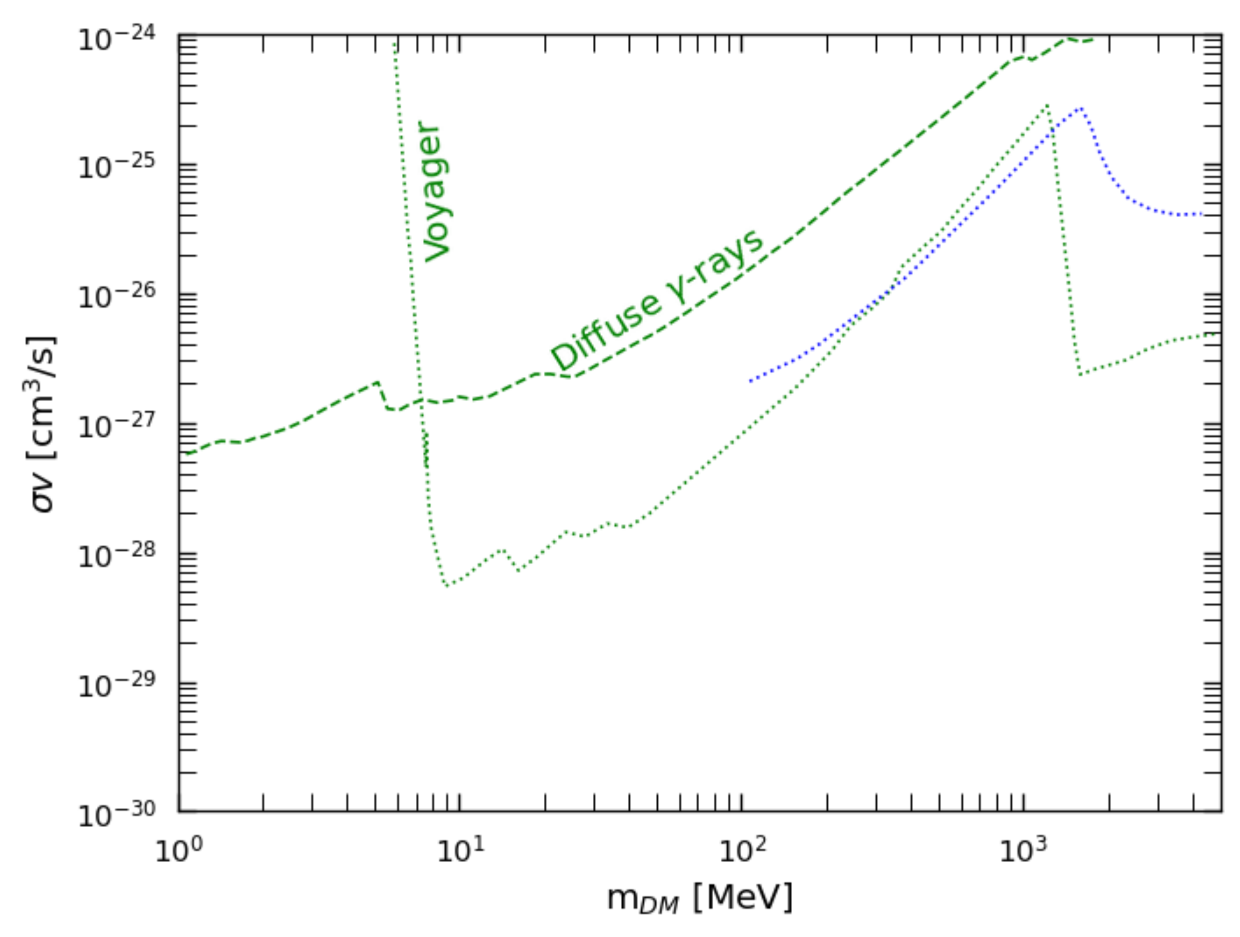

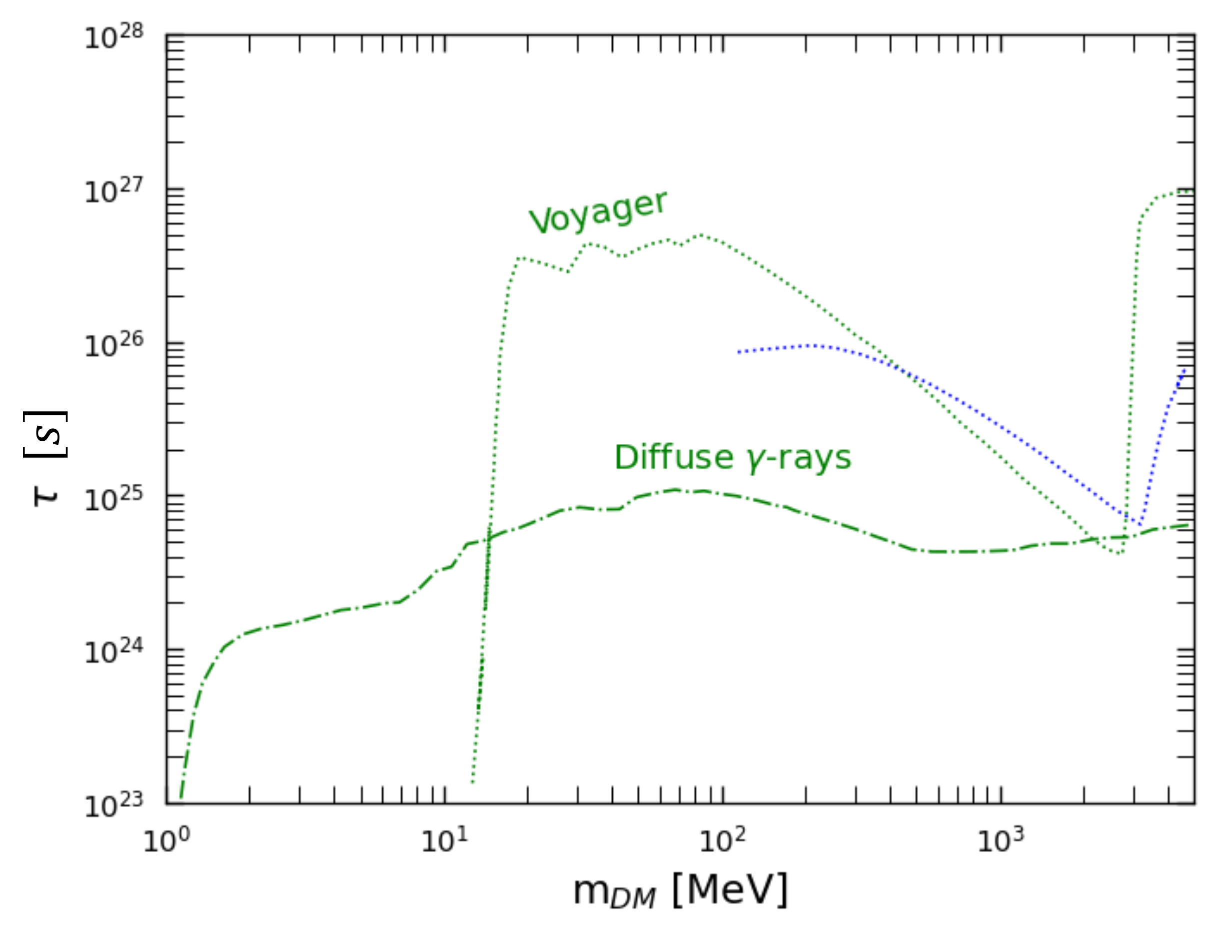

Boudaud et al., Phys. Rev. Lett. 119 (2017) 021103

CMB constraints

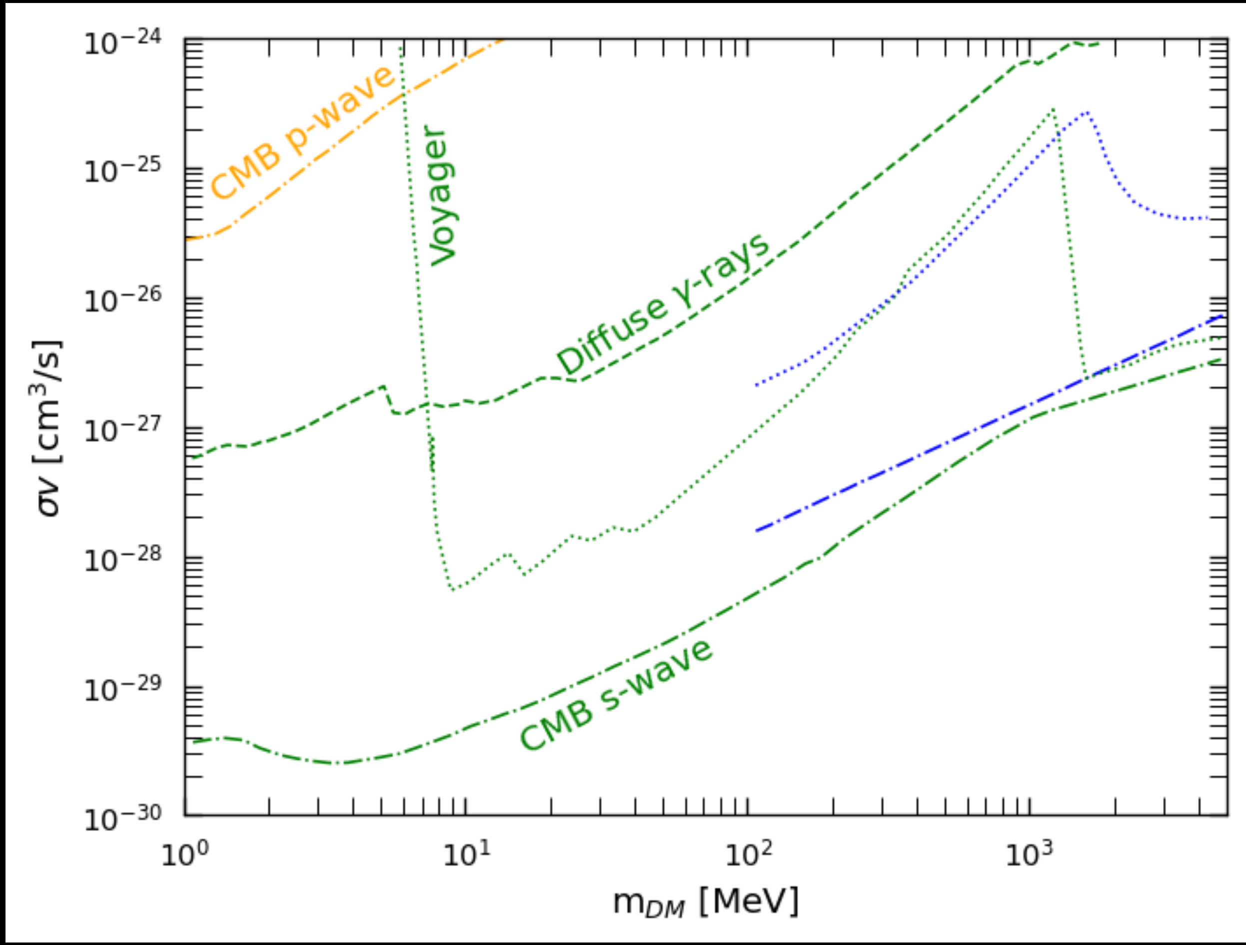

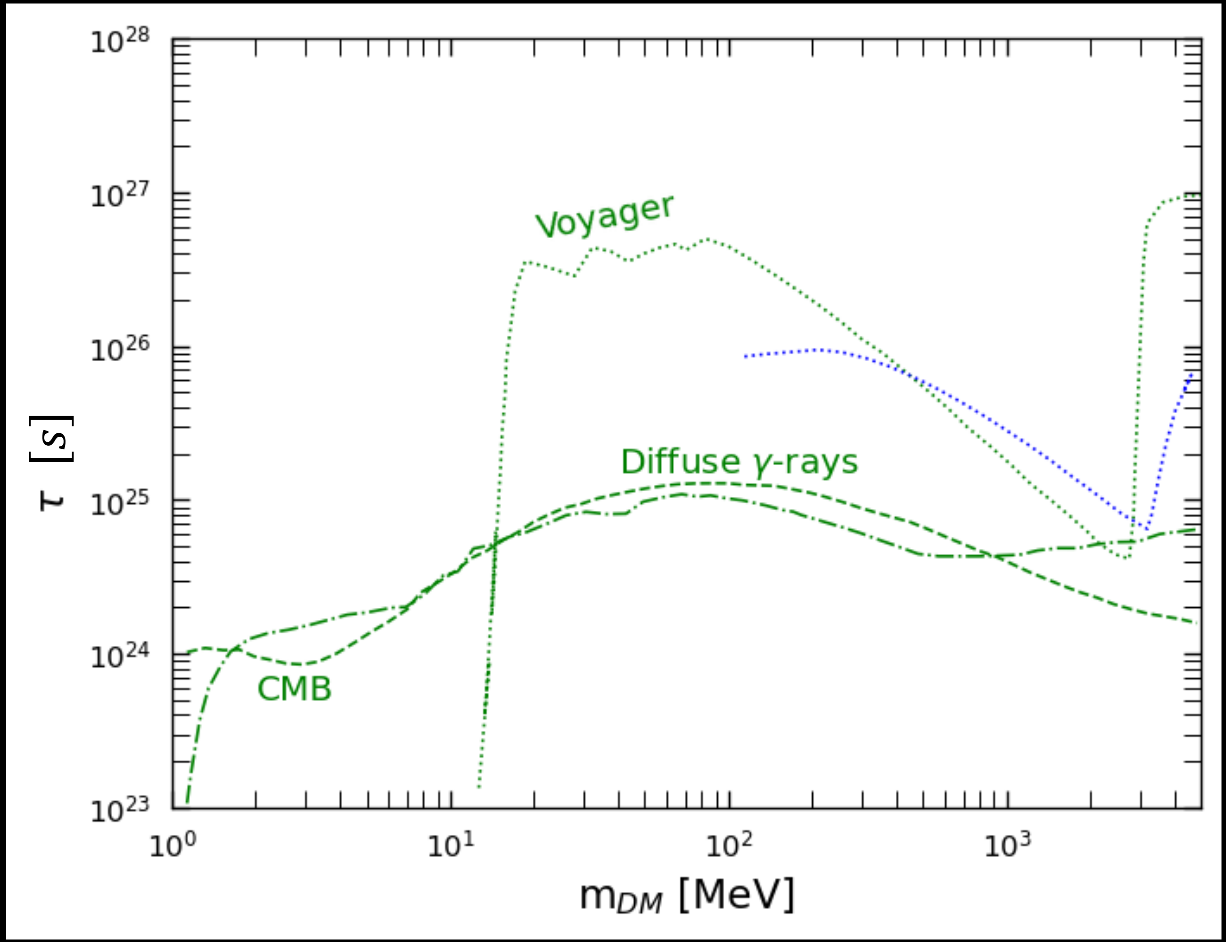

Slatyer, Phys. Rev. D 93 (2016) 023527 Lopez-Honorez et al., JCAP 07 (2013) 046 Diamanti et al., JCAP 02 (2014) 017 Liu et al., arXiv:2008.01084

Leo T constraints

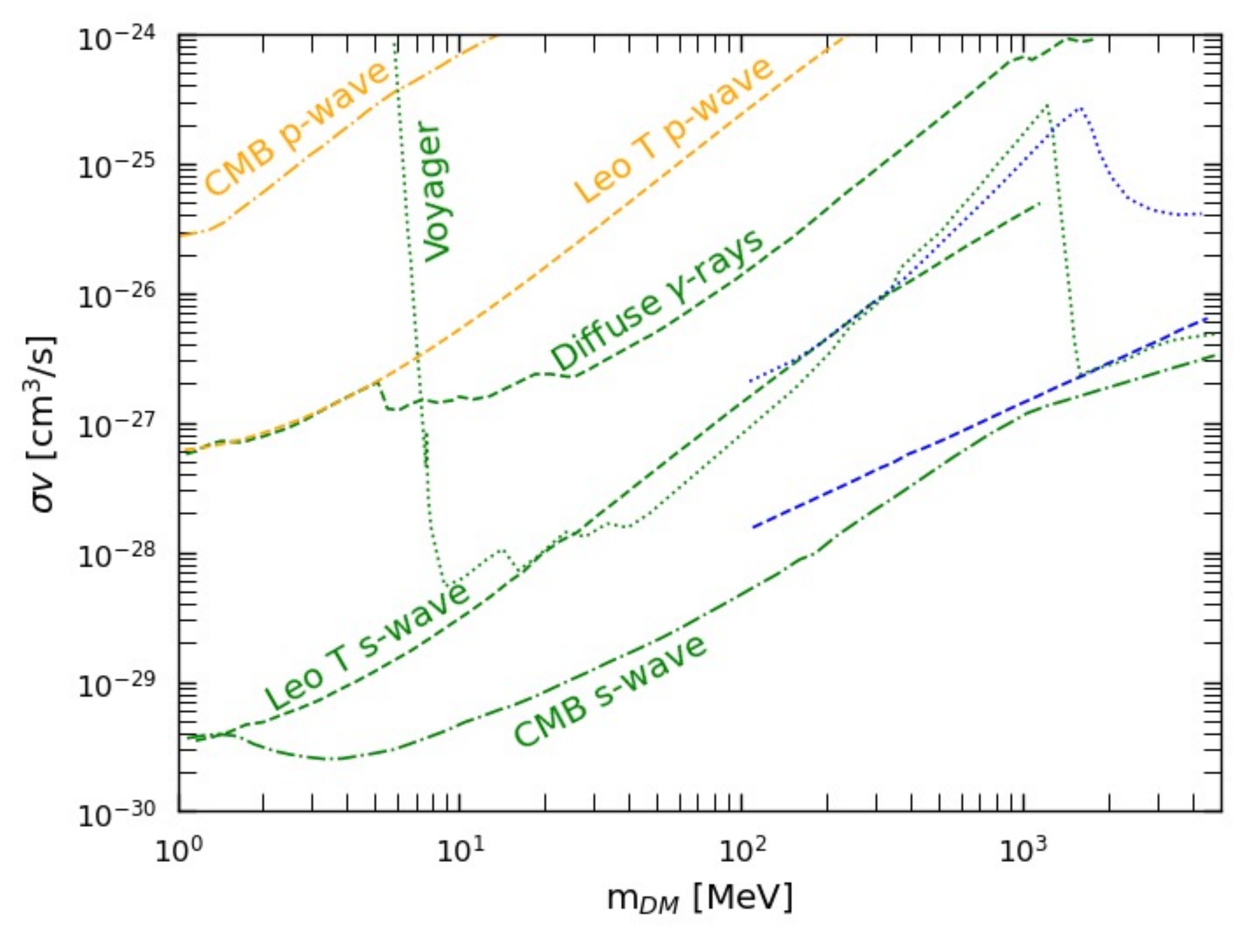

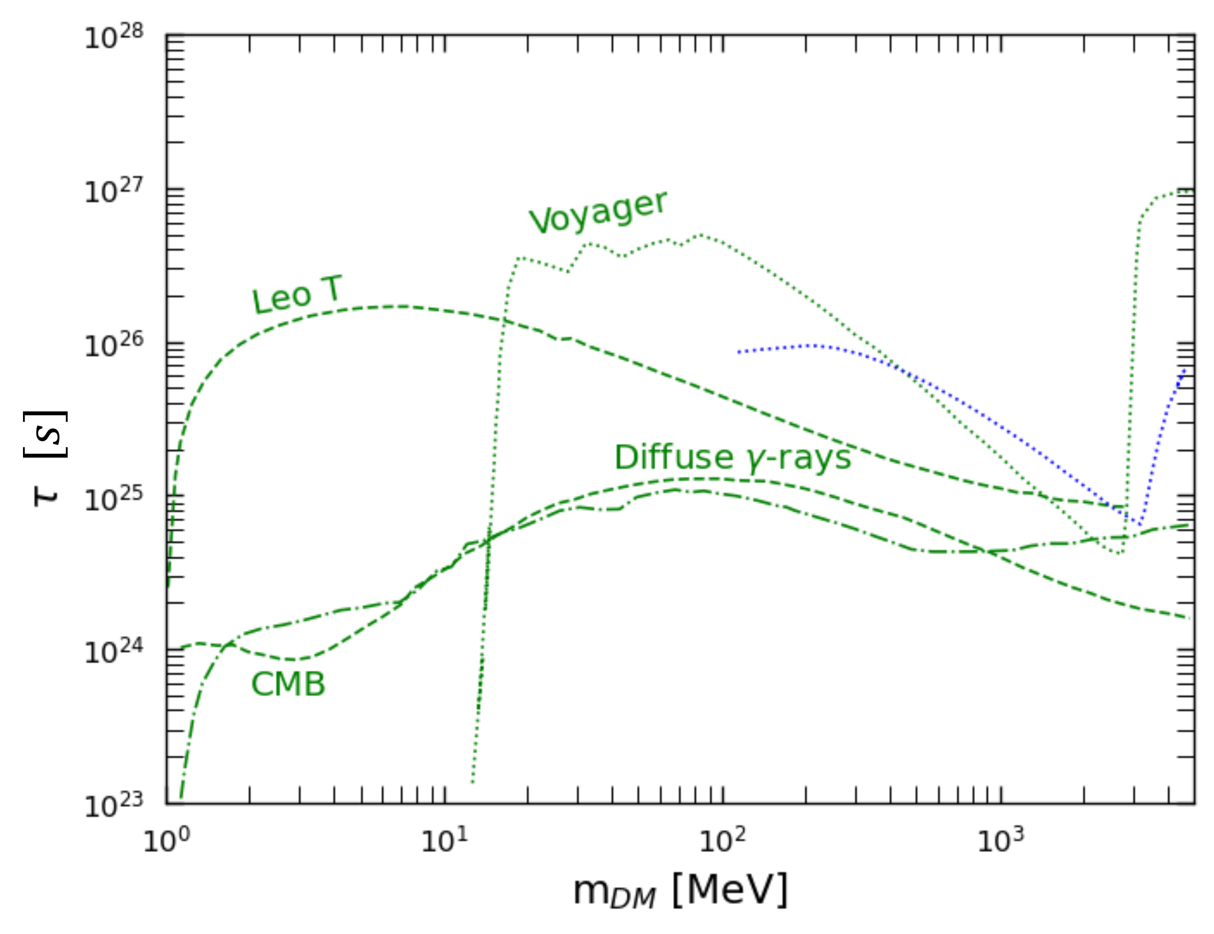

Wadekar and Wang, *Phys.Rev.D* 106 (2022) 7, 075007

Final state radiation with INTEGRAL

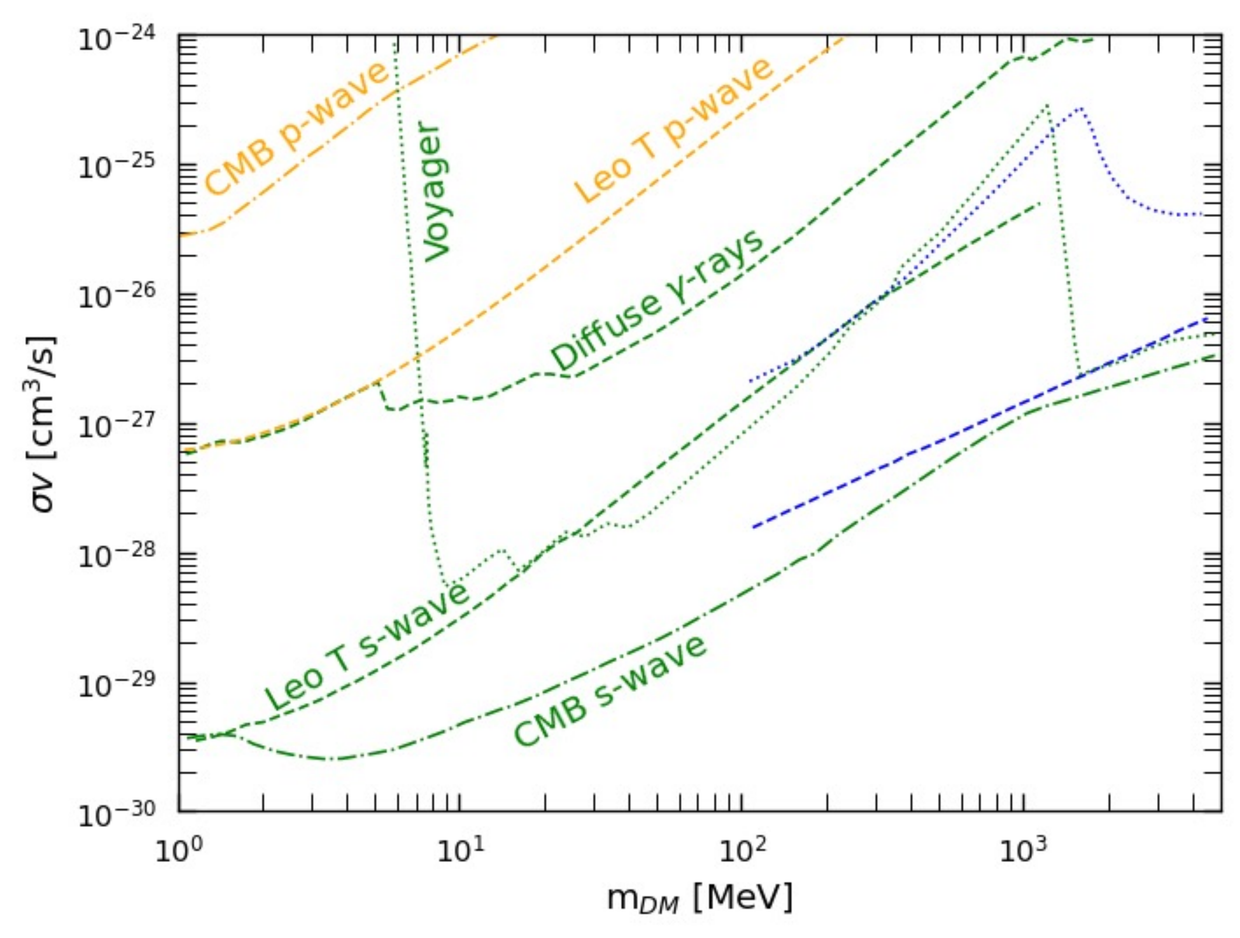

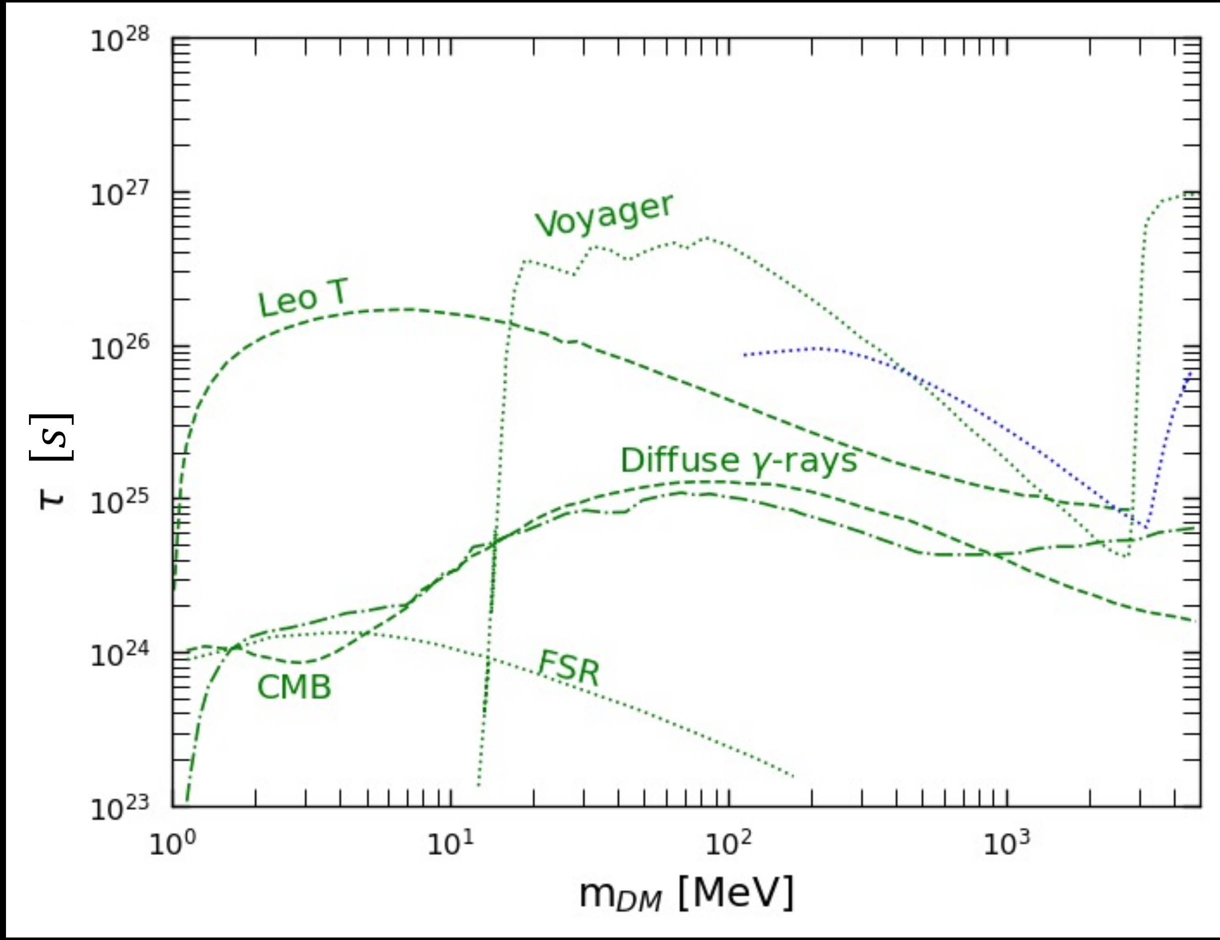

Calore+, Mon. Not. Roy. Astron. Soc. 520 (2023) 4167–4172

Comparison with bounds

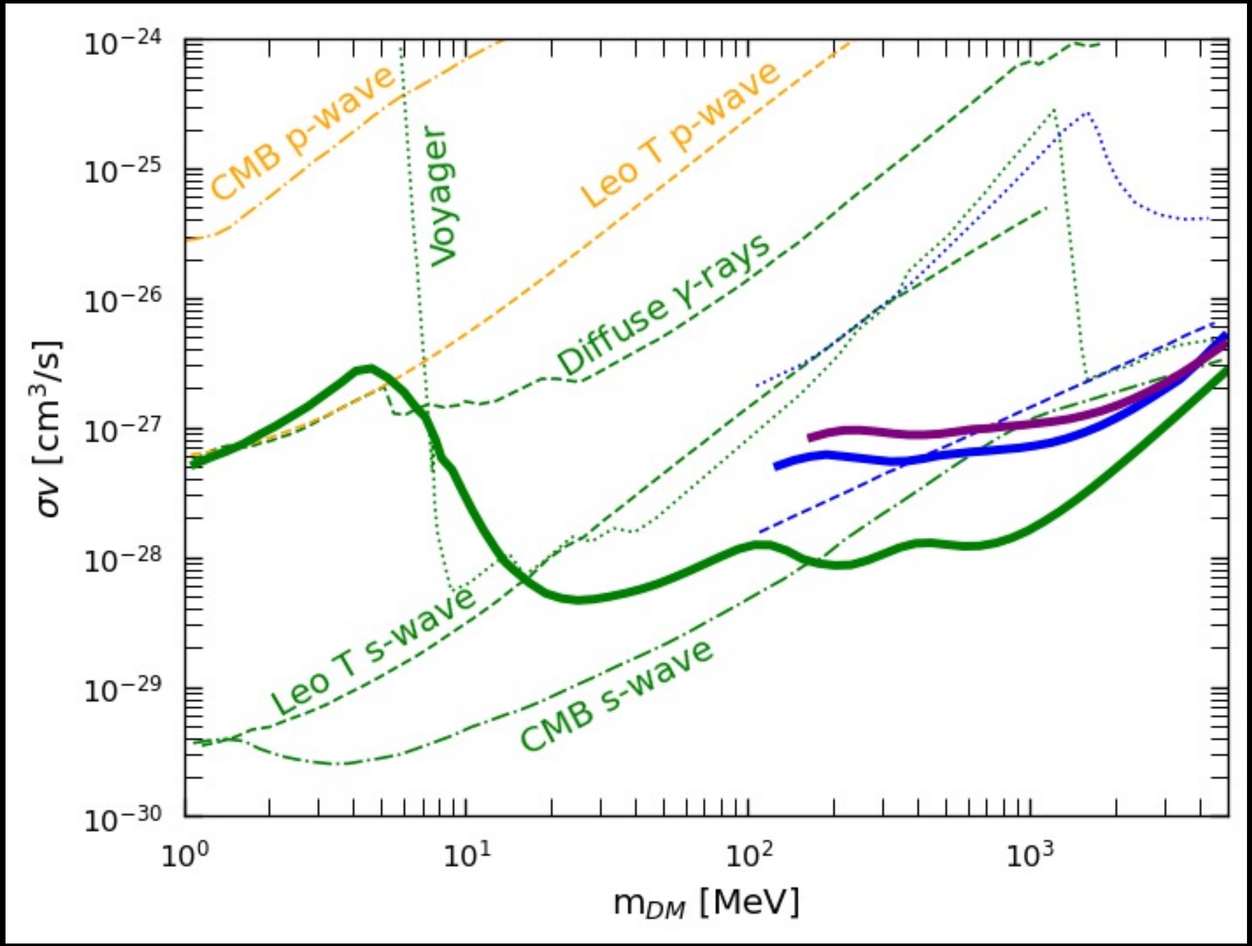

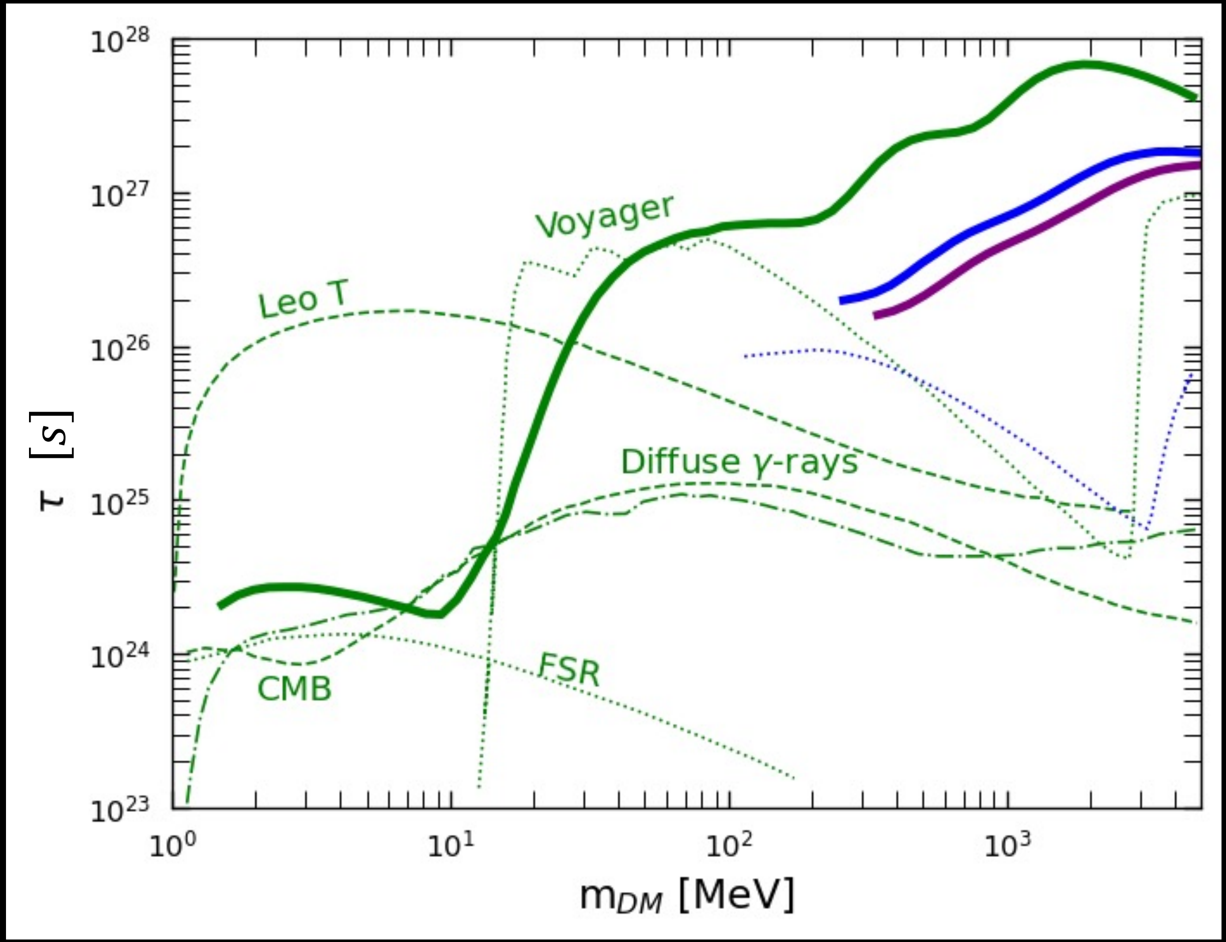

Uncertainties

DM density profile

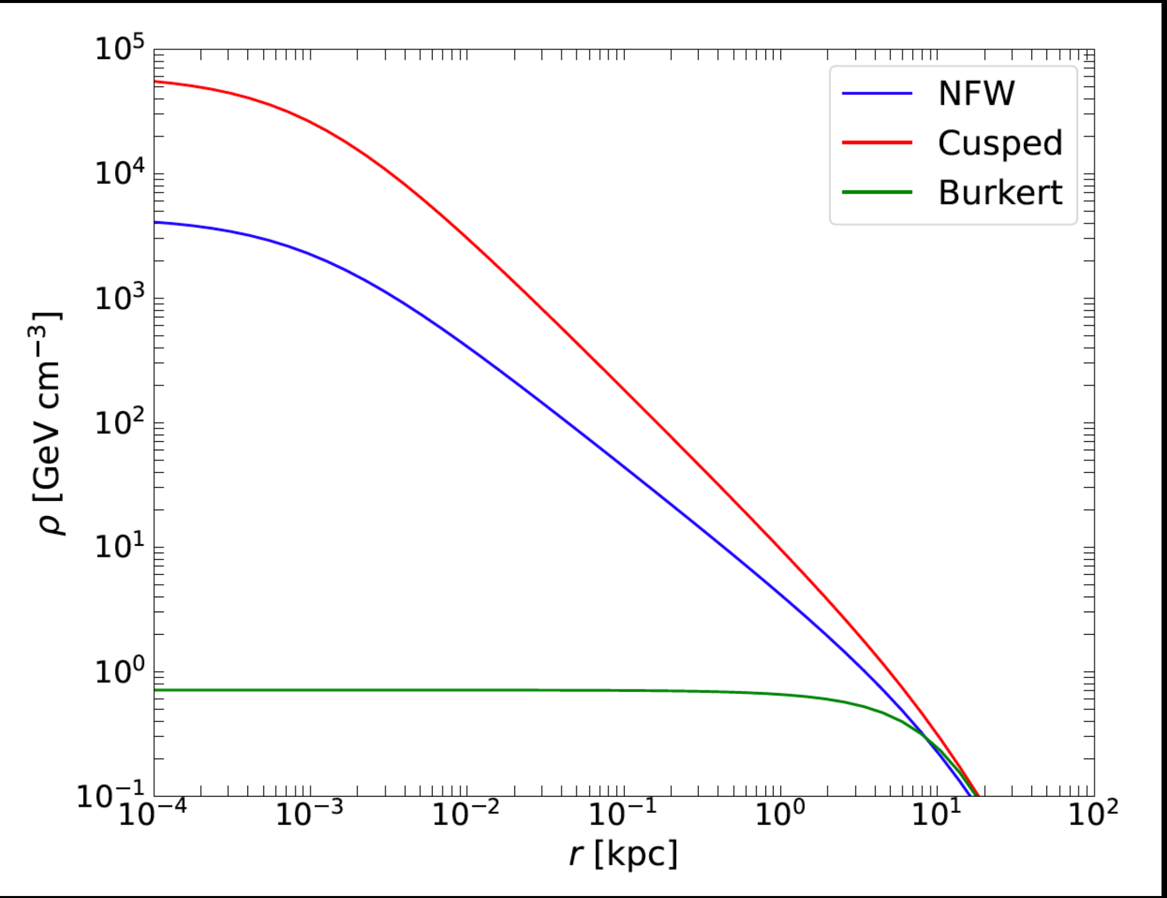

Profile	ρ_s (GeV/cm^3)	r_s (kpc)	γ
NFW	0.184	24.42	1
Cusped	0.184	24.42	1.26
Burkert	0.712	12.67	-

$$\rho(r) = \frac{\rho_s}{\left(\frac{r}{r_s}\right)^{\gamma}\left(1+\frac{r}{r_s}\right)^{3-\gamma}}$$

$$\rho_B = \frac{\rho_s}{\left(1+\frac{r}{r_s}\right)\left[1+\left(\frac{r}{r_s}\right)^2\right]}$$

DM density profile

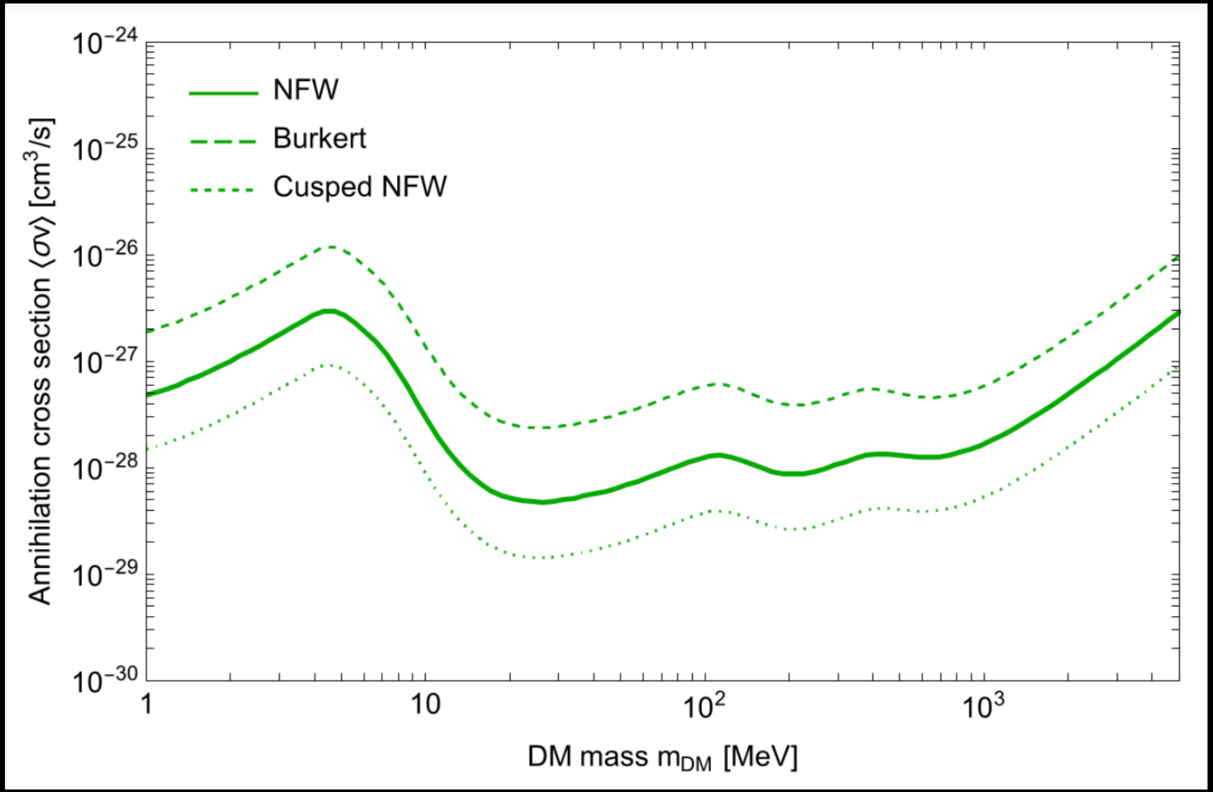

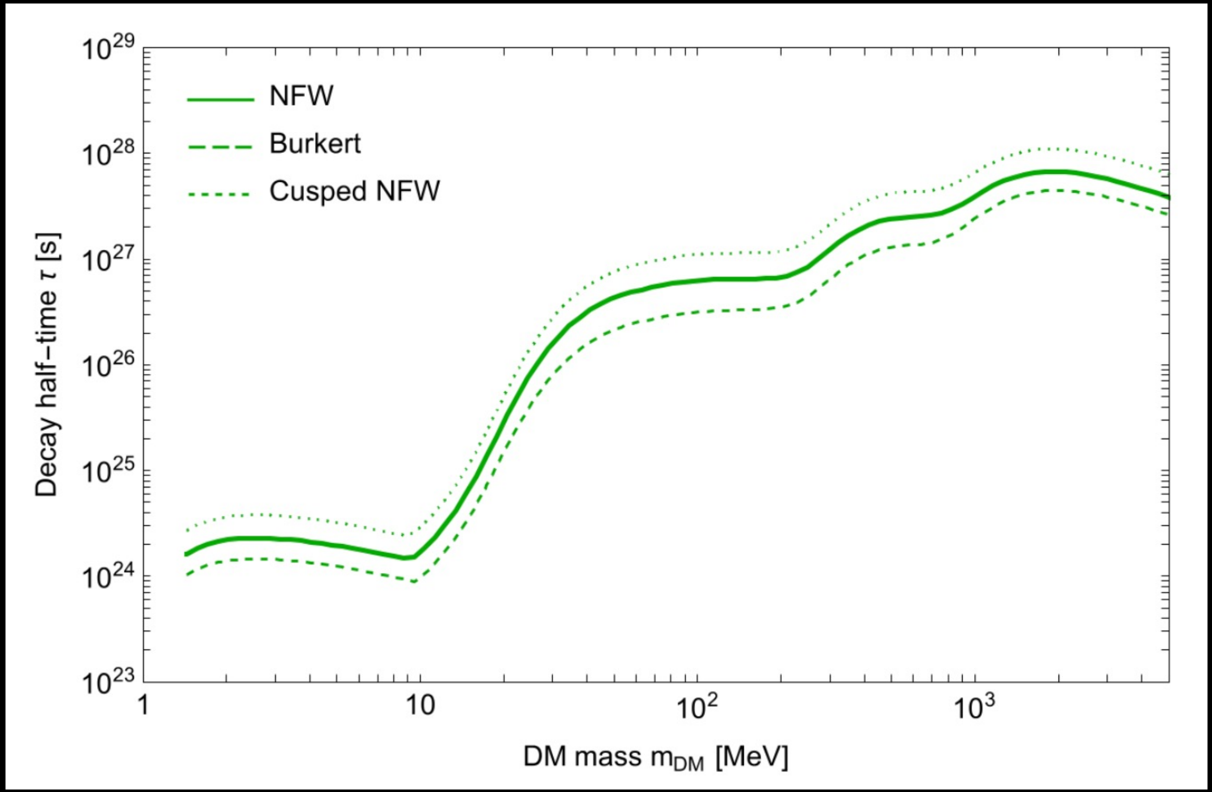

Density of the interstellar medium

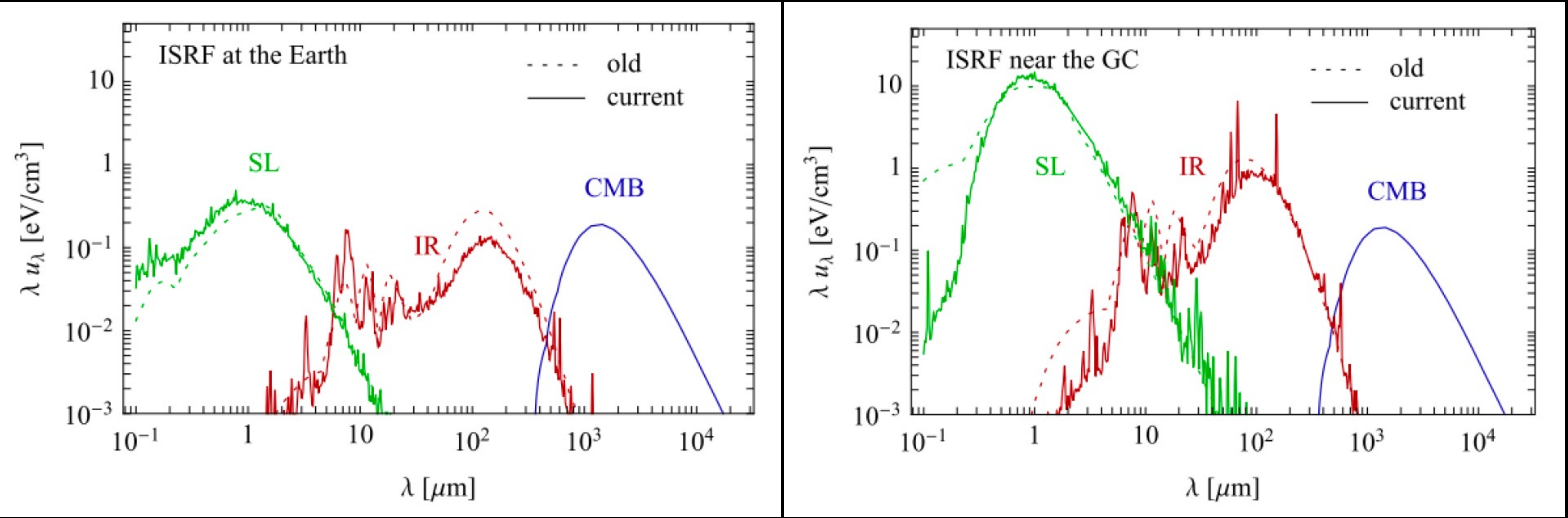

PPPC 4 DM secondary, Buch et al., arXiv:1505.01049

Density of interstellar medium

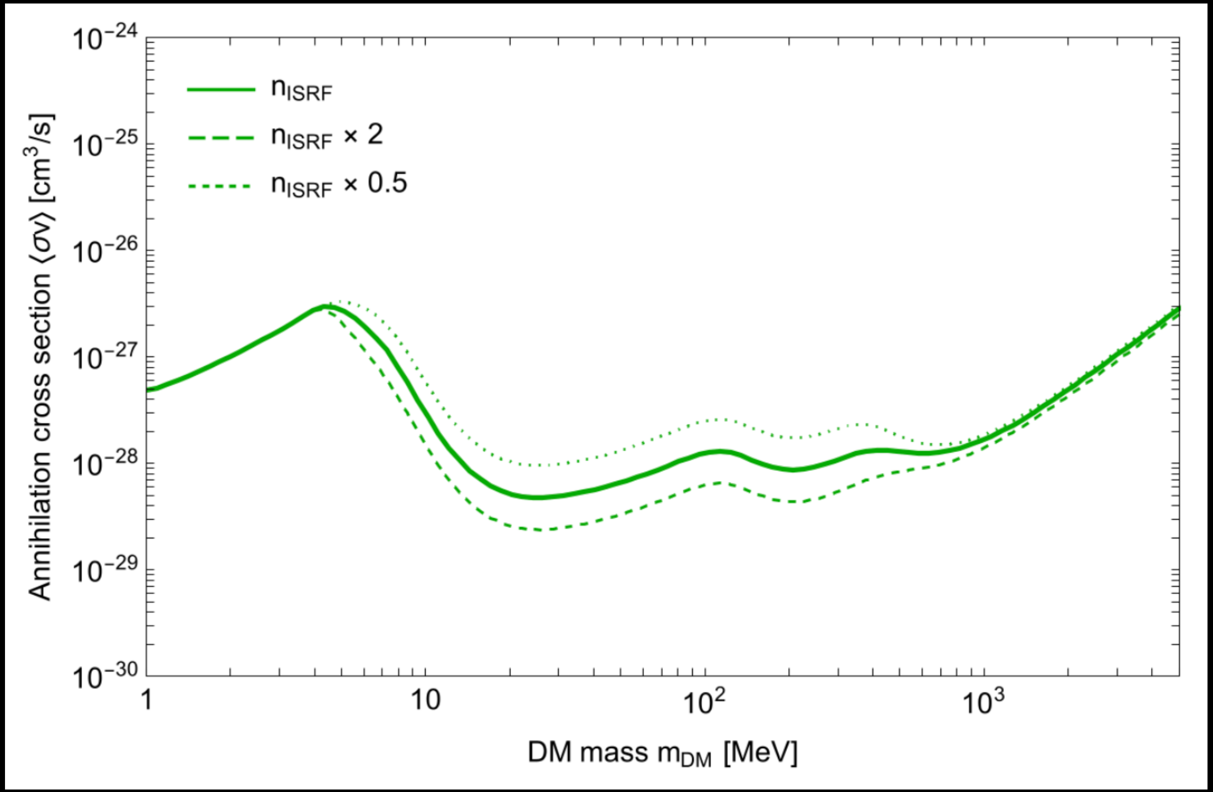

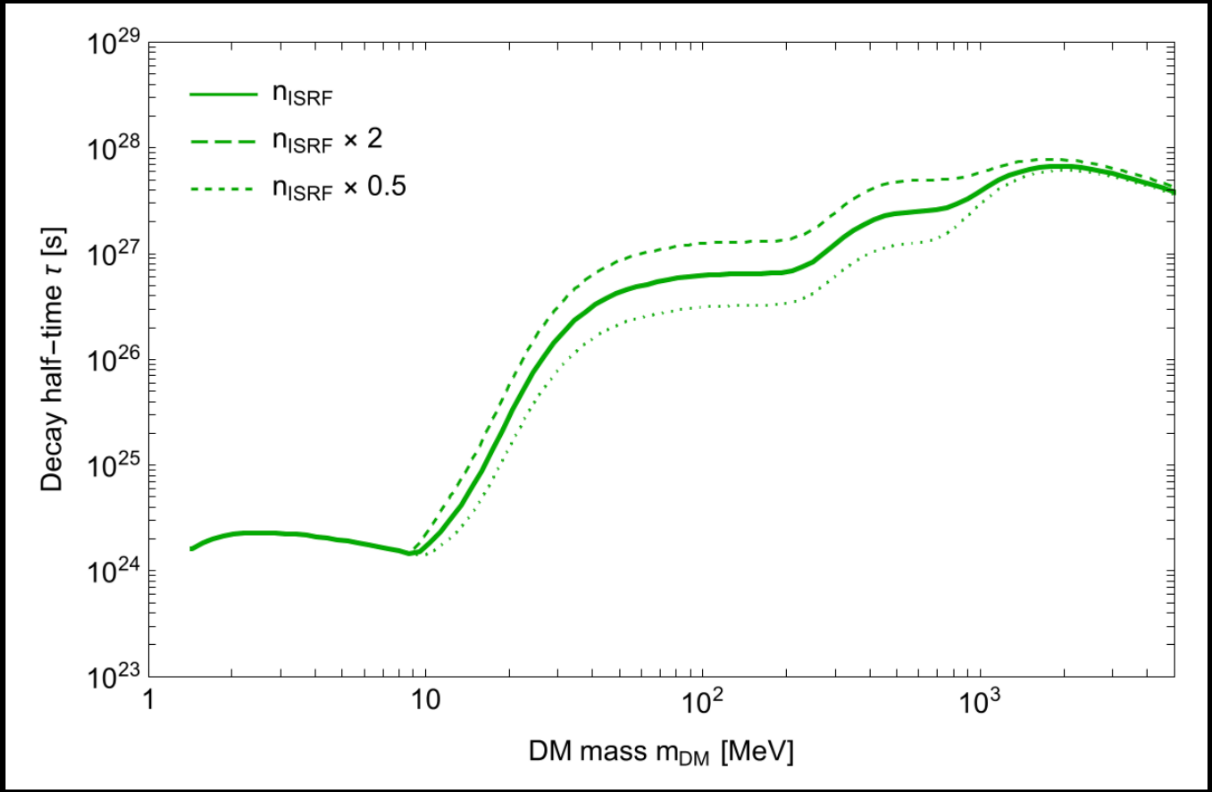

Density of gas

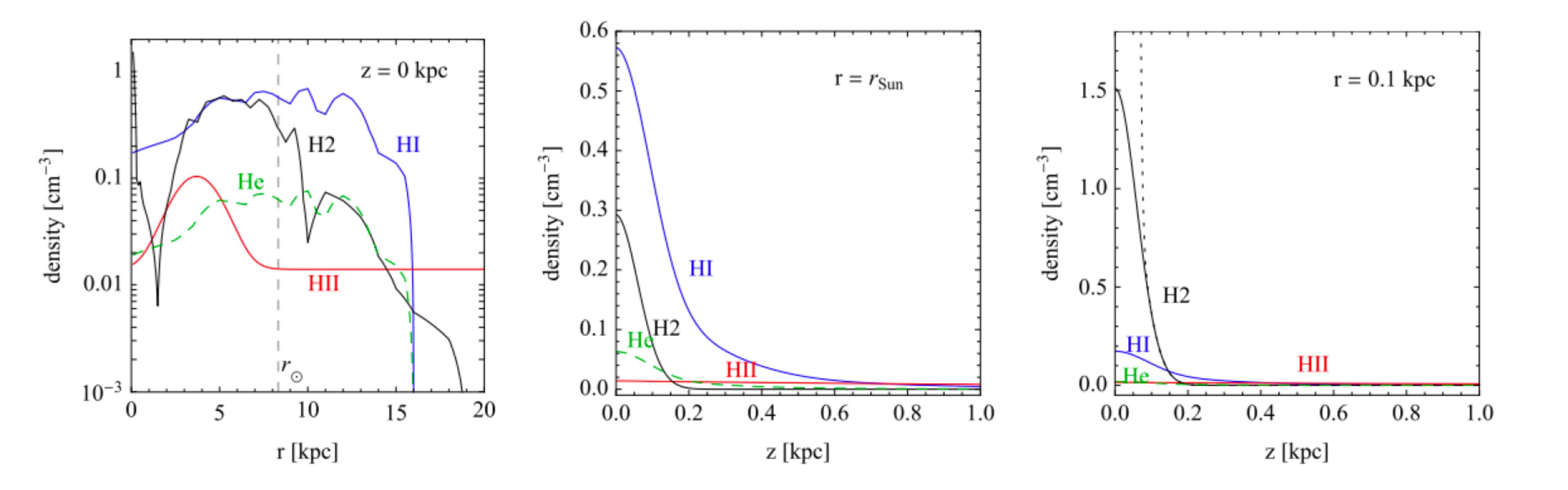

Cirelli+,Matter, JCAP 11 (2013)

Density of gas

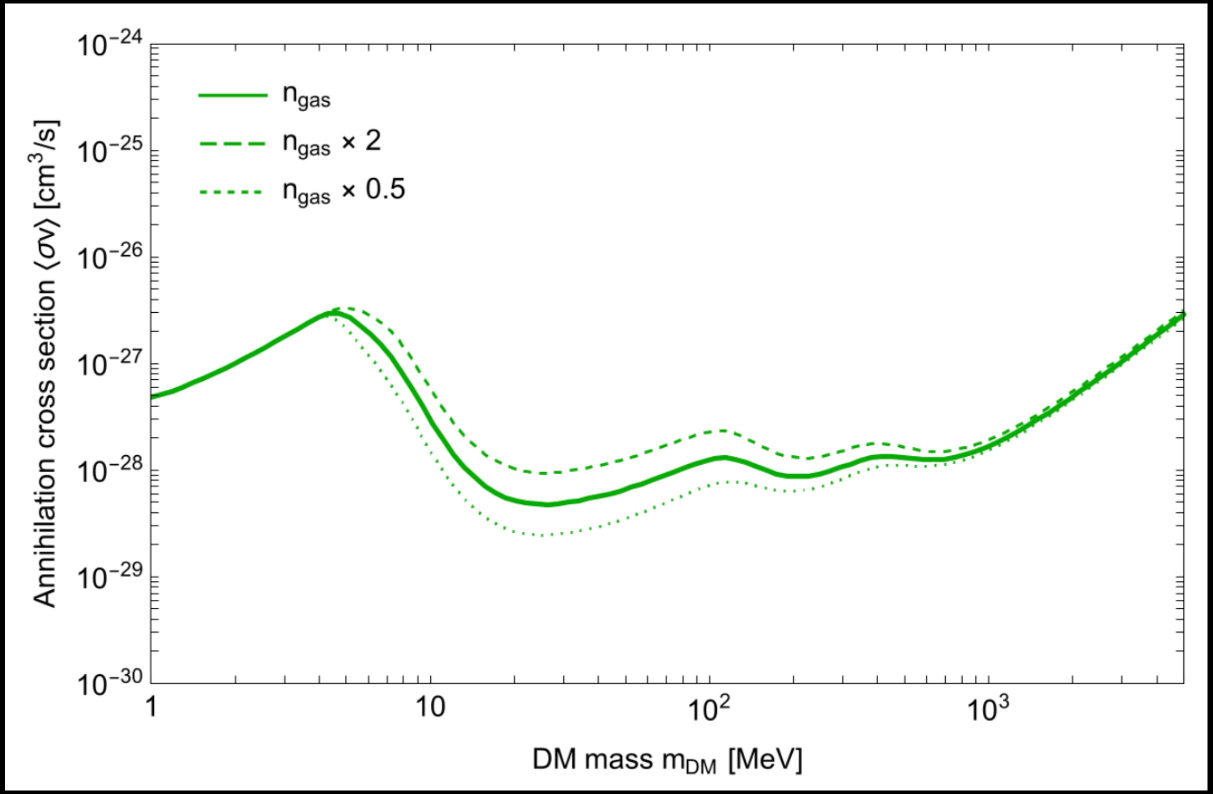

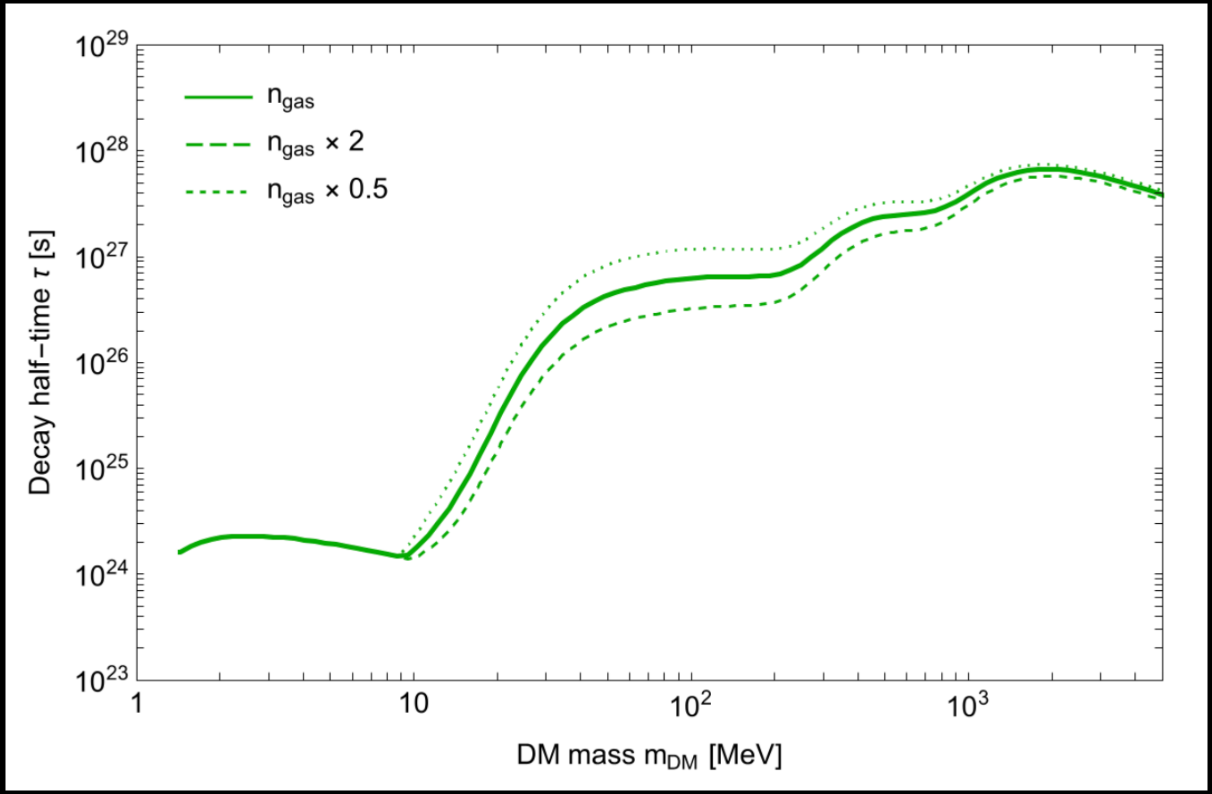

Magnetic field

$$B_{\rm tot} = B_0 \exp\left(-\frac{r - r_\odot}{R_D} - \frac{|z|}{z_D}\right)$$

Model	B_0 (μG)	r_D (kpc)	z_D (kpc)
MF1	4.78	10	2
MF2	5.1	8.5	1
MF3	9.5	30	4

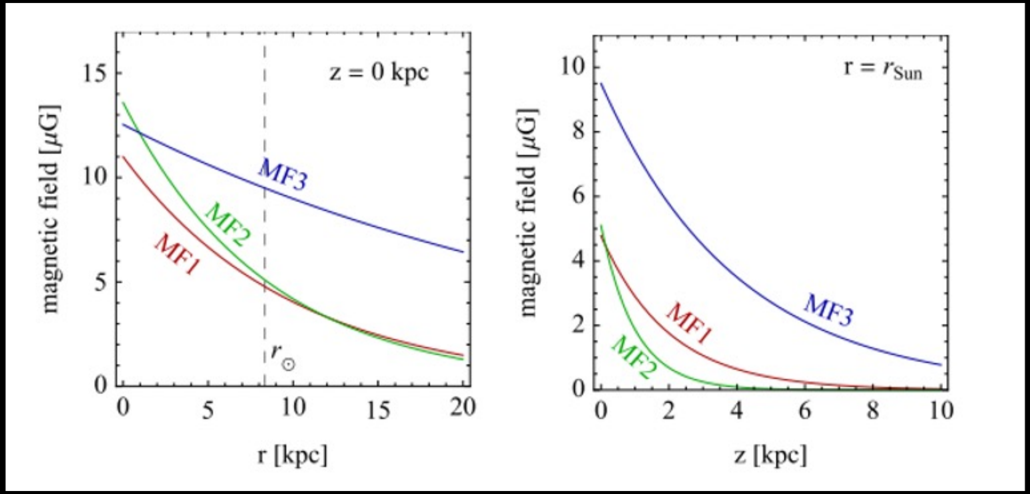

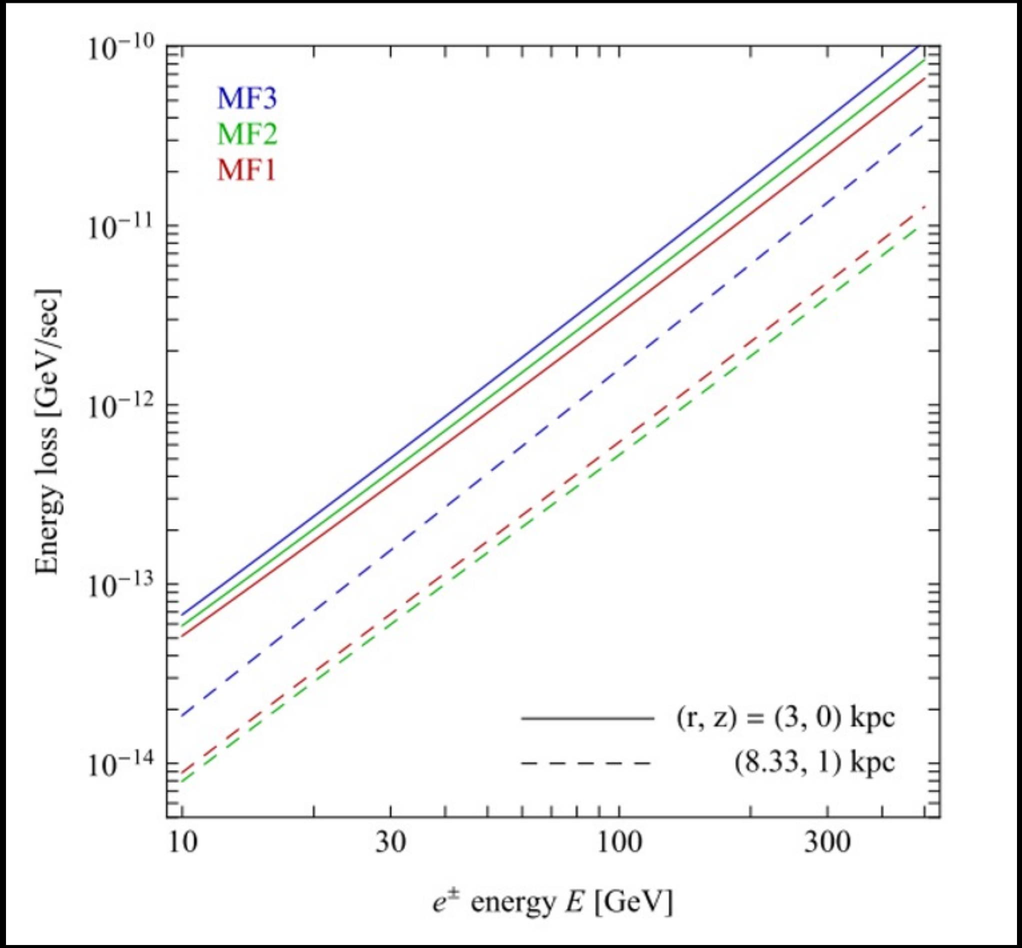

PPPC 4 DM secondary, Buch et al., arXiv:1505.01049

Magnetic field

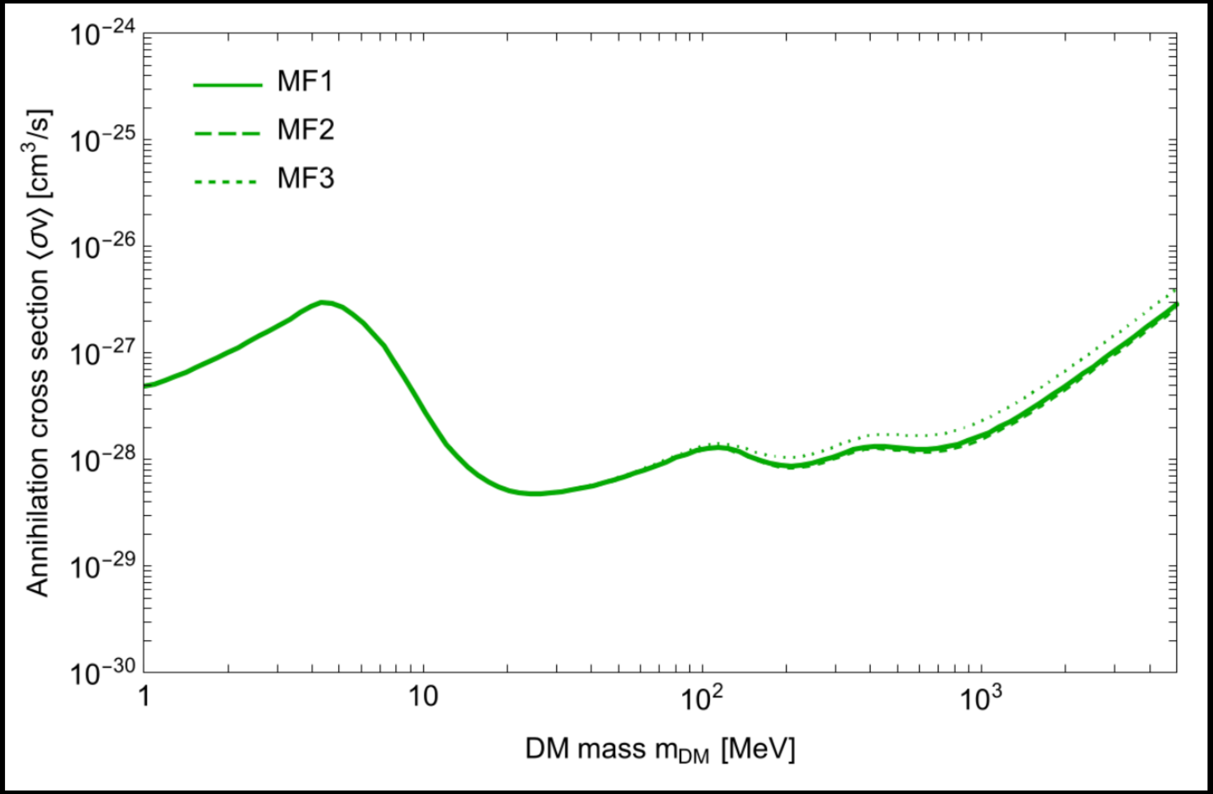

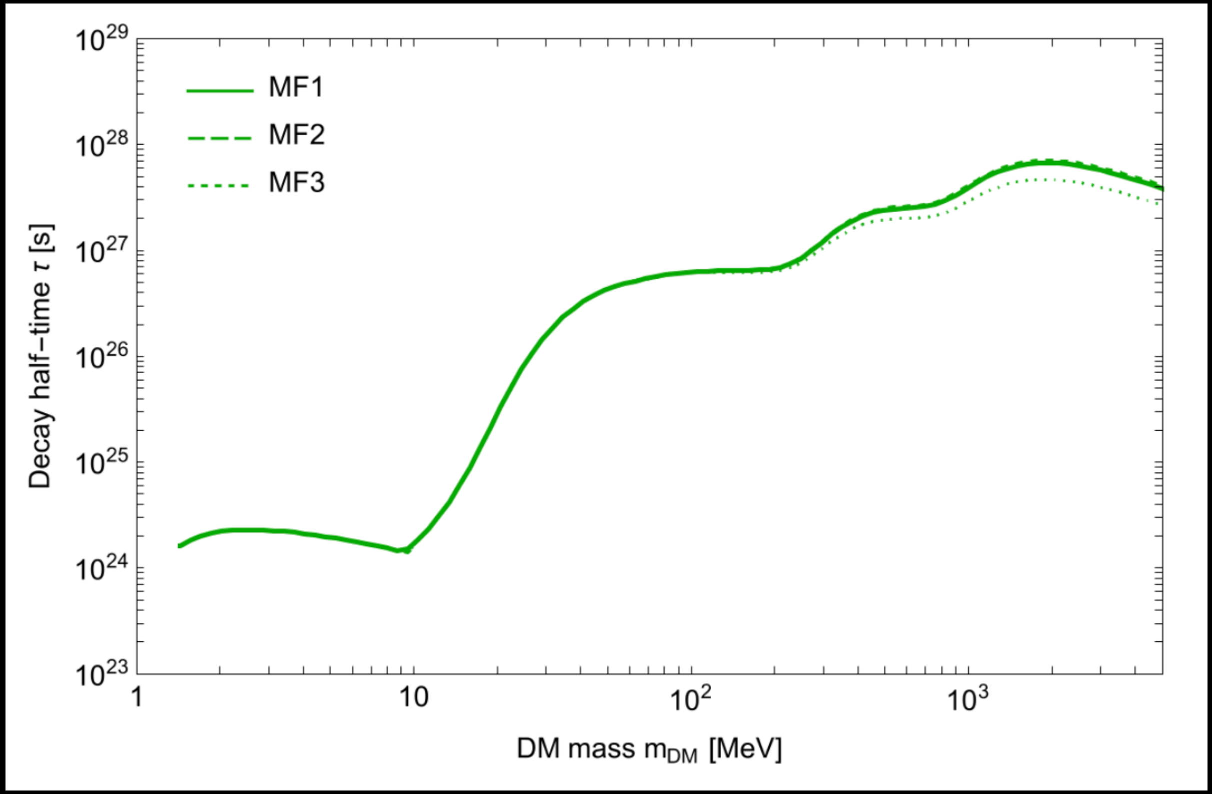

Overall uncertainties

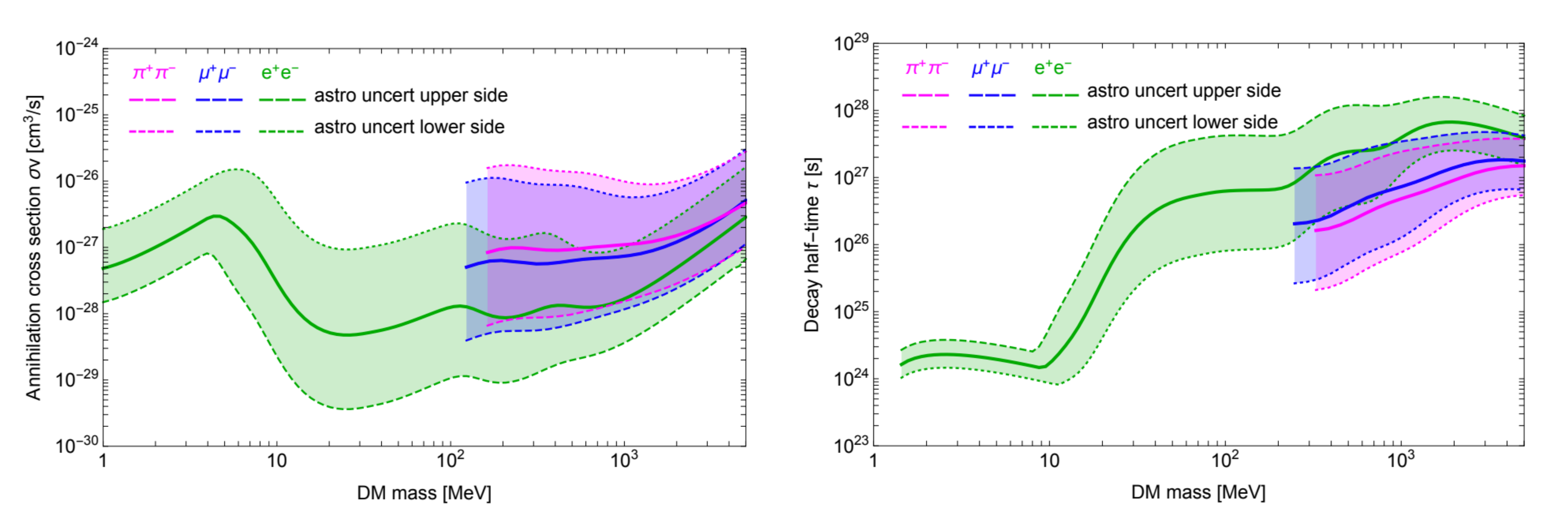

An eye toward the future

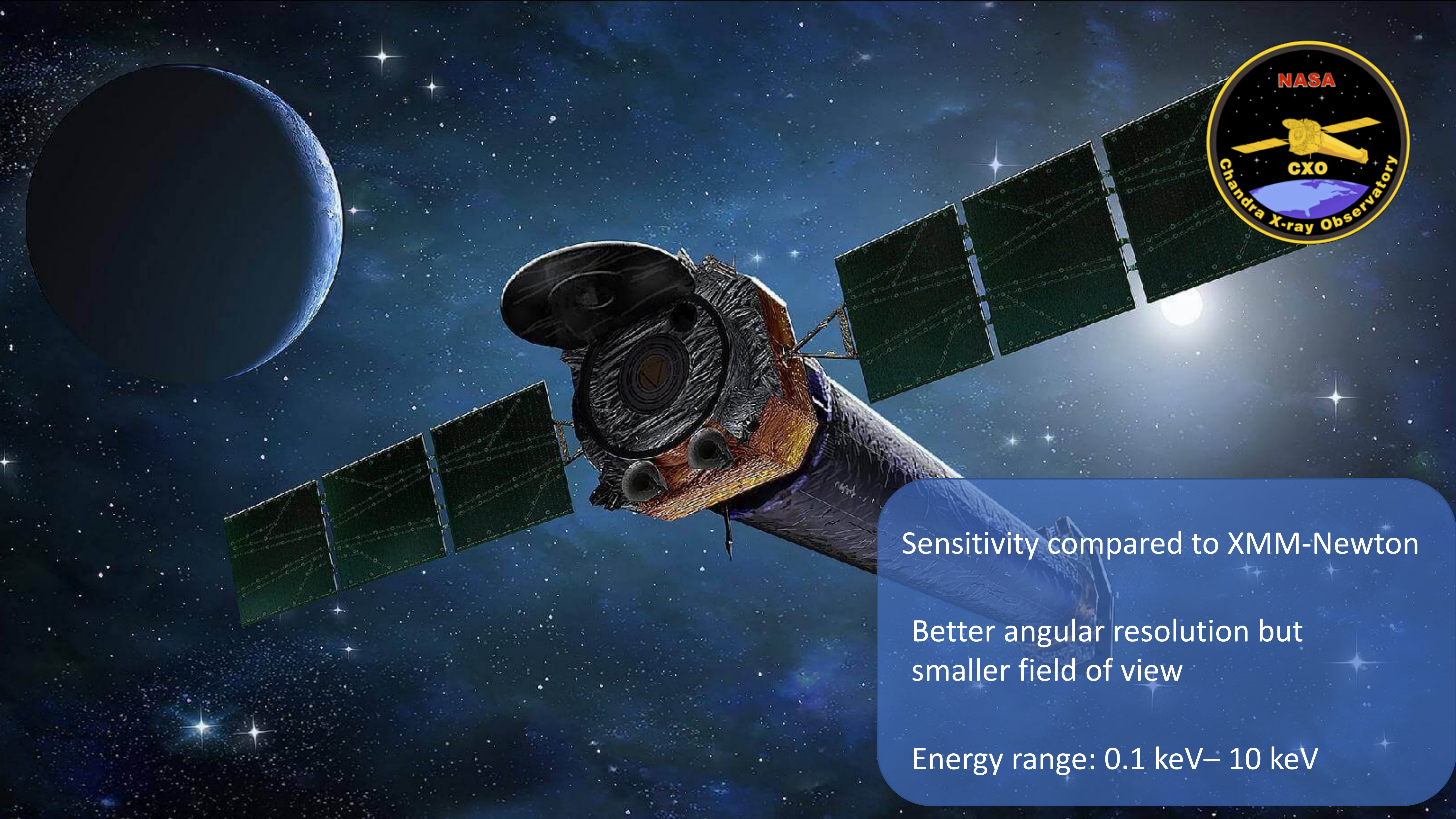

Sensitivity compared to XMM-Newton

Better angular resolution but smaller field of view

Energy range: 0.1 keV– 10 keV

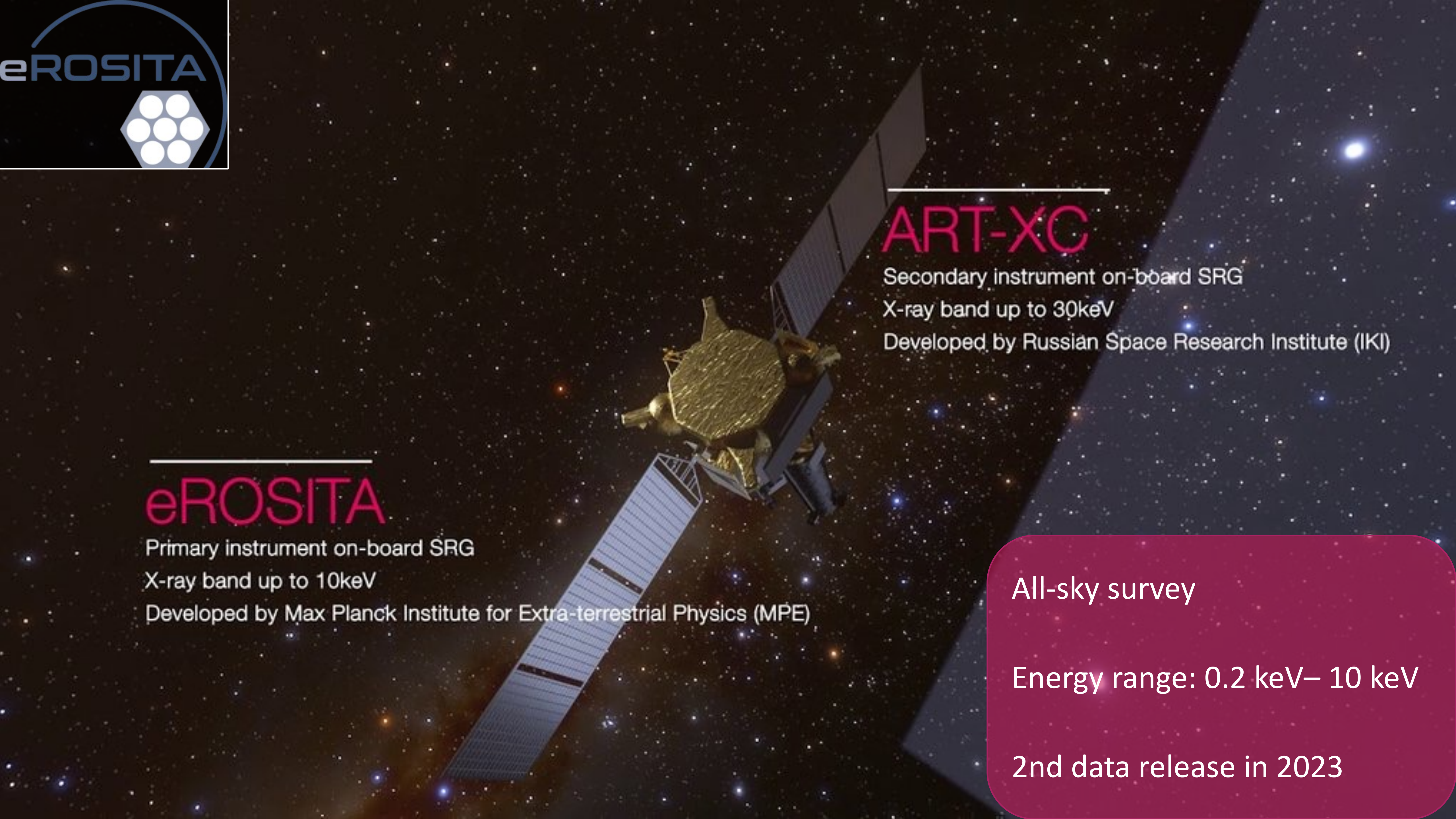

All-sky survey

Energy range: 0.2 keV– 10 keV

2nd data release in 2023

Beyond the Milky Way

Conclusions

1. X-ray telescopes can help in closing the MeV gap

2. Inverse-Compton scattering on the photon bath is a powerful tool to study sub-GeV dark matter

3. Strongest bounds on
   - Annihilating DM (if p-wave): $m_{DM} \geq 20$ MeV
   - Decaying DM: $m_{DM} \geq 100$ MeV

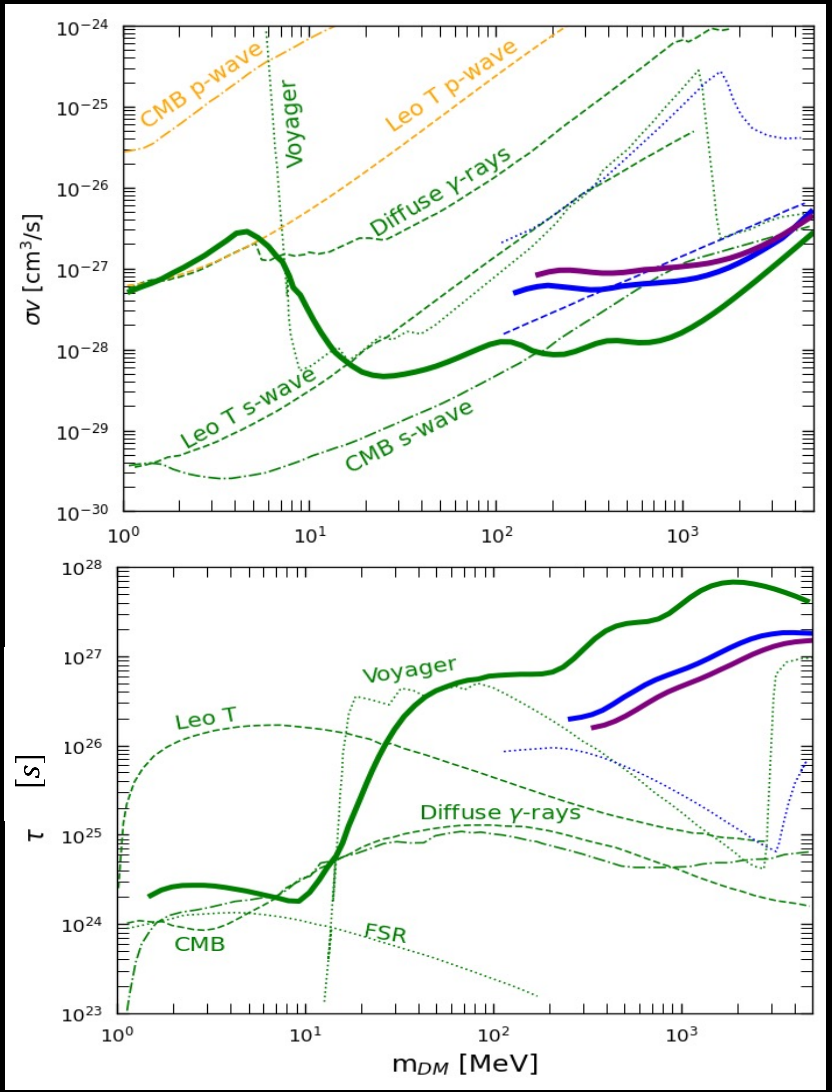

Conclusions

Thank you for your attention!

1. X-ray telescopes can help in closing the MeV gap

2. Inverse-Compton scattering on the photon bath is a powerful tool to study sub-GeV dark matter

3. Strongest bounds on

- Annihilating DM (if p-wave): $m_{DM} \geq 20$ MeV
- Decaying DM: $m_{DM} \geq 100$ MeV

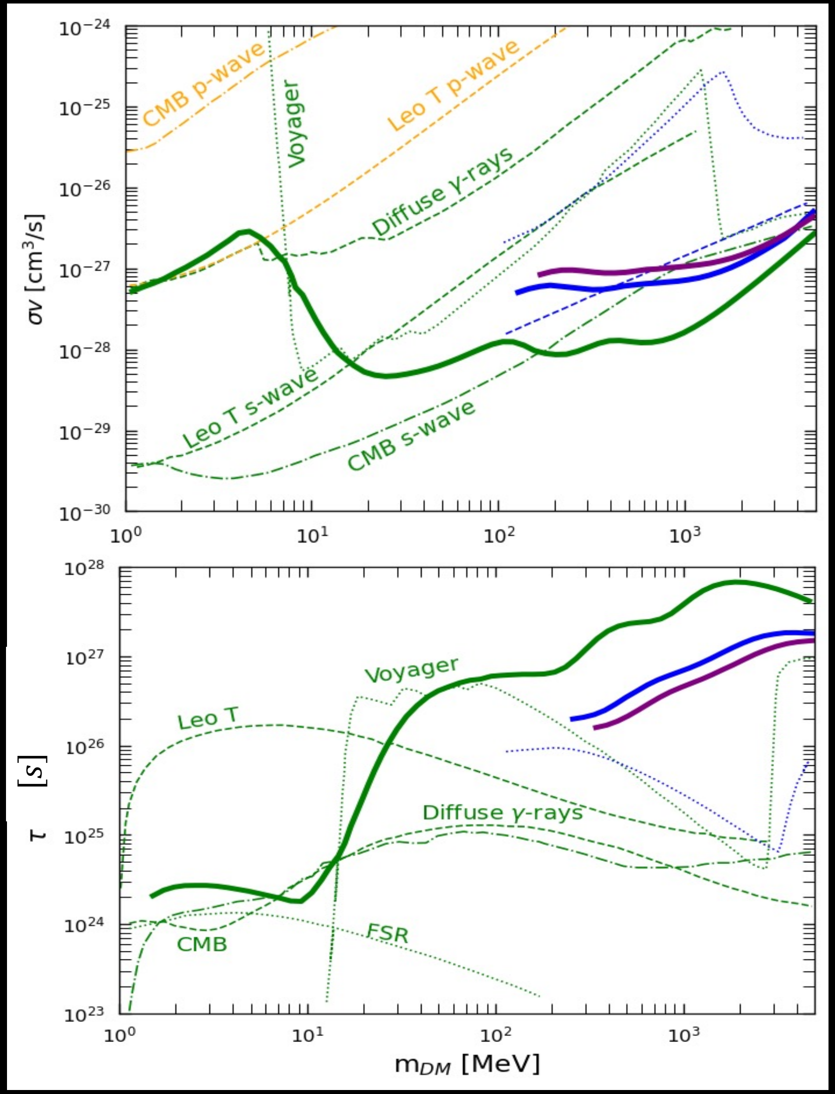

Back-up slides

Data sets

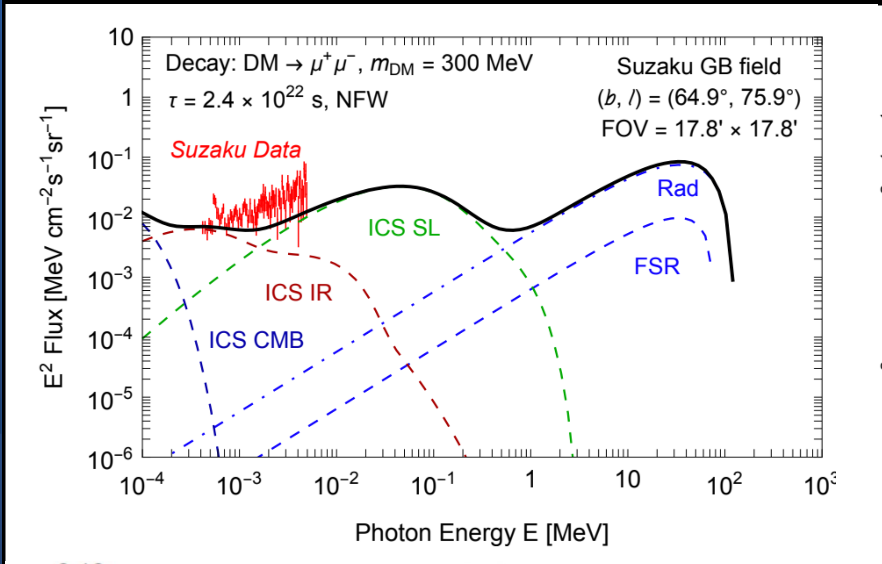
Decay: DM → μ⁺μ⁻, m_DM = 300 MeV
τ = 2.4 × 10^22 s, NFW
Suzaku GB field
(b, l) = (64.9°, 75.9°)
FOV = 17.8' × 17.8'
Suzaku Data
ICS SL
ICS IR
ICS CMB
Rad
FSR
E² Flux [MeV cm⁻²s⁻¹sr⁻¹]
Photon Energy E [MeV]

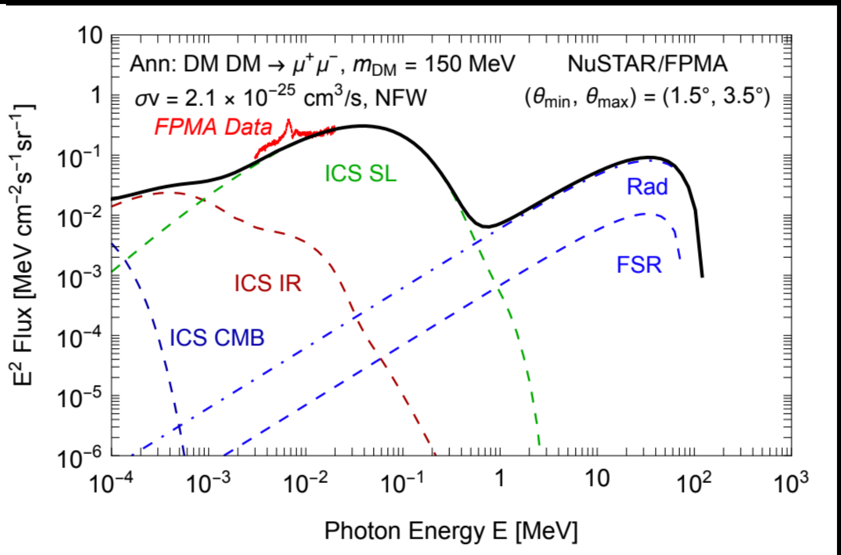
Ann: DM DM → μ⁺μ⁻, m_DM = 150 MeV
σv = 2.1 × 10^−25 cm³/s, NFW
NuSTAR/FPMA
(θ_min, θ_max) = (1.5°, 3.5°)
FPMA Data
ICS SL
ICS IR
ICS CMB
Rad
FSR
E² Flux [MeV cm⁻²s⁻¹sr⁻¹]
Photon Energy E [MeV]

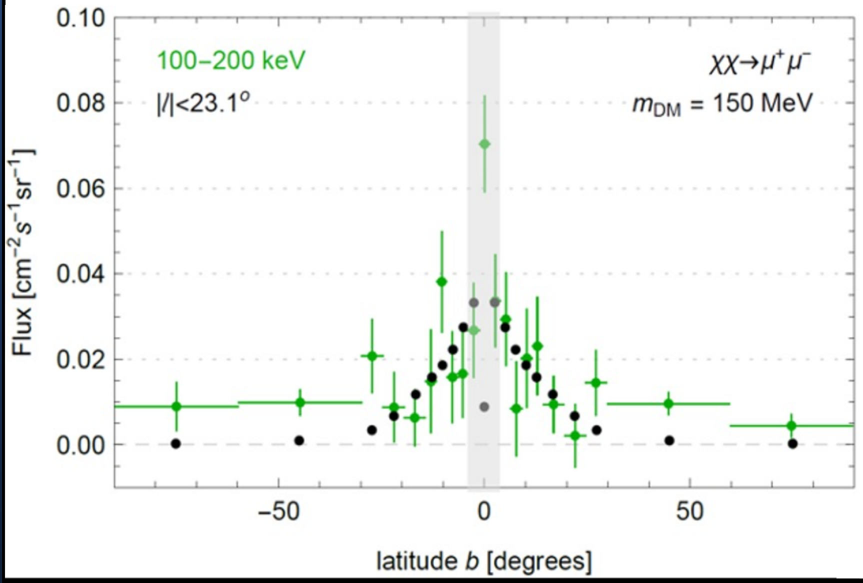
100–200 keV
|l|<23.1°
χχ→μ⁺μ⁻
m_DM = 150 MeV
Flux [cm⁻²s⁻¹sr⁻¹]
latitude b [degrees]

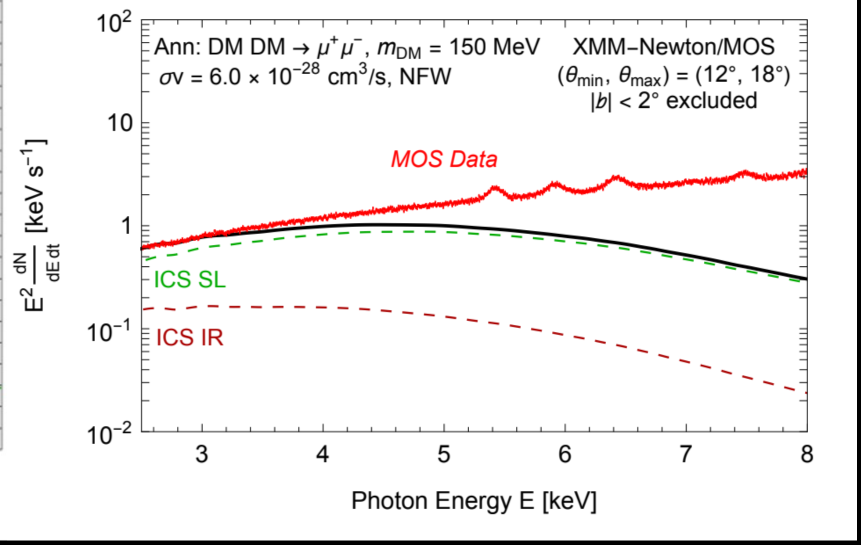
Ann: DM DM → μ⁺μ⁻, m_DM = 150 MeV
σv = 6.0 × 10^−28 cm³/s, NFW
XMM-Newton/MOS
(θ_min, θ_max) = (12°, 18°)
|b| < 2° excluded
MOS Data
ICS SL
ICS IR
E² dN/dE dt [keV s⁻¹]
Photon Energy E [keV]

Annihilation constraints

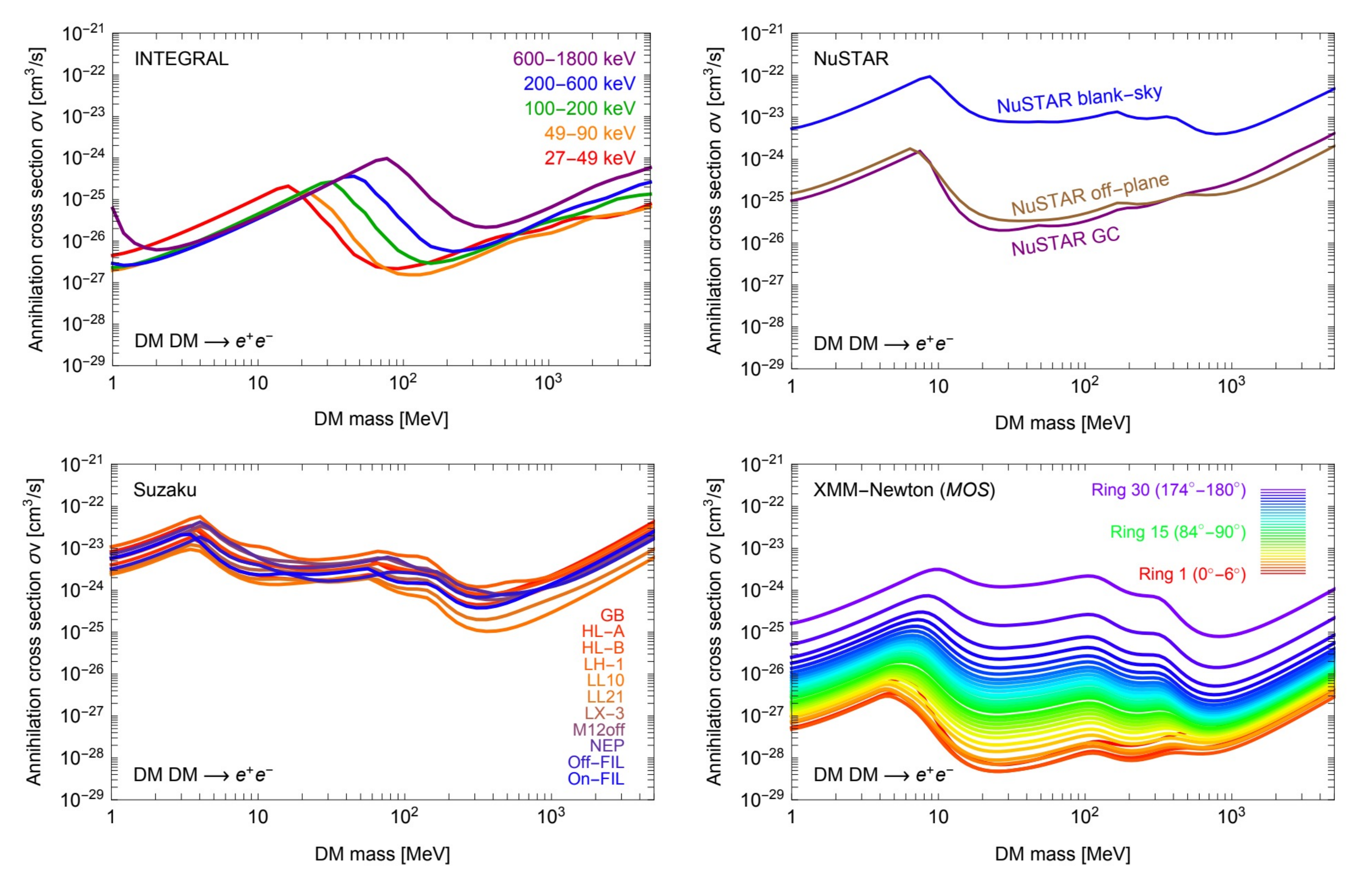

Decay constraints

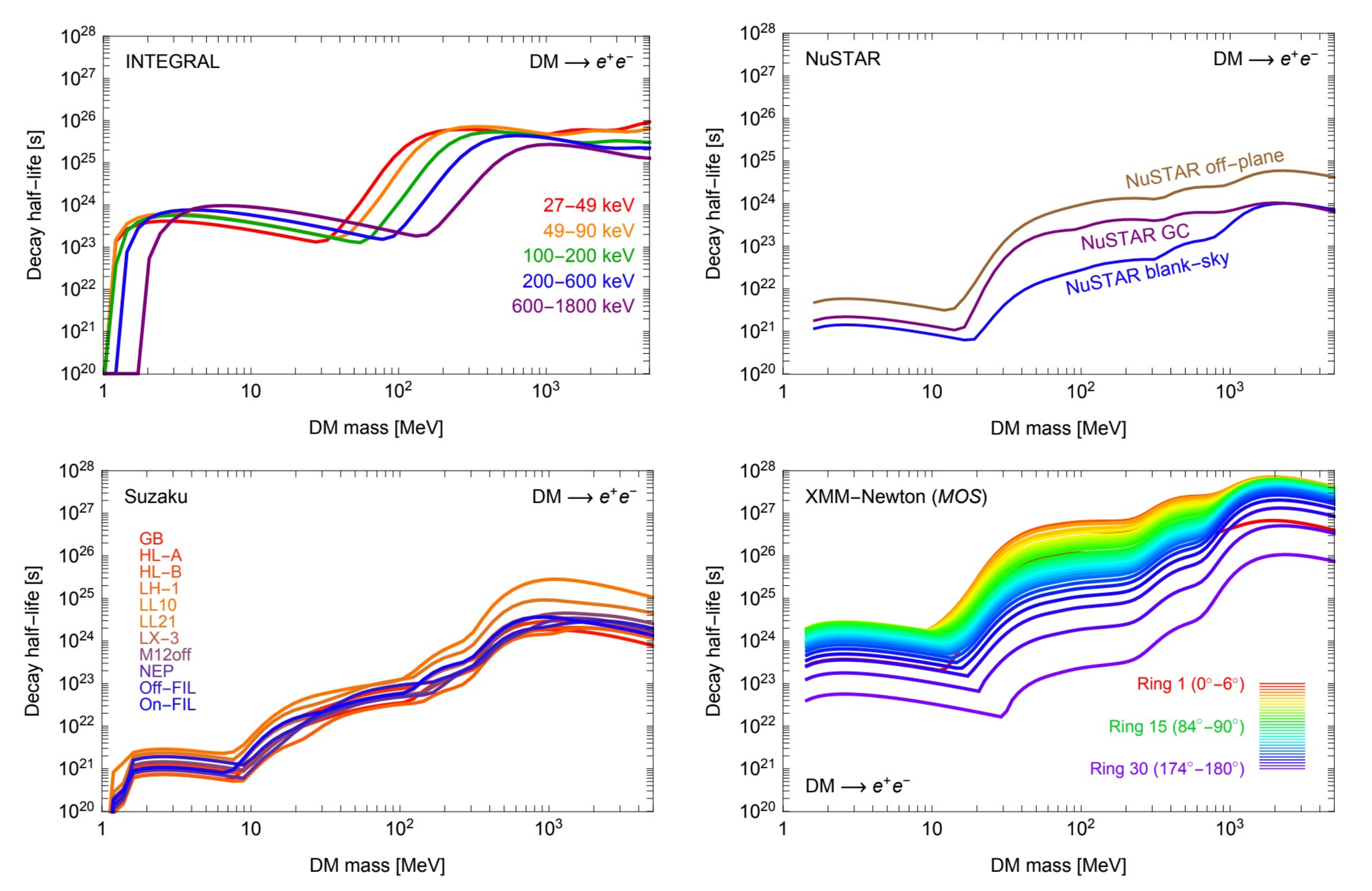

Optimistic constraints

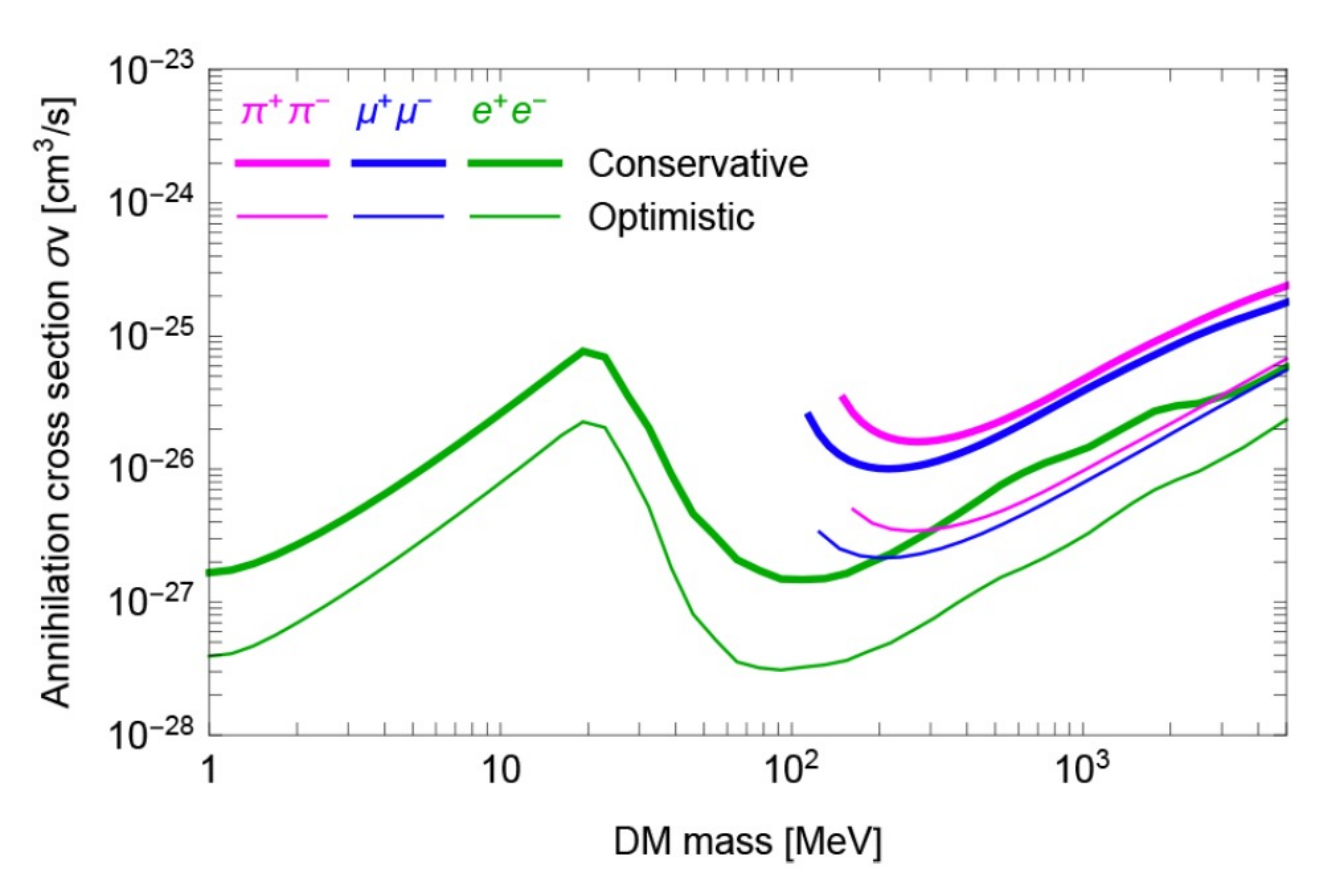

Transport equation

$$\nabla\left(D(E_e,\vec{x})\,\nabla f\right) + \frac{\partial}{\partial E_e}\left(b_{tot}(E_e,\vec{x})\,f\right) = Q_e(E_e,\vec{x})$$

$$f = \frac{dn_{e^{\pm}}}{dE_e}$$

Diffusion

Energy losses

Source term

$$Q_e(E_e,\vec{x}) = \frac{\langle\sigma_{ann} v\rangle}{2\,m_{DM}^2}\,\frac{dN_{e^{\pm}}}{dE_e}\,\rho_{DM}^2$$

On-the-spot approximation

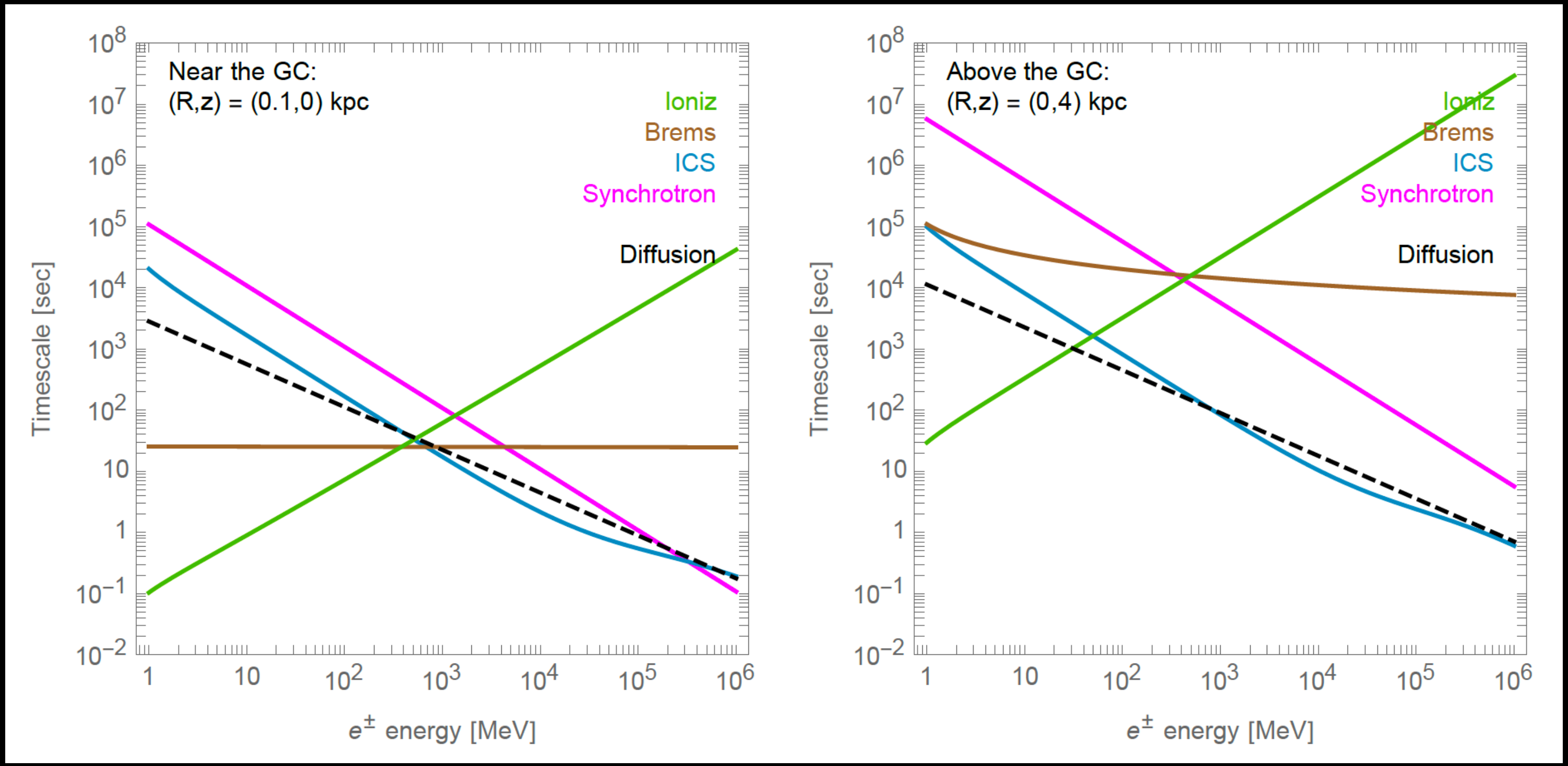

$$\frac{dn_{e^\pm}}{dE_e}(E_e,\vec{x}) = \frac{1}{b_{tot}(E_e,\vec{x})}\int_{E_e}^{m_\chi} d\tilde{E}_e\, Q_e(\tilde{E}_e,\vec{x})$$

On-the-spot approximation

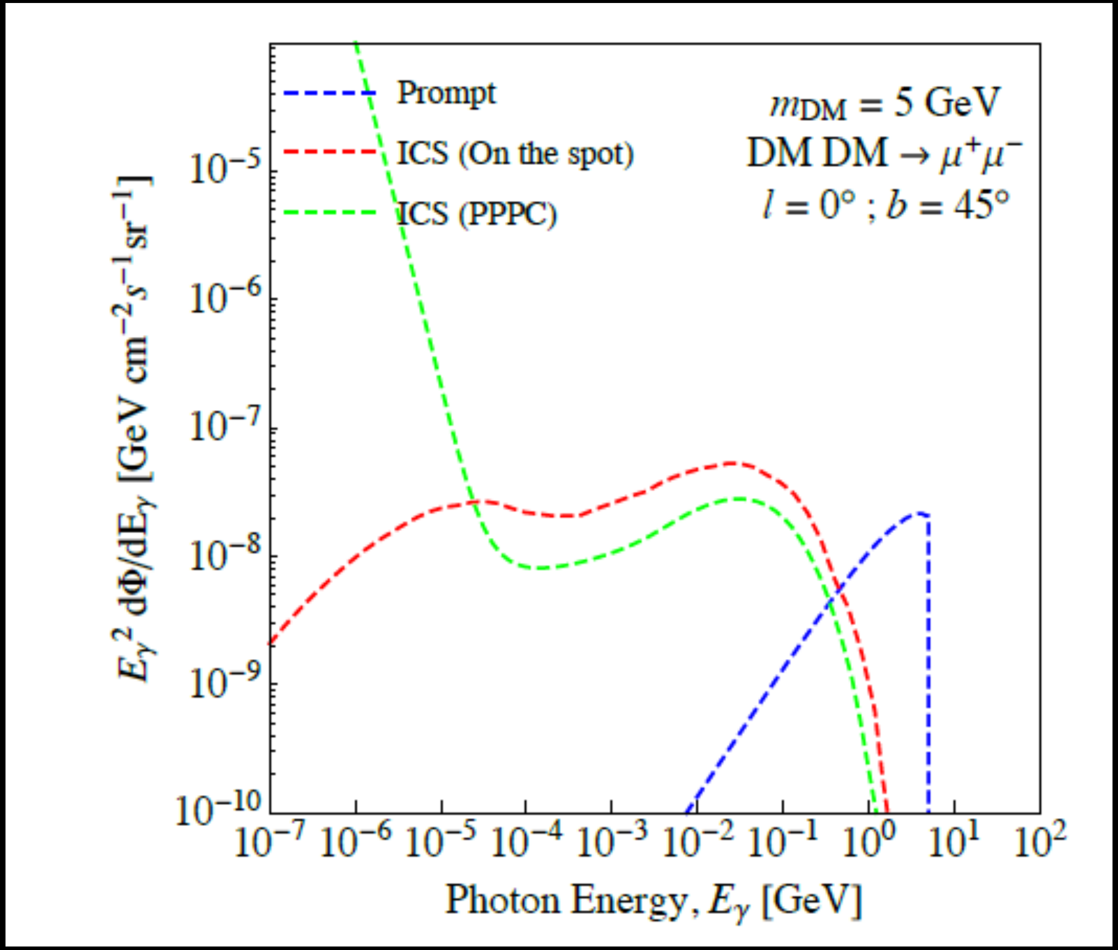

Energy spectrum for FSR

Channels e, μ:

$$\frac{dN}{dE_\gamma} = \frac{\alpha}{\pi\beta(3-\beta^2)m_\chi}\left[A \ln\frac{1+R(v)}{1-R(v)} - 2B \cdot R(v)\right]$$

Channel π:

$$\frac{dN}{dE_\gamma} = \frac{2\alpha}{\pi\beta m_\chi}\left[\left(\frac{\nu}{\beta^2} - \frac{1-\nu}{\nu}\right)R(v) + \left(\frac{1+\beta^2}{2\nu} - 1\right)\ln\frac{1+R(v)}{1-R(v)}\right]$$

$$\nu = \frac{E_\gamma}{m_\chi} \qquad \beta^2 = 1 - 4\mu^2 \qquad \mu = \frac{m_i}{2m_\chi}$$

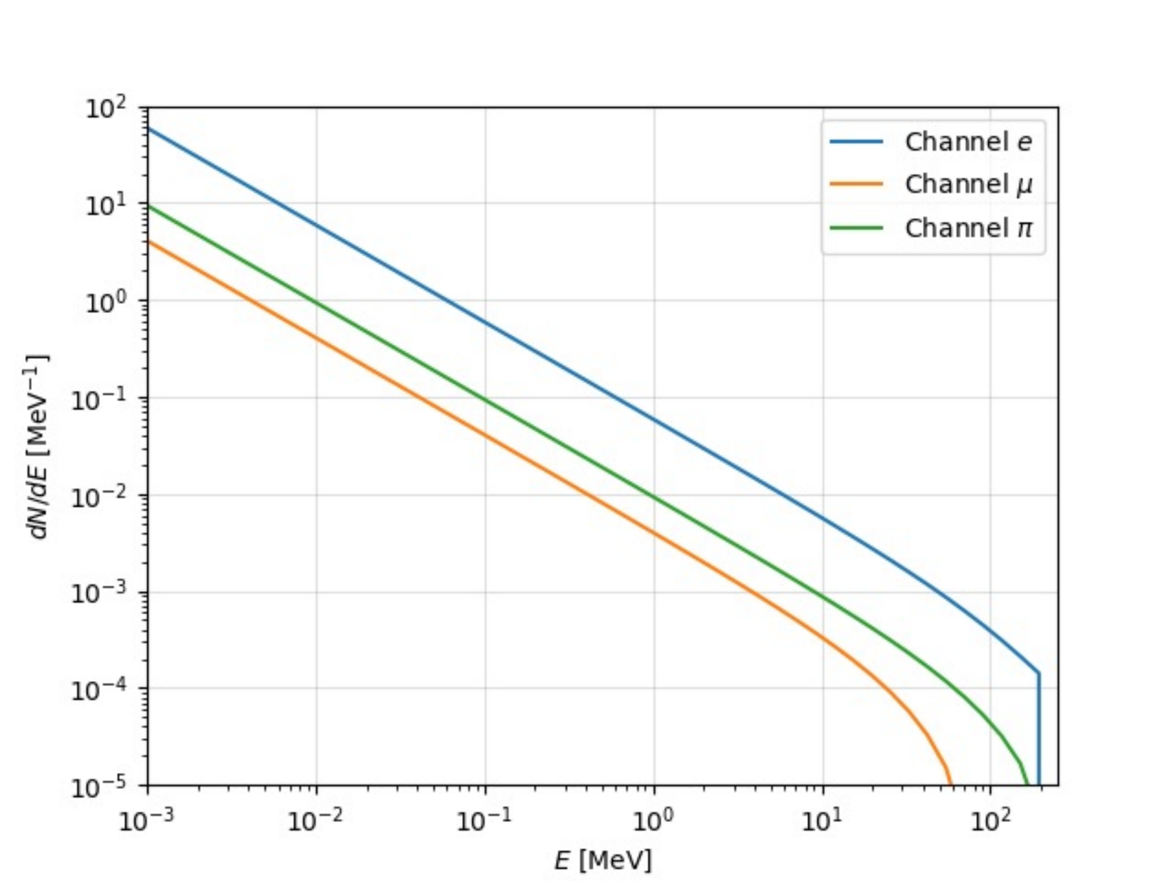

Bystritskiy et al, PRD 72 (2005) 114019

Energy spectrum for radiative decay

$$\frac{dN^{\mu}_{Rad}}{dE_\gamma} = \frac{\alpha\,(1-x)}{36\pi E_\gamma}\left[12(3-2x(1-x)^2)\log\left(\frac{1-x}{r}\right) + x(1-x)(46-55x) - 102\right]$$

$$\frac{dN^{\pi}_{Rad}}{dE_\gamma} = \frac{\alpha\,[f(x)+g(x)]}{24\pi\, m_\pi\, f_\pi^2\,(r-1)^2\,(x-1)^2\, r\, x}$$

$$x = \frac{2E_\gamma}{m_i} \qquad r = \left(\frac{m_e}{m_i}\right)^2$$

$$\frac{dN^{\pi}_{Rad\,Tot}}{dE_\gamma} = \sum_{l=e,\mu} \underbrace{BR(\pi \to l\nu_l)}_{1.23\cdot 10^{-4}} \frac{dN^{\pi}_{Rad}}{dE_\gamma}\Big|_{E_\pi = m_\pi} + \underbrace{BR(\pi \to \mu\nu_\mu)}_{0.999877} \frac{dN^{\mu}_{Rad}}{dE_\gamma}\Big|_{E_\mu = E_*}$$

$$E_* = \frac{(m_\pi^2 + m_\mu^2)}{2m_\pi}$$

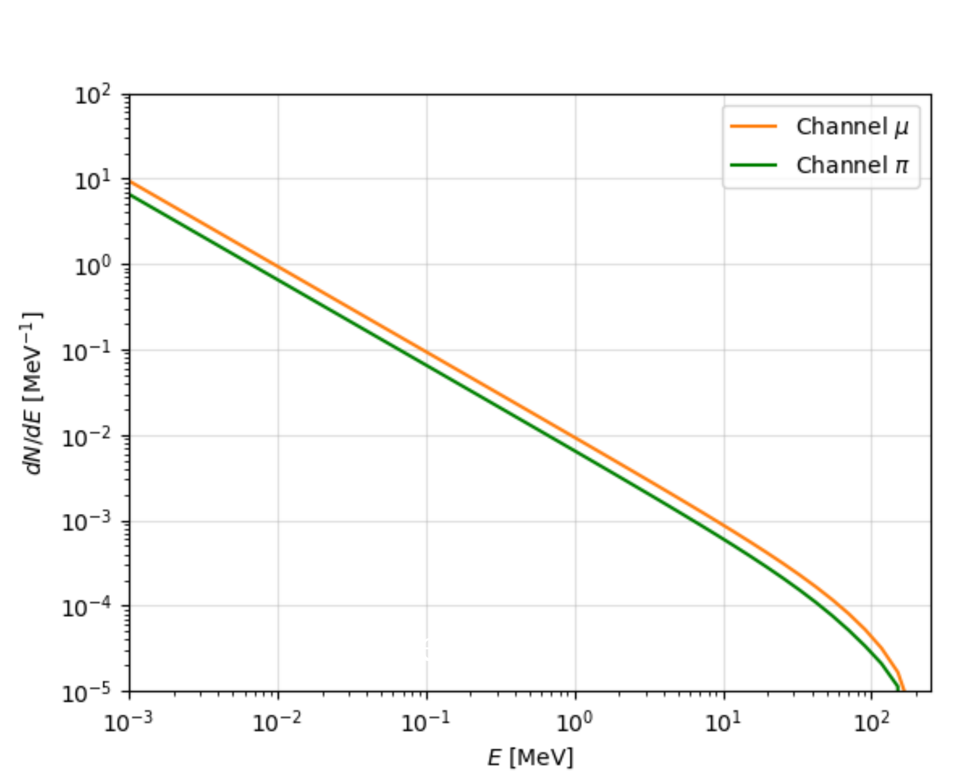

Essig et al, PRD 80 (2009) 023506
Kuno and Okada, Rev. Mod. Phys 73 (2001) 151-202

In-flight annihilation

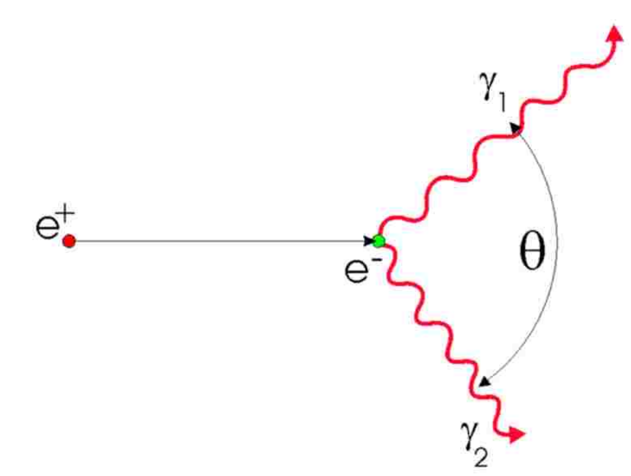

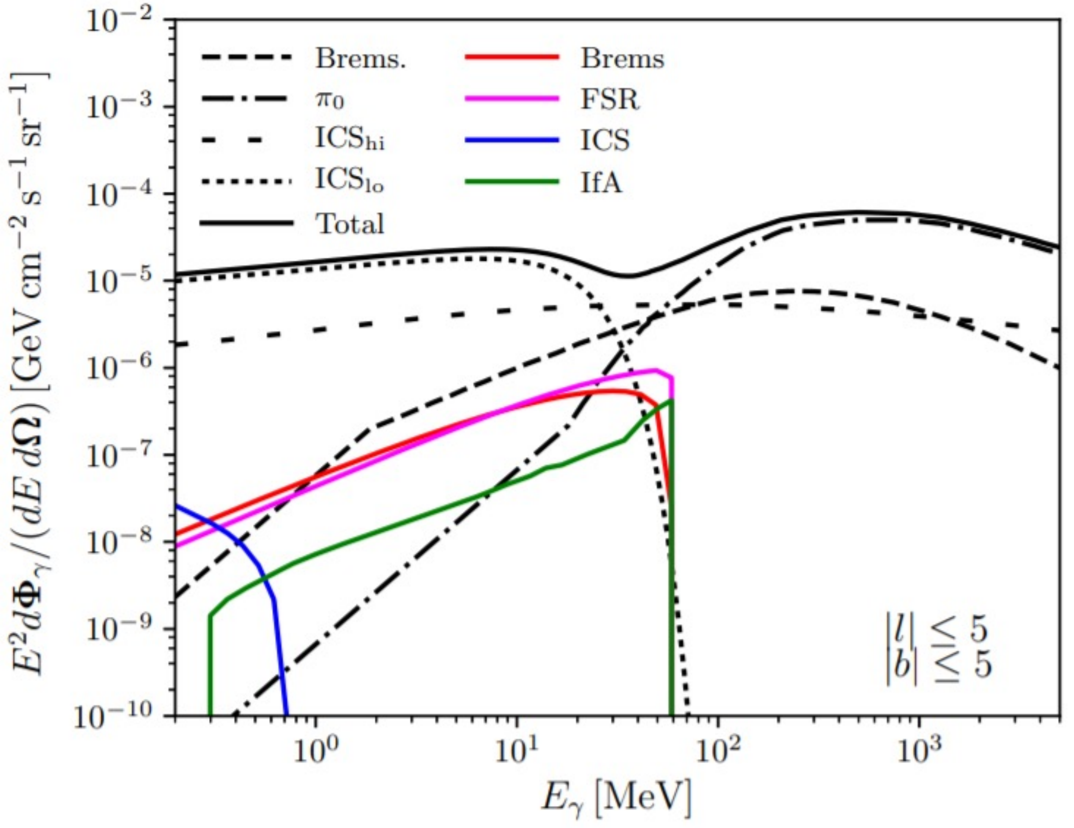

Figure 2: γ-ray spectrum resulting from $\chi\chi \to e^+e^-$ with $\langle\sigma v\rangle = 10^{-28}\,\mathrm{cm^3\,s^{-1}}$ in the inner $10^\circ \times 10^\circ$ of the Galaxy. The DM signal is broken up into individual components: IfA (green), FSR (magenta), bremsstrahlung (red) and ICS (blue). Black lines indicate the various diffuse-background components.

$m_\chi = 60\ \mathrm{MeV}$

Bartels et al,
JCAP 05 (2017) 001

Sensitivity X-ray experiments

Table 28: *Comparison of XMM-Newton with other X-ray satellites*

Satellite	Mirror PSF	Mirror PSF	E range	A_e at 1 keV	Orbital target	Energy resolution
	FWHM [″]	HEW [″]	[keV]	[cm^2] [a]	visibility [hr]	at 1 keV [eV]
XMM-Newton	6	15	0.15 - 12	4650 [b]	36.7 [c]	4 (RGS)
Chandra	0.2 [d]	0.5 [d]	0.1 - 10	555 (ACIS-S)	44.4 [c]	1 (HETG)
ROSAT	3.5	7	0.1 - 2.4	400	1.3 [e]	500
ASCA	73	174	0.5 - 10	350	0.9 [e]	100
Suzaku	96 - 120	108 - 138	0.2 - 600	1760 (XIS)	0.72 [e]	50
RXTE	n.a. [g]	n.a. [g]	2-250	n.a. [g]	1 [e]	n.a. [g]
Swift	8.8	18 [f]	0.2-10 (XRT)	133.5	~0.8 [e]	70
NuSTAR	18	58	3-79	n.a. [g]	~0.8 [e]	n.a. [g]

Velocity distribution

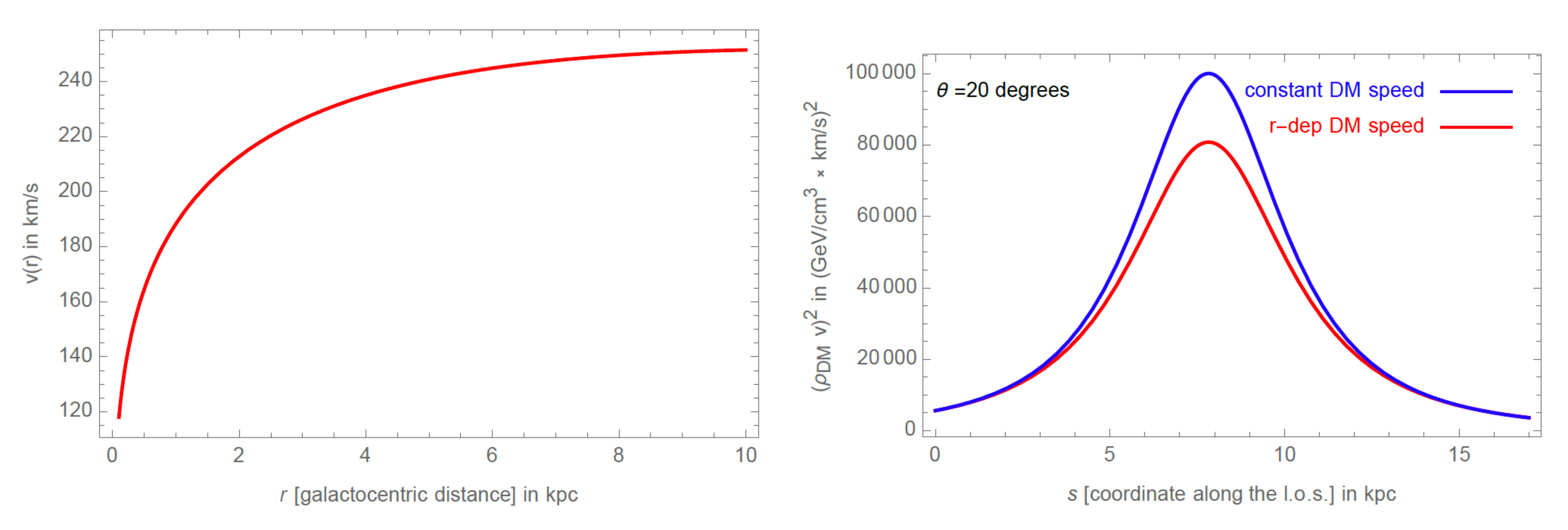

XMM-Newton Telescope

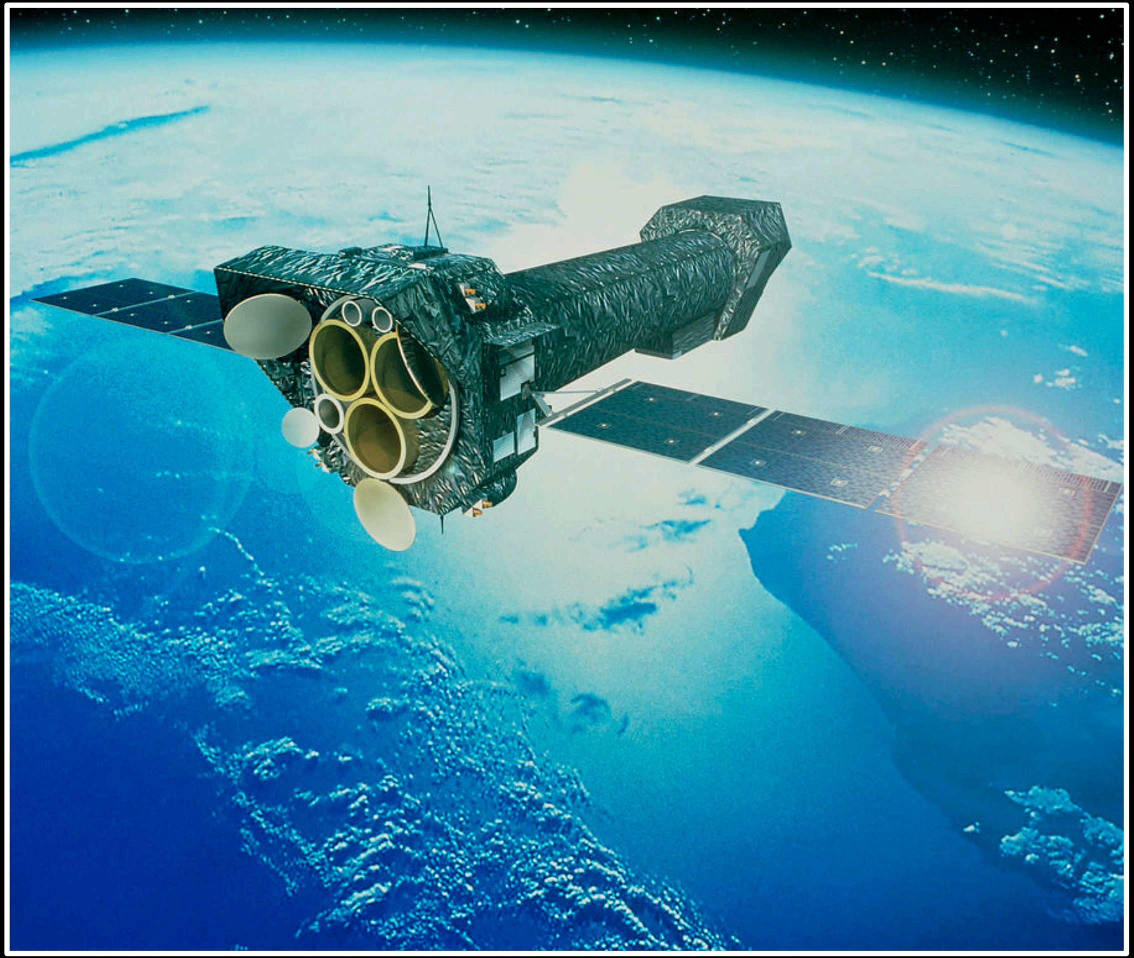

Observation time: 1999-2018

Energy range: 2.5 keV – 8 keV

Data set: 30 concentric rings around the GC

Dessert+, Science 367 (2020)

Foster+, Phys. Rev. Lett. 127 (2021) 051101

https://github.com/bsafdi/XMM_BSO_DATA

INTEGRAL Space Telescope

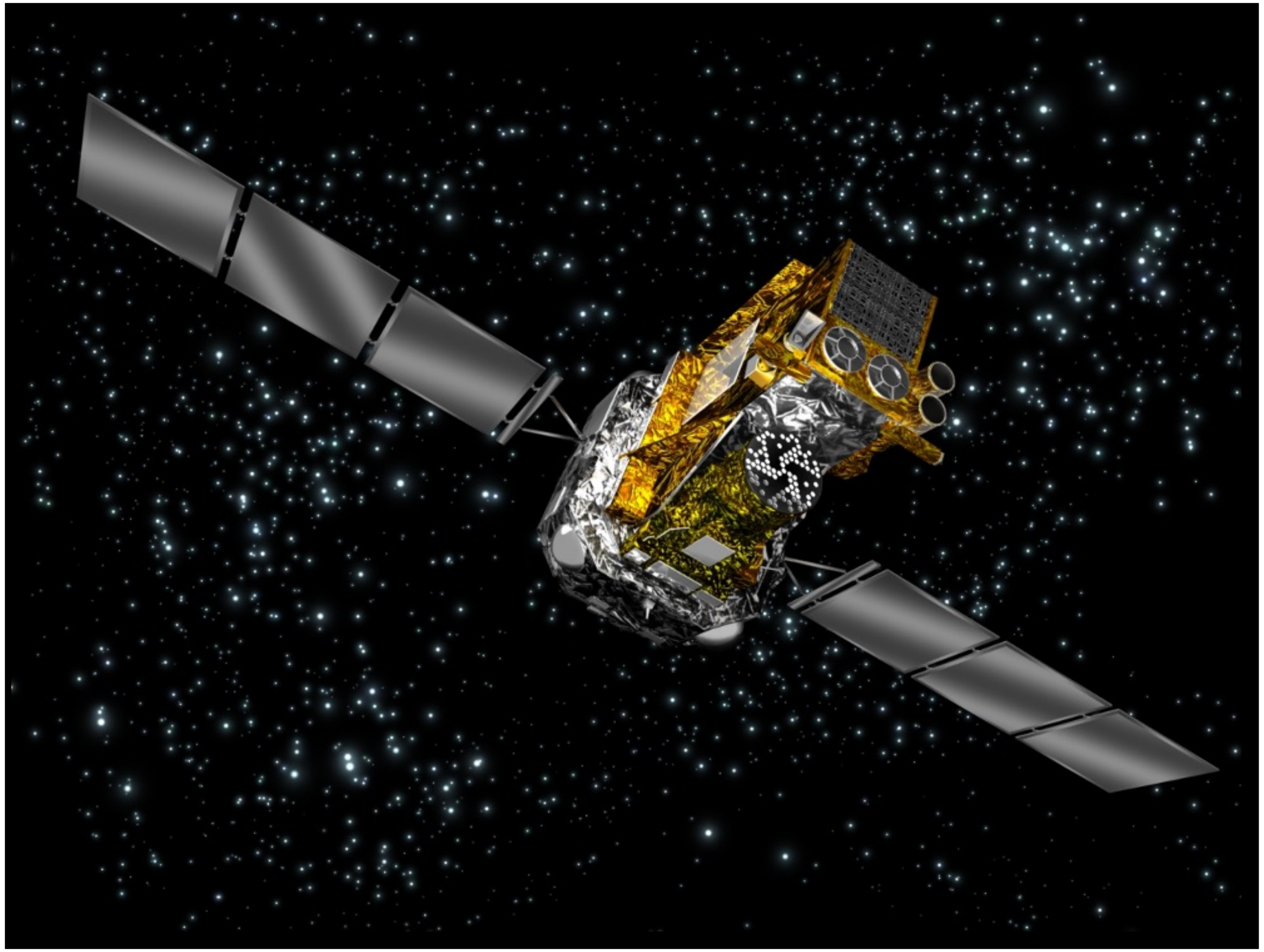

Observation time: 2003-2009

Energy range: 27 keV – 1.8 MeV

- Hard X rays
- Soft gamma rays

Data are provided in two forms:

- Energy flux
- Angular flux

Bouchet et al. (2011), APJ. 739 (2011) 29

Suzaku Telescope

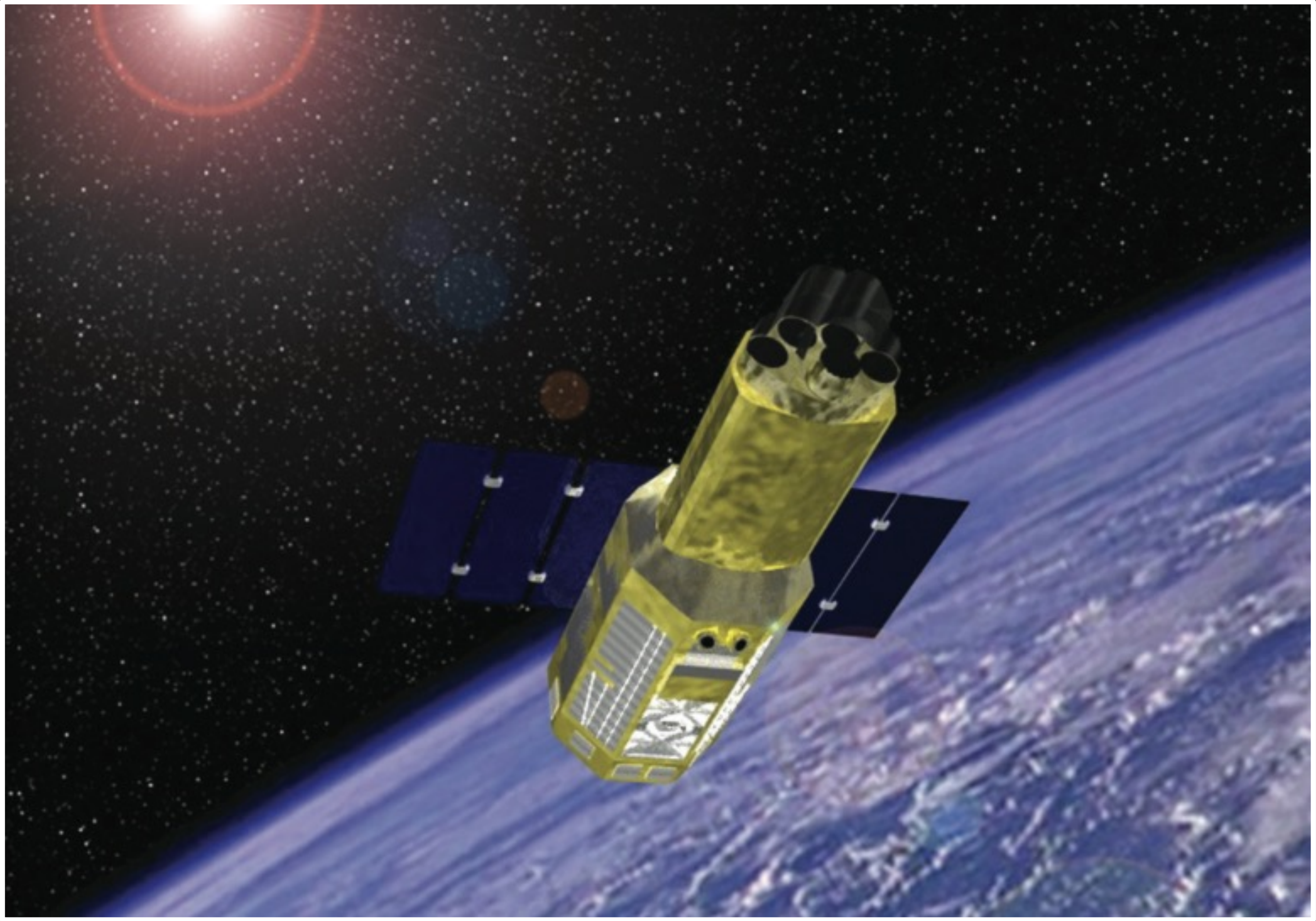

Observation time: 2006-2008

Energy range: 0.4 keV - 5 keV

Energy flux in 11 fields of view

Large Galactic longitudes

Yoshino+, Publ. Astron. Soc. Jap. 61 (2009) 805

NuSTAR Telescope

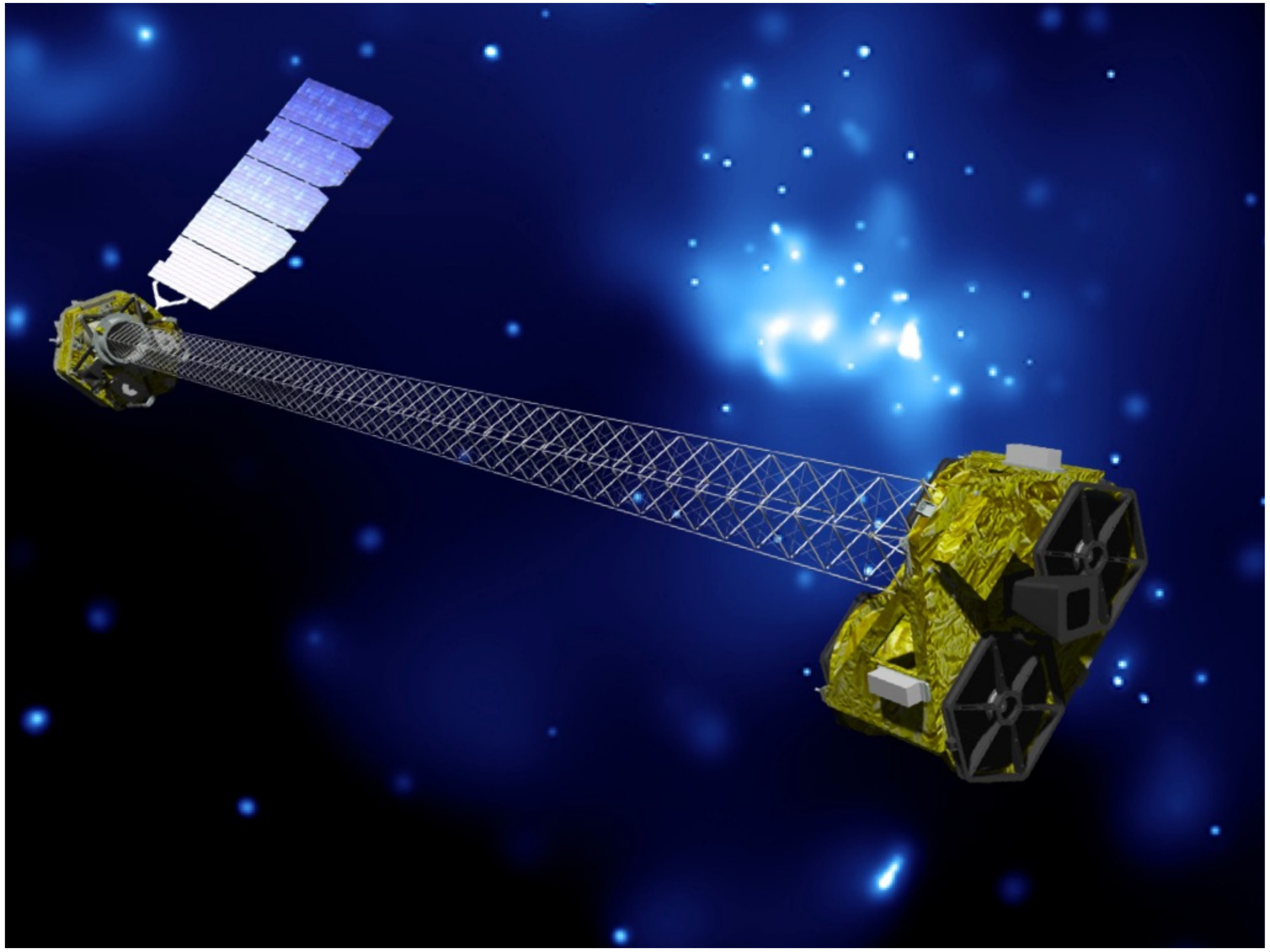

Observation time: 2012-2018

Energy range: 3 keV - 20 keV

Three datasets:
- GC observations
- Off-plane observations
- Blank-sky fields

Krivonos+, MNRAS. 502 (2021) 3966–3975
Perez+, Phys. Rev. D 95 (2017) 123002
Roach+, Phys. Rev. D 101 (2020) 103011

Theory motivations for sub-GeV dark matter

- 511 keV line
- Light scalar dark matter
- SIMP scenarios
- WIMPless idea
- Axinos
- …

Boehm and Fayet, J. Phys. G 30 (2004) 279-286
Boehm and Fayet, Nucl.Phys. B 683 (2004) 219-263
Fayet, PRD 75 (2007) 115017
Boehm+, PRL 92 (2004) 101301
Ahn and Komatsu, PRD 72 (2005) 061301
Boehm+, PRD 77 (2008) 043516
Ema, Sala and Sato, arxiv:2007.09105
Prantzos+, Rev. Mod. Phys. 83 (2011) 1001-1056
Hochberg+, PRL 113 (2014) 171301
Boddy+, PRD 89 (2014) 115017
Hochberg+, PRL 115 (2015) 021301
Choi+, JHEP 10 (2017) 162
Berlin+, PRD 97 (2018) 055033
Feng and Kumar, PRL 101 (2008) 231301
D'Agnolo and Ruderman, PRL 115 (2015) 061301
Covi+, PRL 82 (1999) 4180-4183
Choi+, JHEP 04 (2012) 106
Arhrib+, JCAP 04 (2016) 049
Boehm, Fayet and Silk, PRD 69 (2004) 101302
Hooper and Zurek, PRD 77 (2008) 087302
Essig+, arxiv:1004.0691